UNIVERSITY OF SOUTHAMPTON

FACULTY OF PHYSICAL SCIENCES AND ENGINEERING

School of Electronics and Computer Science

A Study on the Ageing of polymeric materials in the presence of space charge

by

Hisham Alghamdi

A thesis submitted for the degree of
Doctor of Philosophy

January 2016

UNIVERSITY OF SOUTHAMPTON

ABSTRACT

FACULTY OF PHYSICAL SCIENCES AND ENGINEERING
School of Electronics and Computer Science

Doctor of Philosophy

by Hisham Alghamdi

The use of polymeric power cables for high voltage direct current HVDC has become increasingly popular for renewable power sources such as offshore wind farms. The long term reliability of polymeric cables operating under DC conditions is still unknown and therefore of concern to the industry. However, there is no an explicit consideration of how the injected charges can cause effects to the prediction of the life-time. Thus, it is important to develop an ageing model can assist of understanding the effect of these charges on the insulating material.

Regarding to the polymeric material that are used as an electrical insulation, the presence of space charges could be the consequence of material degradations that are thermally activated and accelerated by the presence of electric field. The dynamics of space charge, therefore, can be potentially used to characterise the material. In this direction, an ageing model in which parameters have clear physical meanings has been developed and applied to the material to extrapolate the lifetime. The kinetic equation has been established based on charge trapping and detrapping of the injected charge from electrodes. The local electromechanical energy stored in the region surrounding the trap reduces the trap depth with a value related to the electric field. At a level where the internal electric field exceeds the detrapping field in the material, an electron can be efficiently detrapped and the released energy per detrapped charge can cause a weak bond or chain scission i.e. material degradation. The model has been applied to the electro-thermally aged low density polyethylene LDPE film samples.

To evaluate the damages structure during ageing process, a simulation work was performed on the developed ageing model to investigate the susceptibility of such parameters that can cause an explicit effect to the ageing process. The simulation work is performed on a two-dimensional square grid that is assumed to represent a part of the insulating material. The mesh structure is divided using the finite element method. Based on the nature of polyethylene, its structure is semi-crystalline with a spatially varying morphology. Consequently, each bond in the grid is assigned a set of parameter values. One of these parameters is the critical fraction of trapped charges C^*, which needs to be reached in order to fail a bond. It is chosen at random values from a range centred on the characteristic value obtained from the experimental results. This indicates that the insulation life at varying parameter C^* is lower than its characteristic value.

Contents

List of Figures

List of Tables

Nomenclature

$HVDC$	High Voltage Direct Current
DC	Direct Current
AC	Alternating Current
ICI	Imperial Chemical Industries
PE	Polyethylene
PET	Polyethylene-Terephthalate
$LDPE$	Low-Density Polyethylene
k	Boltzmann constant
T	Temperature
$\Delta G\#$	The Gibbs Energy of Activation
VEC	Voltage Endurance Coefficient
DMM	Dissado-Massanti-Montanari model
h	Planck Constant
PD	Partial Discharge
J	Current Density
N_T	Total of the Traps Density
n_T	Trapped Electron Density
K_T	Trap Coefficient
K_D	Detrap Coefficient
σ_T	Capture Cross-Section
Φ	Energy Barrier Height
N_c	Effective Density of States in the Conduction Band
v_{th}	Thermal Velocity of the Charge
E_T	Trap Depth
C^*	Fraction of Trapped Charges Cause Ageing
Y	Young's Modulus
W_m	Electromechanical Energy
eV	Electron Volt
$SCLC$	Space Charge Limited Current
PF	Poole and Frenkel
PEA	Pulsed Electro-Acoustic
TSC	Thermally Simulated Current

$PVDF$	Piezoelectric Transducer
DOS	Digital Oscilloscope
m_e^*	Electron Effective Mass
FDM	Finite Difference Method

Acknowledgements

Foremost, I would like to express my sincere gratitude to my supervisors Prof. George Chen and Prof. Alun S Vaughan for their guidance, inspiration, suggestions and criticisms during my study. Special thanks are also extended to my colleagues for taking the time to help in some points of my project.

I would also like to acknowledge to the Ministry of Education in Saudi Arabia for sponsoring me to study a PhD at Southampton University.

Finally, I would like to express my special appreciation to my parents for their love and continued support. The deepest thanks are expressed to my family (Mrs Ibtihal and Miss Raneem) for her endless confidence, encouragement, and patience.

Declaration of Authorship

I, **Hisham Alghamdi** , declare that this thesis and the work presented in it are my own and has been generated by me as the result of my own original research.

A Study on the Ageing of polymeric materials in the presence of space charge

I confirm that:

1. This work was done wholly or mainly while in candidature for a research degree at this University;

2. Where any part of this thesis has previously been submitted for a degree or any other qualification at this University or any other institution, this has been clearly stated;

3. Where I have consulted the published work of others, this is always clearly attributed;

4. Where I have quoted from the work of others, the source is always given. With the exception of such quotations, this thesis is entirely my own work;

5. I have acknowledged all main sources of help;

6. Where the thesis is based on work done by myself jointly with others, I have made clear exactly what was done by others and what I have contributed myself;

7. Parts of this work have been published as listed in page 165.

Signed: .....

Date: Tuesday, 19 January 2016

Chapter 1

Introduction

Due to safety, aesthetic considerations and reliability, high voltage cables are used instead of the overhead transmission lines in certain areas, such as residential areas and crossing oceans, to transfer electrical power. Underground cables are covered by insulating materials, instead of only wires in overhead lines, in order to avoid any contact of the conductor with the ground. Over the past few decades, insulation of underground cables consisted of oil-impregnated paper as an insulating medium, and now in most cases this has been replaced by polymeric materials. The advantages, that increase the demand for polymeric materials, are high electrical strength, low dielectric loss, high DC resistivity, good mechanical strength, low maintenance, low effect on the environment compared to paper-oil cables and low cost.

The usage of polymeric cables for HVDC is preferable up to 300 kV with voltage source converters. However, electrical systems with voltage levels of up to 500kV use paper-oil cables due to premature breakdown problems in polymeric cables [1]. The reason behind the lack of reliability in HVDC polymeric cables comes down to the deviation between design stresses in factories and the real stresses withstood in service.

The electric field depends mainly on electrical conductivity in HVDC cables which has an exponential relationship with temperature. Due to the heating produced from Joule losses that result from the conductor resistance, there will be a temperature gradient across the cable. Thus, the electric field profile will be significantly different from that derived if we consider the geometry of the cable to be cylindrical [2].

If the gradient of conductivity is sufficiently large, a field inversion phenomenon can occur. This means that the electric field at the outer semi-con is higher than the inner electric field in the semi-con. Although cable designers have taken this aspect into consideration, the effect of space charge generated by temperature and field inversion is difficult to predict. In fact, accumulation of space charge in polymeric cables is claimed to be the main affective factor that leads to acceleration of insulation degradation in HVDC conditions [3].

1.1 Power Cable Development

The assembly of a power cable usually consists of one or more electrical conductor held together and sheathed with an insulator. Its purpose is to transmit electricity from power stations to multi-consumption points. There are two types of power transmission mediums which are currently in use; overhead lines and underground cables. Figure 1.1 shows the power cable types.

Overhead lines, which are typically used for long distances above land, are bare conductor-based lines. This is cheaper as the insulation cost is less, they have better heat dissipation, are quick/easy to repair or maintain, are cooled by the air and the cables can be thinner. However, there are significant disadvantages to this type of cable. Overhead lines are vulnerable to lightning strikes which can cause interruption. Also, they are considered unsightly as they mar the scenery of the landscape, and there is a much higher risk of electric shock and damage by weather such as high winds.

Underground cables are not as obvious in the landscape, and unlikely to be damaged by weather. They require a narrower band of land to install. There can be difficulties passing though geographic obstructions such as marshes, rivers and hills. For any fault in an underground cable, a longer time is required, with higher cost, to repair it. Other disadvantages need to be considered such as they are difficult to access, expensive to install, they suffer heating losses and need insulation. In some cases, underground cables need to be rerouted to accommodate other underground structures such as sewage lines or pipelines. It is important to mark underground cables with sign boards to prevent accidents when excavations are carried out in the same area.

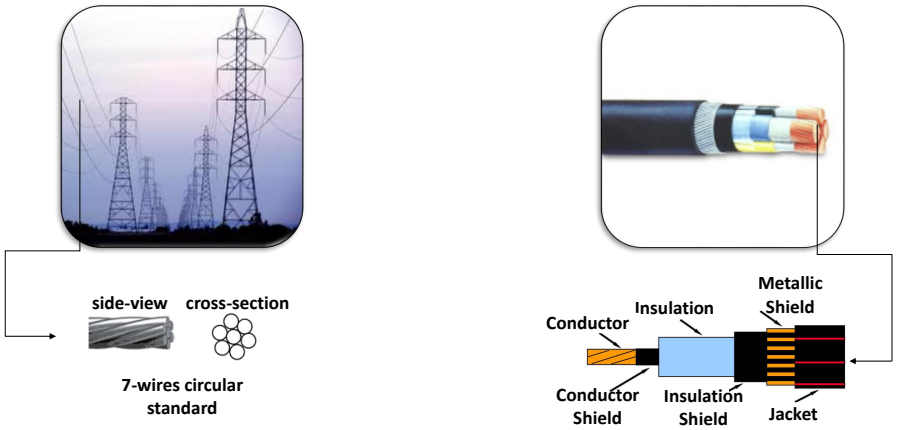

FIGURE 1.1: Types of the transmission lines; [a] overhead transmission lines with representing a single line of 7-wires circular standard type, [b] underground cable with construction details of a single line in the cable.

As the underground cable is the type considered in this study, a brief explanation is given here of the journey of the cables development. Every year, due to energy losses, there is a distinct percentage of energy in the world that does not reach the end user. This loss occurs from using alternating current AC where the electron flow changes direction rapidly, moving around the conductor surface leading to excessive waste heat. With direct current DC, the electrons can only flow in one direction and pass further into the conductor. The later is preferable as the conductor becomes more efficient, less heat is lost and there is less wasted energy. Figure 1.2 shows the flow of electrons in the two types of current in the conductor.

The question that should be asked 'why was this option not chosen earlier?'. To reach the answer, there are several factors that should be considered when choosing the current type. The technology to transmit electricity over long distances in the form of DC was costly. However, the cost of energy today is being questioned and engineers are working on developing DC cables with cost-effective solutions. One of the solutions is that the ultra high performance converters transform high voltage AC into DC. Thereafter, the current is transported as a direct current via underground cables over distances of up to several thousand kilometres. At the end, there is a converter station which transforms the DC back into AC to feeds it into the distribution grid.

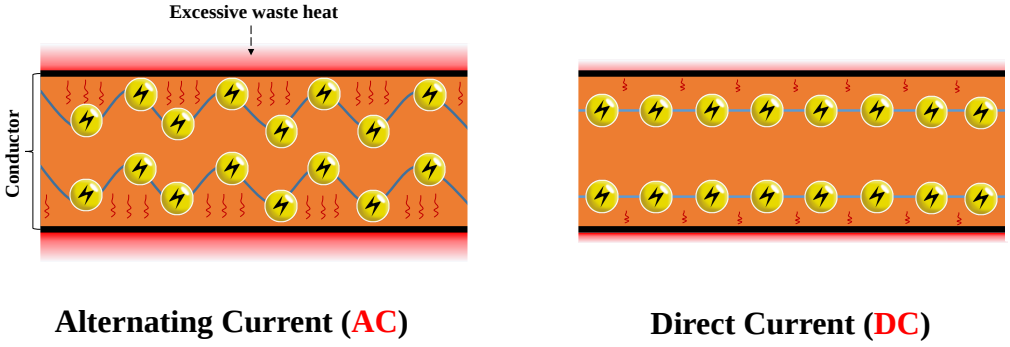

FIGURE 1.2: Scheme the electron flow in a conductor. It changes direction in AC which produces excessive waste heat, while the waste heat energy is less in DC.

In addition to the core converter technologies of high voltage DC systems, underground and undersea transmission cables are often used for high voltage DC as well, including the integration of offshore renewable energy. As the demand for renewable sources has increased due to energy needs and climate issues, the number of wind farms has increased worldwide. It is necessary to deal with the right and appropriate insulation material for these cables to survive to their utmost and reduce side effects. To develop insulation materials, the actual structure of materials needs to be understood. Here, a precise selection of polymeric insulations exists widely in most of the popular insulations.

1.2 Polymeric Insulating Materials

1.2.1 History of Polymer Science

The term Polymer has been used since 1866 by Berthelot [4] who observed that styrolene (styrene), heated at 200^oC for a period of few hours, transforms itself into a resinous polymer. This observation was the first recognised synthetic polymer. However, Hermann Staudinger [5] in the year 1920 was the first to propose the concept of polymers in the sense we use today. He was awarded the Nobel prize in 1953 for his work which was the basis of the science of macromolecules.

Man [6] used naturally-occurring polymers for clothes, shelter, decoration, tools and other uses. Moreover, the polymer industries at the end of 19^{th} century transformed natural polymers into artificial polymers. Thus, they created a chemical compound called nitrocellulose (celluloid, artificial silk) for the replacement of many materials, presenting new properties likely to generate new applications (ebonite by extreme vulcanization of natural rubber).

In 1933, there was a success in the polymerisation of ethylene for the first time by the firm ICI (Imperial Chemical Industries). The result was a completely new material: low density polyethylene. This material is a polymer of extreme importance that is produced nowadays on the scale of several tens of million tons for various purposes.

During the same decade (in 1938) [7], a research team discovered polyamides (nylons) and showed that the chemistry of polymers is able to generate materials whose mechanical characteristics could be higher than those of natural polymers.

In the next decade, polymers were used instead of a number of traditional materials. These substitutions were carried-out based on the results of research in the industrial and academic laboratories that showed improvements in reducing and eliminating the principal defects of the polymers. Currently, polymers are used for the most sophisticated applications and the most advanced fields of technology.

Due to their economic applications, polymer industries have produced a multitude of research tasks and stimulated, upstream, academic research to make a great quality of products. This is strongly supported by industrial circles with their strength in developing basic research into products.

The universality of polymers is now well established. They can be seen in most fields of industrial production as additive or structural materials. The improvement in polymer properties gradually eliminated their bad reputation and, at the present time, we can now state that ‘There are no bad polymers, only bad applications of them’.

1.2.2 Engineering Properties of Polymers

The most common way to describe the classifications of polymers is shown in Figure 1.3, in which polymers are initially classified into three groups: thermoplastics, elastomers and thermosets. Thermoplastics are separated into crystalline, semi-crystalline and amorphous. These classifications are based essentially upon the structure of polymers which all have advantages compared to others.

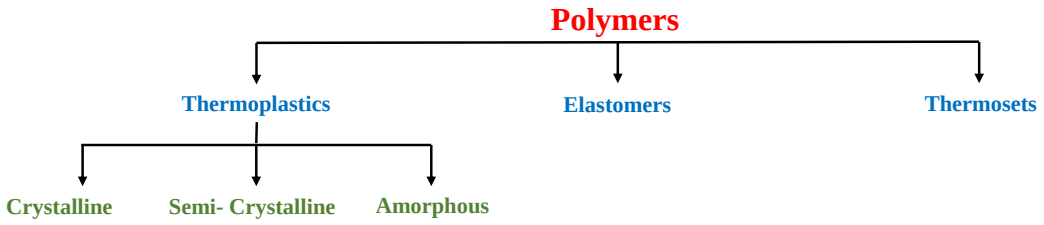

FIGURE 1.3: Classification of polymers.

Thermoplastics refer normally to linear or branched polymers which enter a liquid phase when exposed to heat. One of their advantages is that they can be moulded and re-moulded easily and economically, using modern techniques, into a final product[8]. On the other hand, thermoplastics do not easily crystallize from a liquid state to a solid state when cooled enough, due to the considerable requirements of coiled and entangled macromolecules. In reality, the form of crystallinity cannot properly exist in polymeric materials but instead they can be semi-crystalline materials containing both crystalline and amorphous phases. Crystalline phase, refers to the degree of structural order in a solid, that can be characterised based on the melting temperature T_m, above which such polymers can be converted into artefacts by conventional polymer-processing techniques.

Amorphous phase of semi-crystalline polymers is characterised by its glass transition temperature T_g. Glass temperature is the temperature at which polymers transfer from a glass state to a rubbery state abruptly (i.e. from a hard to a soft state). Below glass temperature, polymer chains are unable to move (frozen). While above glass temperature, polymer chains correspond to the onset of chain motion. Figure 1.4 shows a representation of amorphous and crystalline polymers.

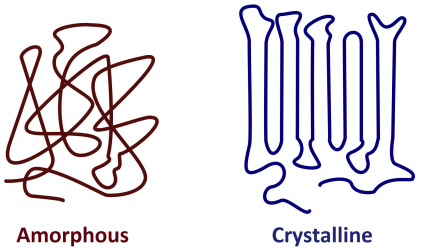

FIGURE 1.4: Scheme of amorphous and crystalline regions in polymers.

Elastomers, which are the second classification of polymers, are cross-linked rubbery polymers. This type of polymer can be stretched easily to a high range of extension (i.e. 3 to 10 times the original dimension) and rapidly return back to the original dimensions when the applied stress is released. The network density in elastomers is classified as low cross linking density. Rubber is the preferable word used instead of elastomers for rubbery polymers that do not have cross-linking in their structure.

Thermosets are rigid materials with a high degree of cross-linking. Chain motions in thermosets are greatly restricted. Once this type of polymer is formed, it becomes intractable rather than fluid with the application of heat. Therefore, their processing into artefacts needs a minimum amount of flow to be performed.

Based on the above, we can deduce that polymers consist of long-chain molecules which have many identical repeating units known as monomers. The formula of the monomer is $[A]_n$ where A is the monomer and n is the degree of the polymerisation which represents the number of monomers composing the chain. For example ethylene monomers of polyethylene PE Figure 1.5. Ends of chains have different molecular units as CH_3 in polyethylene. Since the order of monomer units ranges between 10^3 to 10^5 for each chain, the effect of end groups of the bulk of the material is still minimal, but they may have a significant influence on net space charge since traps originate from these chains [9].

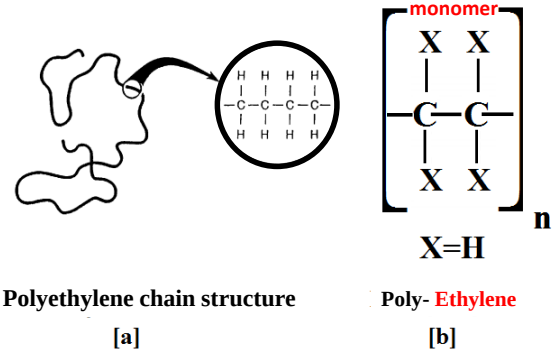

FIGURE 1.5: Polyethylene chain unit (monomers).

Polymers such as polyethylene (PE) and polyethylene terephthalate (PET) are widely used in insulating materials due to their good advantages. These materials are made up of mixed crystalline and amorphous regions and can be classified as semi-crystalline polymers. Hence, characteristics of both crystalline and amorphous systems are applied as they have both glass transition for amorphous regions and melting temperature for crystalline regions. Formation of crystalline regions involves creating long ribbons which are called lamellae, while the amorphous portion is outside the lamellae as shown in Figure 1.6. The lamella grows like the spokes of a bicycle (sometimes known as lamellar fibrils). When the fibrils grow out in three dimensions, the form becomes like spheres

and the whole assembly is called a spherulite. In a small sample, there are many billions of spherulites. Among the crystalline lamellae, there are disordered regions which are called the amorphous regions.

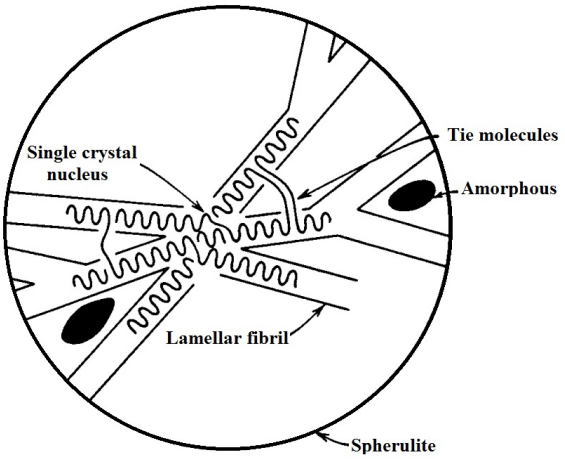

FIGURE 1.6: Spherulite formed from many lamellae for semi-crystalline region [10].

Polymeric materials also can be classified based on the chemical type of the monomers into homopolymers which consist of the same type of monomers, and copolymers which are different repeating units. The copolymers can be separated into two types based on the arrangement of the monomers; random copolymers (different repeating units are distributed randomly), alternating copolymers (alternating sequences of different monomers) and graft copolymers (a chain made from one type of monomer with branches of another type). All these classifications are shown in Figure 1.7.

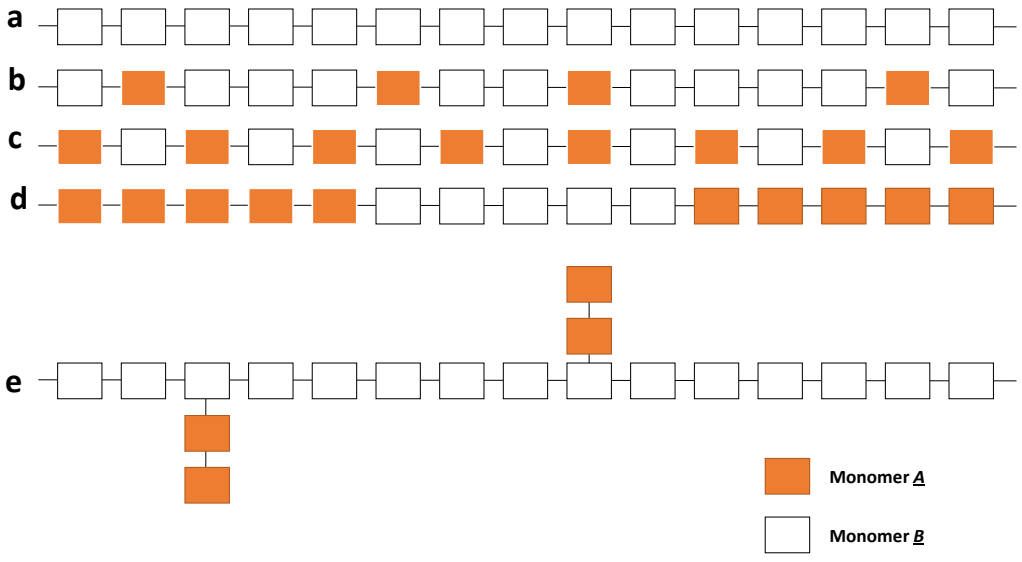

FIGURE 1.7: (a) Homopolymer; (b) random copolymer; (c) alternating copolymer; (d) block copolymer; (e) graft copolymer.

1.3 Research Objectives and Scope

The general objective of this thesis is to obtain a better knowledge of the ageing process of polymeric HVDC cable insulation, and analyse possible ageing mechanisms that the insulating materials experience during ageing. From a narrow view, the study was maintained to investigate the effect of space charge in the insulating material. A number of competing theories existing in the literature have been discussed broadly in Chapter 2, and each model is based on different physical mechanisms without obvious connection to the space charge. Although all the models predict relationships between the material life and the applied field and temperature which give good fits to the experimental lifetime results, they tend towards the chemical direction rather than the electrical.

This study, however, aims to develop a new ageing model based on the charge trapping and detrapping process. In order to understand the developed model, it is important to know the physics behind the chosen parameters. In a simple way, the model can be separated into three parts; electron injection process, trapped space charge, and detrapping the captured electrons. To identify the injection process, conductivity measurements were performed on low density polyethylene LDPE samples. The results were obtained at different applied temperatures. In regards to space charge, it was essential to extract and determine the model parameters. The main concept of the ageing mechanism is derived from the released energy after detrapping the captured electrons. Finally, the model results were verified with electro-thermal aged samples.

1.4 Contributions

This thesis contributes to the understanding of space charge effects on the ageing process in polymeric insulating materials through theoretical modelling, experimental investigations and simulating the breakdown growth. A new ageing model is developed which is derived from the electro-thermal dynamics of space charge in polyethylene under a DC electric field, based on trapping and detrapping of the injected electrons. Due to the accumulation of charges in traps, electromechanical stress is created which leads to induced electromechanical energy. The local electromechanical energy stored in the region surrounding the trap reduces the trap depth with a value related to the electric field. At a level where the internal electric field exceeds the detrapping field in the material, an electron can be efficiently detrapped and the released energy per detrapped charge can cause a weak bond or chain scission i.e. material degradation.

Throughout, the simulation results show that a fraction of the insulating material needs to be broken to fail the sample. This supports the experimental results such as growing electric tree. In addition, investigating the effect of the model parameters on the ageing

process can be performed through the simulation. A clear study was carried out on the effect of the fraction of trapped charge to the ageing.

1.5 Thesis Outline

The project in this thesis is mainly focused on interpreting the effect of injected space charge on polymeric insulation materials. Through a narrow window, the thesis explains a newly developed ageing model based on the trapping and detrapping process. To represent the model in an obvious way, several steps were performed on low-density polyethylene samples to validate the model. The thesis is broadly summed up as follows:

Initially, it is worthy of attention to review the ageing models describing the basis and the physical mechanism behind each model. This is most likely to assists the reader by providing a large view of the research in this area. Chapter 2 describes in more detail the ageing models that are reported in the literature.

Besides the literature, Chapter 3 shows the steps and the basis of the developed ageing model in the thesis. The model illustrates explicitly the effect of space charge on insulation life. The lifetime expression is derived from the electro-thermal kinetic equations that are based on trapping and detrapping the injected electrons. In addition, the effect of the released energy from detrapping process to the trap is covered in this chapter.

The developed ageing model is based on the trapping process, and the injected current is the intrinsic parameter in the trapping process. Chapter 4 describes the compatible mechanism for the injection process. The chosen mechanism is verified by taking conductivity measurements of LDPE samples.

The model parameters can be described as a chain, the rest of the parameters can be reached when part of the model's parameters are extracted. To do this process, space charge profile at decay stage is a convenient method to extract the initial parameters which lead to a solution for the rest of the parameters. Chapter 5 discuss the steps in more detail based on the experimental results of space charge.

A major step in verifying the developed ageing model is to compare the life results with the experimental results. Chapter 6 covers the experimental set-up of the electro-thermal ageing at fixed fields and temperature. The results were analysed using the Weibull distribution function.

As a step forward in the work, the ageing model is simulated in two-dimensions. The purpose of the simulation is to investigate the effect of the variation of the model parameters on the ageing results. Furthermore, the simulation is a suitable way to represent the growth of the breakdown path through the sample. Both of these points are discussed clearly in Chapter 7.

Chapter 8 is the conclusion and suggests future work on the developed ageing model. In this chapter, the whole project is summarised and some further work is suggested.

Chapter 2

Polymeric Ageing Models Review

2.1 Introduction

The purpose of developing ageing models, as described in literature, is to obtain useful information about the insulation life to keep the products working normally. In earlier research works, the developing ageing models were subjected to more severe conditions (in short times) than normal in order to induce early failures. This way can save time and expenses as long as the results can extrapolate the life at service conditions. With the advancement of science, this approach was found to be weak as it does not have firm theoretical basis. In addition, the power law regime from short time tests does not fit for long time results, which limits the validity of this way for extrapolation [11].

The term of ageing is defined in accordance to International Electro-technical Commission IEC Publication 505 [12] as "irreversible deleterious change to the serviceability of insulation systems and such changes are characterized by a failure rate which increases with time". From this definition, two important aspects should be brought into account: ageing as a concept does not apply only for the insulating material itself but to the insulation systems. Another point is that ageing process is related to the serviceability of the insulation systems. Thus, ageing is subjective and determined by the insulation system.

Based on IEC Publication 505, there are four parameters that have been defined as ageing factors: temperature effect, electrical stress, mechanical stress and environmental factors. The insulation can be subjected to either a single or multiple factors simultaneously. Damage to the significant parts of the insulation during the ageing process eventually causes a failure to the system. Obviously, the endurance of an insulation system is for a long period of time before failure occurs. Thus, accelerated test procedure must be applied for evaluating the ageing properties of the insulation system. The lifetime can be predicted at conditions that differ from the accelerated testing conditions

used in the ageing models. Chinh Dang et al.[13] reported that around a dozen theories and models were published without any of them reaching a reliable end-of-life-prediction. Obviously, a thorough evaluation should be made to keep only the models that give a fair agreement with actuality.

Basically, a couple of mathematical expressions have to be considered for creating an ageing model. First is the ageing rate expression which explains the thermodynamic principle of the ageing. Second is the solution of the rate equation to achieve the ageing model as a function of the ageing factors.

This project focuses on two factors of ageing: thermal and electrical effects. With respect to electricity, ageing models dealing with high-voltage direct-current (HVDC) are discussed here with their validity to insulating materials highlighted. There are several reasons behind choosing DC ageing models rather than AC. In regards to DC, it allows the transmission of huge amount of electric power (five times more electricity on conventional HV lines) from remote places to where it is needed in the most efficient manner, and transmission losses are typically lower than with AC systems at the same voltage and power. In addition to that, engineers are working on developing DC transmission cables as the DC sources can be classified as clean energy sources. Consequently, the chance of ageing models focused on HVDC applications reflects these industry shift to DC.

Due to the demand of transferring large amount of current from power-plant stations to distribution points, underground cables should be able to carry the required currents with less effects of temperature. Unfortunately, increments in temperature adversely affect the useful working life of underground cables and may irreversibly damage the insulating materials. The correlation between loading power and temperature in underground cables is limited to the maximum allowable operating temperature. Thus, the temperature of the conductors should be confined to provide longer life and protection to the insulation.

Electric stress is another major factor that plays a significant role in the ageing process. During the application of an electric field, electrons inject into the insulations and ions causing space charge. The term of space charge is used to describe the accumulation of the injected charges from the cathode into an insulating material. These charges affect the distribution of the electric field in the insulation when a DC voltage is applied across it. Consequently, the resulting mechanical stress in areas that have high fields will have greater influence [14, 15] in accelerating the degradation process. At voids with a high concentration of space charge, the local field strength increases and may exceed the breakdown strength of the insulation. This leads to an increased degradation rate of the insulation due to the increment in the electromechanical stress. As a result of the degradation process, modifications occur on the chemical-physical bonds between the

atoms of the insulating materials. Ultimately, bond properties are lost due to weakness or brokenness and thus leads to dielectric failure.

Significance of studying the endurance of insulation properties subjected to DC fields raises as the interest of choosing polymeric materials as insulation for transmission cables increases as well. Accordingly, a brief discussion of the single DC ageing models has been reviewed, while the most focus is a placed on multi-factor DC ageing models on polymeric insulating materials.

2.2 Single Factor Ageing Models

The appropriate classification of ageing models is single factor models and multi-factors models as shown in Figure 2.1. Ageing models of single factors such as thermal effects, environmental effects, electrical stresses and mechanical stresses have been singly applied for many years. An example of a thermal model is known as the Arrhenius model, the inverse power and exponential models for electrical and mechanical stresses have been widely used for insulation materials[16, 17, 18]. The mentioned models are applicable for constant stress amplitude and the resulting life expectancy lines are straight lines in appropriate coordinate systems. Majority of the studies on ageing were found to focus on thermal and electrical effects. Therefore, this chapter will focus only on these two factors.

2.2.1 Thermal Models

Thermal ageing is associated with the rate process of degradation that is thermally activated. Some of thermal ageing examples are rupture of chains, breaking of bonds and oxidation. At the occurrence breakdown, the insulation features become unable to operate the system satisfactorily. Therefore, the necessity of expecting the lifetime of insulation before failing electric systems becomes more important to avoid these system stop working during the repair time.

The initial studies, with regards aging, were mainly focused on thermal endurance by developing thermal aging models which, at that time, were well assessed for thermal stress. In 1930s, Montsinger[19] began to study the behaviour of insulating materials at high temperatures in order to discover a relation between the applied temperature and the failure time. The relation that Monstinger found is an exponential model. Based on this empirical relationship, several researchers, thereafter, attempted to infer an ageing mechanism due to temperature. Consequently, Dakin proposed an interesting approach which shows a similarity to the well-known Arrhenius equation. The thermal ageing

rate was then given by:

$$R = A \exp\left[-\frac{B}{kT}\right] \tag{2.1}$$

where A is an empirical factor, B is the so-called activation energy, k is the Boltzmann constant and T is the absolute temperature. Since the lifetime is inversely proportional to the ageing rate, the life model can be written as:

$$L = K_t \exp\left[\frac{B}{kT}\right] \tag{2.2}$$

where$L$ is the thermal life and $K_t = 1/A$. The Arrhenius constant, K_t, is the life for $T = \infty$. Due to the lack in the physical sense of the constant A and the difficulty in predicting it and because plots of $\log t$ vs. $1/T$ do not often yield straight lines, Eyring[20] developed an alternative to the Arrhenius equation. The rate theory says, in its simplest form, that the required time to cross an activation energy barrier of $\Delta G\#$ height is

$$L = \frac{h}{kT} \exp\left[\frac{\Delta G\#}{T}\right] \tag{2.3}$$

Eyring equation is verified when the results are plotted on $\ln(L * T)$ versus $1/T$ graph and yield straight slope ($\Delta G\#/T$). A generally accepted development of Eyring to cover the case of multi-factor ageing and give fit result is shown in the second section (2.3).

2.2.2 Electrical Models

Certainly, electrical ageing claims the main attention when insulation materials are concerned. However, research about the nature of electrical ageing has not yielded full the knowledge of this factor. For example, partial discharges are believed to be an important feature of electrical ageing but are not fully understood. Moreover, charge injection at sites of strong field enhancements plays an important role in ageing and the way these charges affect the material properties is still not clear [21]. Due to the limited knowledge of electrical ageing, it was necessary to develop electrical ageing models. These models fit reasonably well to the experimental results.

Two simple voltage endurance models have quite a small number of parameters which can be estimated experimentally. They are the inverse power law and the exponential law as represented in Eqs. 2.4 or 2.5 respectively.

$$L = \frac{C_1}{E^n} \tag{2.4}$$

$$L = C_2 \exp[-bE] \tag{2.5}$$

where E is the magnitude of the electric field. C_1 and C_2 are constants which, in most cases, depend on the material. n and b are called the voltage endurance coefficient

(VEC). The larger value of VEC leads to better insulation endurance, therefore, the VEC is a fundamental parameter for insulation characterization. Although both models can be used for constant stress test, the inverse power law is the preferred and widely used model as it is in agreement with Weibull statistics where designing of extruded cables is often carried out on a statistical basis[22, 23]. As these simple models do not provide any details about the ageing mechanisms, sufficiently describing or modelling the lifetime of insulations become more difficult as the key affected factors are unknown. Thus, further studies were carried out to develop a more comprehensive electro-thermal ageing model simultaneously.

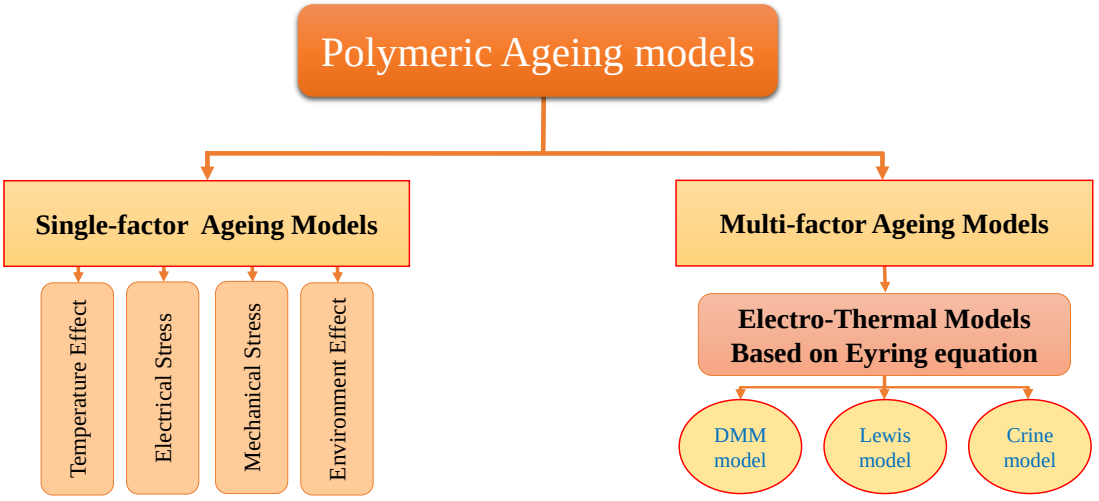

FIGURE 2.1: General diagram of polymeric ageing models based on IEC Publication 505 [12], with adding most popular multi-factor (electro-thermal) ageing models that developed by reducing the electrical-mechanical term from the activation energy in Eyring model.

2.3 Multi-Factor Ageing Models

Subjecting an insulating system to multiple ageing factors may lead interactions to be involved in the ageing process itself. Two types of interaction can affect the ageing[12]. The first type is called direct interaction which results from factors that act simultaneously, while the other type is known as an indirect interaction in which the interaction essentially remains the same whether the ageing factors are applied either sequentially or simultaneously. A well-known example of the direct interaction is oxidation - both oxygen and elevated temperature is required to give synergy effect at the same time [24]. For the case of indirect interaction, the result of mechanical or electrical stress can

be given as an example. Mechanical stress can create micro-voids that may give rise to partial discharge activity. The ageing process proceeds at a faster rate at interaction compared to the sum of the corresponding single stress rates.

Several mechanisms have been inferred for the electro-thermal ageing process that apply for insulating materials. These models are aimed to derive usable life expressions, and have followed two prevailing directions without and with physical meaning. Models without an explicit physical meaning such as Simoni's model[25], Ramu's model[26] and Fallou's model[27] are not covered in this thesis. However, electro-thermal ageing models based on the modifications of the Eyring thermal model (Eq.2.3) have a physical meaning, and are discussed and compared with each other. Crine, Dissado-Massanti-Montanari (DMM) and Lewis models[28, 14, 29] are well-know models for the later direction, and all fitted to the empirical results. The extra parameter, that was added to the Eyring model, is related to the applied electric field. Just recall Eq.2.3, the Eyring model can be rewritten as:

$$L = \frac{h}{kT} \exp\left[\frac{\Delta G\# - W_{em}}{T}\right] \tag{2.6}$$

where W_{em} is the induced energy from electrostatic field. The ageing process is assumed to be thermally activated, and accelerated by the presence of electric field in the form of term W_{em}. Different explanations of W_{em} have been made in these models. Crine [11] specified this term as the electrostatic energy of a charge particle that is released to the polymer and the particle displaces in the direction of electric field. Another explanation offered by Lewis was that the electro-mechanical energy stored in a form of a sub-microscopic crack will exist in a practical solid dielectric and the energy associated with this stress will most likely be sufficient to extend the crack[29]. DMM model has suggested that the stored electromechanical energy around a trapped space charge centre may cause local deformations which eventually coalesce into nanometre size voids and subsequently to micrometer size voids [14].

2.3.1 Dissado, Mazzanti and Montanari (DMM) Model

Basically, the concept of ageing process in DMM model is not attributed to a specific physical mechanism[30, 14, 31]. Therefore, it could be used for explaining several ageing processes as long as they use chemical reaction rate as an ageing process, reversible process, and could include bond breaking or untangle polymer chain[32].

DMM model is similarly explained by the methods describing the rest of the electro-thermal models. Initially, the model was applied to the case of thermal activation, and then was developed to the case of an existing electric field.

- **Physical Concept of the Model**

At the beginning, DMM assumed that the polymer is in a non-equilibrium state, and all of the moieties are in the unaged state with free energy G_1. Moieties will be able to move forward and backward between unaged and aged states, when the moieties has sufficient energy, to be part in the reaction. As time goes on, the state of polymer moves towards an equilibrium. This means that equilibrium can be reach when a fraction of moieties moved to the aged state. At an irreversible movement of a fraction of moieties in any local area, ageing can start. This critical fraction is denoted as A^*. For breakdown to begin, a polymer just needs to exceed the critical fraction in any local part of the polymer (not the whole polymer). Afterwards, the lifetime is likely to be very short. Indeed, several factors can have a significant effect on the fraction of moieties such as temperature and barrier height.

- **Model in Case of Thermal Activation**

Polymer is assumed in DMM model to be produced of many moieties (or group of atoms). These moieties move from a free energy configuration to another due to the effect of temperature. The movement of moieties between the energy configurations (which will be described later) is asumed to be reversible as long as product and reactant states are not separated[30]. Figure2.2 shows the forward and backward movement of moieties.

Based on Gibbs free energy concept, G_1 and G_2 are known as the free energy of unaged state and aged state respectively. The peak energy between these energies is a transition state in which the moiety state changes from product to reactant and vice versa. The activation energy barrier $\Delta G\#$ is defined as the difference between G_a and the mean of G_1 and G_2, and consists of an enthalpy part as well as an entropy part. As the structure of polymers are mostly inhomogeneous, the value of the activation energy is likely to be different for each moiety. Thus, $\Delta G\#$ will have a different value from one moiety to another. For purpose of simplification, single value parameters are used in Cirne, DMM and Lewis models, and the extracted values are well-fit to the experimental results [30, 33, 34].

To explain the mathematical equation of the model, its basis starts from the forward and backward reaction for the moieties. They can be represented as:

$$\frac{dc_1}{dt} = -K_f c_1 + K_b c_2 \tag{2.7}$$

$$\frac{dc_2}{dt} = -K_b c_2 + K_f c_1 \tag{2.8}$$

where c_1 and c_2 are the concentration of unaged and aged moieties at a given time, respectively. The reaction rate constants are based on the Eyring concept and given as:

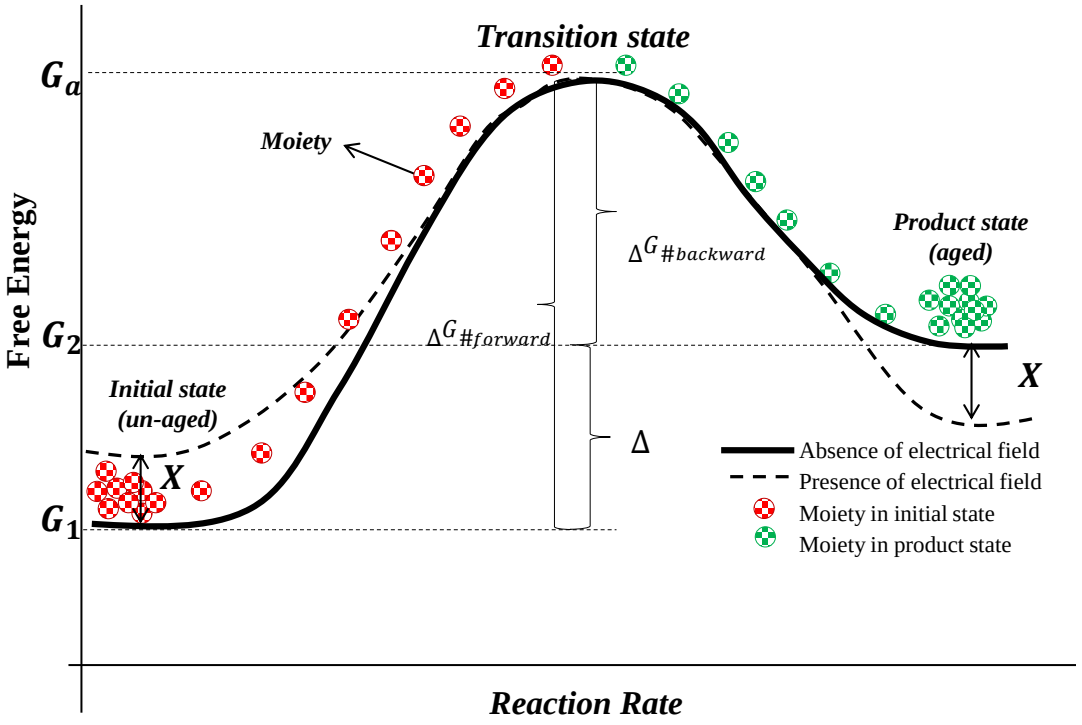

FIGURE 2.2: Schematic diagram of Gibbs free energy, (solid line) represents in the absence of electric field whereas (dotted line) represents in the presence of electric field.

$$K_f = \left[\frac{kT}{h}\right] \exp\left[-\frac{G_a - G_1}{kT}\right] \tag{2.9}$$

$$K_b = \left[\frac{kT}{h}\right] \exp\left[-\frac{G_a - G_2}{kT}\right] \tag{2.10}$$

where k is Boltzmann's constant, h is Planck's constant and T is the absolute temperature.

By assuming $X = \frac{c_2}{N}$ where N is the total concentration of the reacting moieties, and subtracting $\frac{dc_1}{dt}$ from $\frac{dc_2}{dt}$, and then substituting X and N for c_1 and c_2, leading to:

$$\frac{dX}{dt} = K_f - (K_f + K_b)X \tag{2.11}$$

Initially, the moieties are assumed to be in unaged state, so $c_2 = 0$ and therefore, $X = 0$. At the end life of the polymer, concentration of the aged state reaches the critical value is c_2^*, and therefore $X = c_2^*/N$.

By integrating equation 2.11 from $X = 0$ to $X = A^* = c_2^*/N$, it gives the thermal life time as :

$$L(T) = \frac{1}{K_b + K_f} \times \left(- \ln \frac{A_{eq} - A^*}{A^*} \right) \tag{2.12}$$

where the thermal equilibrium value is given by:

$$A_{eq} = \frac{K_f}{K_f + K_b} \tag{2.13}$$

The thermal life-time can be calculated if the equilibrium is greater than or equal to the critical value A^*, otherwise $L(T)$ goes to infinite.

- **Model in case of electro-thermal activation**

In the presence of an electric field, DMM assumed that space charge trapping within the polymer modifies the ageing process describe above. Experimentally, space charge either on both anode and cathode interfaces or injected into the bulk has been observed. It has been reported that charge is most likely to be trapped at defect regions, and in between crystalline and amorphous interface as well as at sites of chemical inclusions and impurities [30, 35, 36, 37]

At positions in the polymer in which space charge is trapped, the distribution of local electric field will be modified. Consequently, electrostatic and electromechanical forces, which depend on the electric field, will reach maximum values at the boundaries of space charge regions[30, 14]. The electrostatic force is presented from space charge, and affect all of the energy levels (aged and unaged states), therefore there is no effect to $G\#$, rate constants or lifetime of polymer. As space charge will not be removed or neutralised during ageing process, the electrostatic force will remain constant.

With regards to electromechanical force, it causes a mechanical strain that is assumed to affect the unaged state (only G_1). This strain will be released when a moiety moves to an aged state. At enough fraction of moieties that have moved to an aged state, the released electromechanical strains lead to a crack or tree formation [30]. The amount of free energy that will be added, G_1, is related to the amount of trapped charges. The amount of charges is not governed by a well developed relationship, but by assuming that the model is a function of the magnitude of the applied field. The modification of free energy in unaged state is written as:

$$G_1(E) = G_1 + C \times E^{4b} \tag{2.14}$$

where C is a function of material parameters such as (electrostriction coefficient, Young's modulus, permittivity and radius of space charge centre), b is the power constant related to the material from this relation ($q \propto E^b$).

The eletro-thermal life-time of Equation 2.12, after applying the effect of electric field on the forward rate constant becomes as:

$$L(T,E) = \frac{h}{2kT}\exp(\frac{\Delta G\# - CE^{4b}/2}{kT}) \times \ln\frac{(\frac{A_{eq}}{A_{eq}-A^*})}{\cosh(\frac{\Delta - CE^{4b}}{2kT})} \tag{2.15}$$

where $\Delta G\#$ (Activation free-energy) = H# (Enthalpy) - T (Temperature) $\times$ S# (Entropy). Δ is the required energy to create a single local elemental modification in the ageing process (see Figure 2.2). The field-dependent equilibrium A_{eq} is:

$$A_{eq} = \frac{1}{1+\exp(\frac{\Delta - CE^{4b}}{kT})} \tag{2.16}$$

2.3.2 Lewis Model

The ageing model of Lewis is close to the DMM model dealing with moieties that move forward and backward during the ageing reaction. However, Lewis model differs from DMM in the physical process it describes namely the way the chemical bonds linking the moiety to the rest of the polymer chains alter with time[38, 29]. Simply, the unaged state in DMM model corresponds to an unbroken bond, and the aged state in DMM corresponds to a broken or weakened bond between molecules.

- **Physical Concept of the Model**

The polymeric ageing process in Lewis model is similar to DMM model as it assumes a reversible process. It is thermally activated in the absence of applied field, and the acceleration of ageing process is increased when the electric field is applied.

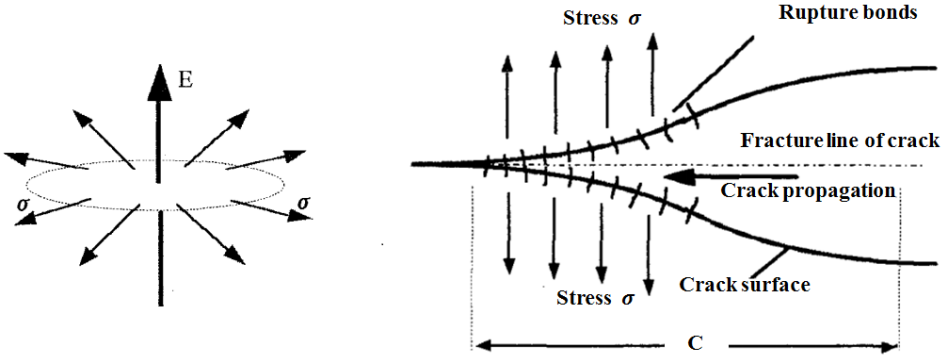

FIGURE 2.3: Schematic diagram of electric field and mechanical stress on dielectric materials. (a) Electric field orthogonal to dielectric materials (b) Griffith half-crack in the material with length c[33].

The insulation is subjected to a mechanical stress, εE^2, at the application of electric field. This stress tends to expand the insulation against the cohesive force in perpendicular direction to the electric field lines. Figure2.3 shows the effect of electric field to the insulation. Further details are given in the next section when the electric field is applied.

- **Model in Case of Thermal Activation**

The mathematical details are nearly similar to those in DMM model which was described in the previous section. From the rate equation, the forward (at which bonds are broken or weakened) and backward (at which bonds can be repaired) reaction rate constants are:

$$K_B = \left(\frac{kT}{h}\right) \exp\left(-\frac{U_B}{kT}\right) \tag{2.17}$$

$$K_R = \left(\frac{kT}{h}\right) \exp\left(-\frac{U_R}{kT}\right) \tag{2.18}$$

where U_B is the required energy to break or weak a bond and it is similar to $G_a - G_1$ in the DMM model, U_R is the required energy to repair a bond which is equivalent to $G_a - G_2$ as well. This is shown in Figure 2.4.

Following the derivation of DMM model, N represents all of the bonds that take part in the ageing process. In Lewis model, C_1 represents the concentration of unbroken bonds and C_2 the concentration of broken or weak bonds. $X = C_2/N$ represents the fraction of broken bonds, and it's expression for the change in the fraction of broken bonds with time is:

$$\frac{dX}{dt} = K_f - (K_f + K_b)X \tag{2.19}$$

- **Model in Case of Electro-Thermal Activation**

The assumed mechanism to accelerate the ageing process in Lewis model is different from DMM model in the presence of an electric field. A generalised form of the Lippmann electro-chemical equation is applied in Lewis model[33, 39, 40]. The Lippmann electro-chemical equation states that the change in inter-facial tension is generated by a change in potential difference across an interface, it is given as:

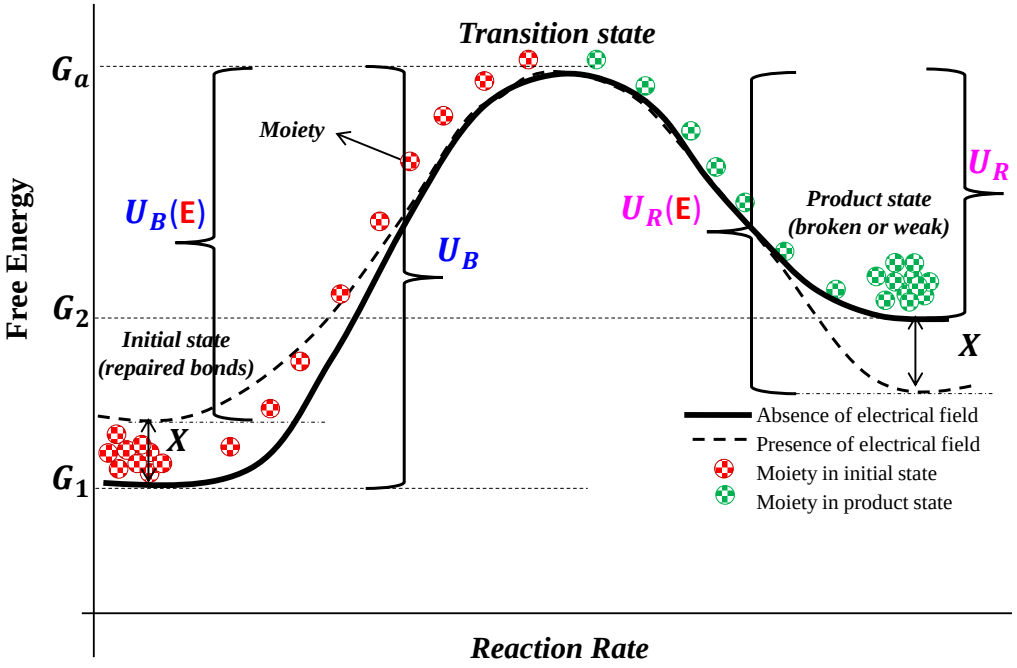

FIGURE 2.4: Schematic diagram of Gibbs free energy, (solid line) represents in the absence of electric field whereas (dotted line) represents in the presence of electric field.

$$\nabla\gamma = -q\nabla V \tag{2.20}$$

where q is the charge separation across the interface, and ∇V is the free volume.

Once the electric field is applied, an expanding action of the mechanical stress is assumed to reduce the required energy for breaking bonds. In contrast, the energy needed to repair bonds is increased. The ageing process will be accelerated by reducing U_B and increasing U_R . The assumed amount by which these energies are changed is proportional to the mechanical force. The field dependent energy barriers for the forward and backward can be written as:

$$U_B(E) = U_B - \gamma_B \varepsilon E^2 \tag{2.21}$$

$$U_R(E) = U_R + \gamma_R \varepsilon E^2 \tag{2.22}$$

where γ_B and γ_R represent the effective volume change for the forward reaction (i.e. strain) and for the backward reaction (i.e. relaxation), respectively, ε is the permittivity and E is the electric field. This leads to field modified rate equations such that:

$$K_B = \left(\frac{kT}{h}\right) \exp\left(-\frac{U_B - \gamma_B \varepsilon E^2}{kT}\right) \tag{2.23}$$

$$K_R = \left(\frac{kT}{h}\right) \exp\left(-\frac{U_R + \gamma_R \varepsilon E^2}{kT}\right) \tag{2.24}$$

Equivalent integration in Lewis model is made for the reacting rates as was in DMM model, from $X = 0$ to $X = b$ (note: $b = K_B/(K_R + K_B)$). It gives an equation for the lifetime:

$$L(E,T) = \frac{1}{K_B + K_R} \times \left[-\ln\left(\frac{b_{eq} - b^*}{b^*}\right)\right] \tag{2.25}$$

where b_{eq} is the equilibrium fraction of broken bonds that is equivalent to A_{eq} in the DMM model.

2.3.3 Crine Model

In the same way as previous models, Crine designed an ageing model based on the Eyring equation with different physical concept of the electric field effect to the thermal energy barrier. Crine used a preliminary linear relationship between the energy of barrier deformation and the applied field[34]. Later on, this energy is represented in general form by proportioning the energy to the square of the electric field[41]. Further details are described in the coming section.

- **Physical Concept of the Model**

Crine model is based on the assumption that high electric field can deform mechanically polymer chains by fatigue process. This process leads to submicrocavity formation. When the electric field is applied, molecular chains are deformed over a distance λ, and the activation free-energy is reduced by an amount equal to the work of deformation applied on the barrier $W = e\lambda E$ as shown in Figure 2.5. This definition is shared with Lewis in which a moiety moves from unbroken state to broken state.

Subsequently, Crine generalised the definition of the work of deformation by using the Maxwell stress induced by the electric field in the activation volume, i.e. the strained volume. The general form of the deformation energy can be applied to AC and DC fields as long as ageing is associated with the formation of cavities. These cavities are generated when the energy supplied by the field was larger than the energy of cohesion of the polymer.

- **Model in Case of Thermal Activation**

The energy barrier in Crine model is assumed to be symmetrical (or nearly symmetrical)

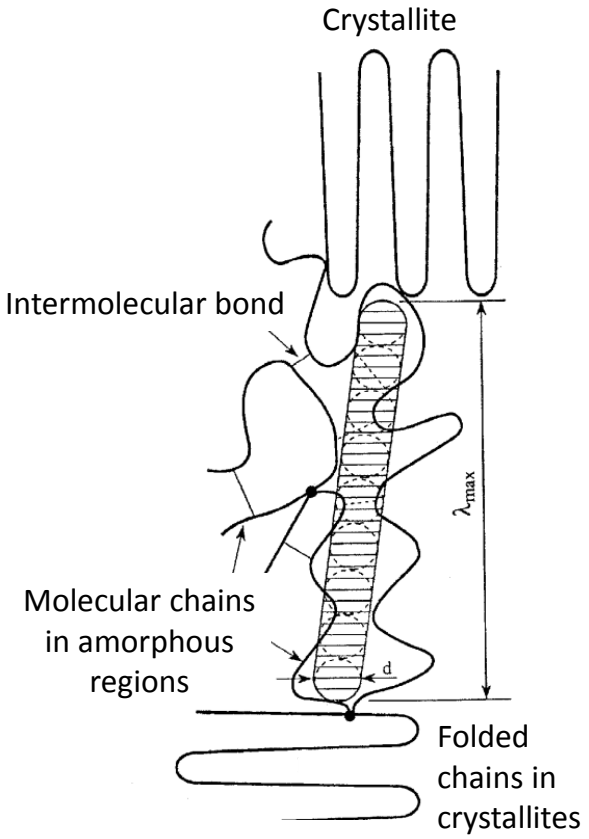

FIGURE 2.5: First schematic representation of the physical concept of Crine model[34]

as shown in Figure 2.6. This assumption is in contrast to what is stated in DMM and Lewis. The final (i.e. aged) state in Crine model should have less energy compared to the initial (unaged) state. Intuitively, the energy for aged and unaged states in Lewis and DMM models seem to be unrealistic as it shows that the aged state could have a higher energy than the unaged state. This means that the required activation energy to get moieties back to the unaged state would be smaller than the one required for moving them to aged state[42]. Unfortunately, this assumption would never be valid for any ageing!

The mathematical equations of the forward and backward thermodynamic rates are similar to the previous models

$$K_F = \left(\frac{kT}{h}\right) \exp\left(-\frac{U_F}{kT}\right) \tag{2.26}$$

$$K_B = \left(\frac{kT}{h}\right) \exp\left(-\frac{U_B}{kT}\right) \tag{2.27}$$

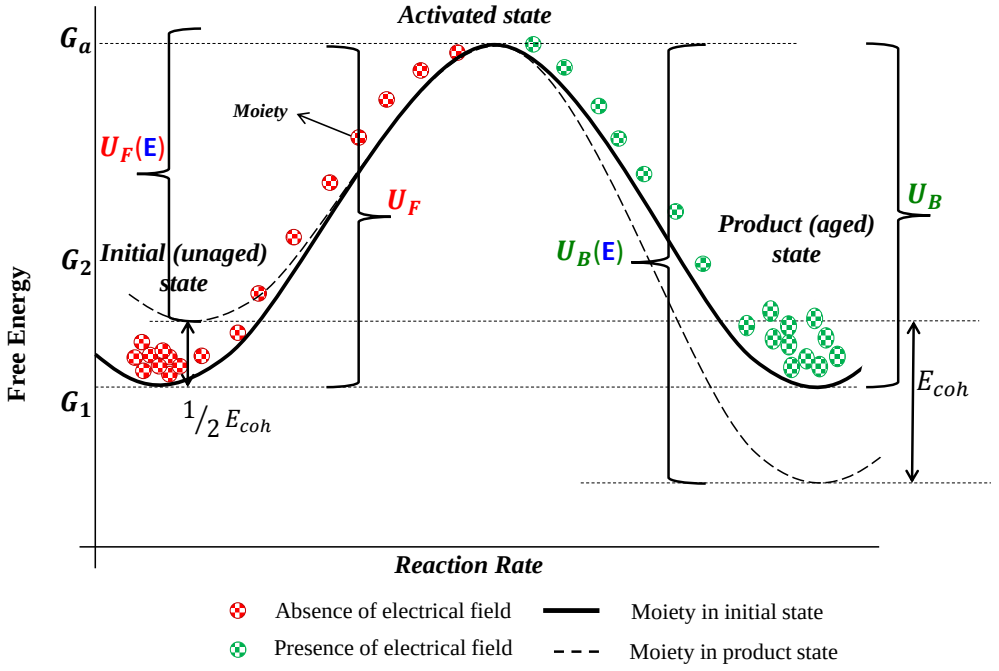

FIGURE 2.6: Schematic diagram of a free energy barrier in the absence of electric field(bold line), and in the presence of electric field(dot line) for Crine model.

where U_F is the required energy to move moieties to aged state. It is the energy difference between the unaged state energy level and the transition energy. U_B is the opposite required energy to moving moieties from aged state to unaged state. This energy is equal to the difference between the transition energy and the aged state energy.

The same case in Crine model with regards X, it represents the concentration of aged moieties to the total concentration of unaged and aged moieties. The thermodynamic expression of X is given as:

$$\frac{dX}{dt} = K_F - (K_F + K_B)X \tag{2.28}$$

- **Model in Case of Electro-Thermal Activation**

The basis of Cirne model, which is based on the rate theory, assumes that electrical aging is a thermally activated process. Thus, for moieties to go from the original (unaged) state to the final (aged) state require a jump in energy over an activated energy barrier

$\Delta G\#$. When the electric field is applied, the local mechanical stress varies with the square of the applied field (Maxwell stress). The energy barrier is then deformed by the amount of energy $0.5\ \varepsilon\ \Delta V E^2$. The field dependent energy barriers for the forward and backward can be written as:

$$U_F(E) = U_F - 0.5\ \varepsilon\ \Delta V E^2 \tag{2.29}$$

$$U_B(E) = U_B + 0.5\ \varepsilon\ \Delta V E^2 \tag{2.30}$$

where ε is the permittivity, ΔV is the activation volume and E is the electric field. According to Crine, a crack is generated when the deformation energy exceeds the cohesive energy. When the cohesive energy E_{coh} equals to σ_G the stress required to generate a crack times ΔV, cracks are then formed for

$$E_{coh} = \sigma_G\ \Delta V = (\gamma Y/628L)^{0.5}\Delta V \tag{2.31}$$

where γ is the surface tension, Y is the Young modulus and L is the length of the crack.

The rate equations in the presence of electric field become as:

$$K_F = \left(\frac{kT}{h}\right)\exp\left(-\frac{U_F - 0.5\ \varepsilon\ \Delta V E^2}{kT}\right) \tag{2.32}$$

$$K_B = \left(\frac{kT}{h}\right)\exp\left(-\frac{U_B + 0.5\ \varepsilon\ \Delta V E^2}{kT}\right) \tag{2.33}$$

When the final state is reached, i.e. when the energy barrier has been overcome, chemical bonds that are in the breakdown path of the insulation have been broken. This will generate some free space or submicrocavities, after a critical fraction of moieties that have been moved to the final (aged) state.

By integrating Equation 2.28 from $X = 0$ to $X = s$ while s is a fraction of the aged moieties concentration to the total concentration, the time to reach the state of bond disruption can be written as:

$$L(E,T) = \frac{1}{K_B + K_R} \times \left[-\ln\left(\frac{s_{eq} - s^*}{s^*}\right)\right] \tag{2.34}$$

or in another form after the substitutions

$$L(E,T) = \frac{h}{2kT}\exp\left[-\left(\frac{\Delta G - 0.5\ \varepsilon\ \Delta V E^2}{kT}\right)\right] \tag{2.35}$$

2.4 Comparison of the Electro-Thermal Ageing Models

2.4.1 Threshold Conditions

All of the electro-thermal ageing models have a threshold condition in which the electro-thermal ageing process has an effect on the lifetime of the insulation. It is noted that DMM model equilibrium parameter A_{eq} must exceed A^*, similarly b_{eq} and s_{eq} in Lewis and Crine models must exceed b^* and s^*, respectively.

In the DMM model, the threshold or critical field takes the form of a critical fraction of moieties in the aged state that needs to be exceeded for ageing to occur. As the two states of moieties during the reaction do not assign for a specific physical meaning, difference processes can be applied to the change in free energy. It is derived from the ageing model which gives [14]:

$$E_c = \left\{ \frac{\Delta - T \ln \left[(1 - A^*)/A^* \right]}{C} \right\} \tag{2.36}$$

According to Lewis, a critical fraction of the bonds in the insulating material had to be broken[33, 29]. Supported experimental results in [43] show that polyethylene C-C bonds are indeed ruptured during the electro-thermal ageing. The critical field is based on the Griffith criterion concept [44], and it is given in the propagating direction of the crack as:

$$E_c = \left(\frac{2\zeta Y}{k\varepsilon^2 c} \right)^{0.25} \tag{2.37}$$

where ζ is the fracture energy required to create unit area of new crack surface by breaking bonds, c is the half-length of the crack, k is a constant.

With regards to the critical condition in Crine model, when the electric field is less than the critical field there is no submicrocavities generated in the insulation, and then the lifetime should be extremely long. However, lifetime will be very short when the deformation energy, ($W_{coh} = 0.5\varepsilon {E_c}^2$), is larger than the cohesive energy E_{coh}. Therefore, the induced stress is bigger than the cohesive energy between the bonds. It is given in [45, 46] as:

$$E_c = \left(\frac{2 * W_{coh}}{\Delta V} \right)^{0.5} \tag{2.38}$$

2.4.2 Effect of Electric Field

The major difference between the electro-thermal ageing models is in their way of explaining the effect of the applied field to the activation energy of the ageing process, and the physical mechanism by which this is assumed to occur in the insulation. All of the model, as mentioned previously, have a critical or 'threshold' field and no ageing could occur below this field.

In DMM model, energy of a moiety in initial state G_1 raises by an amount of energy equal to CE^{4b}, where C and b are factors relate to the insulation. The transition from product state to initial state is unaffected. In reality, this term links the electric field to the trapped space charge in the bulk of the insulation. The applied electric field is able to make the transition between initial and product states.

With regards to Lewis model, the applied field increases the energy of initial state, G_1 by $\gamma_B \varepsilon E^2$. So, the transition from state G_1 to G_2 becomes more likely as $G_a - G_1$ is reduced. On the other hand, the application of electric field lowers the product state G_2 by $\gamma_R \varepsilon E^2$, and the transition becomes less likely on application of electric field since $G_a - G_2$ is increased.

In Crine model, $(0.5\ \varepsilon\ \Delta V E^2)$ the amount of energy that depends on the square of the applied field will be able to increase the moieties energy in state one to cross over the barrier to the aged state (creating submicrocavities). However, the same amount of energy makes the transition from aged state to unaged state much difficult as the aged level decreases.

The physical mechanisms by which the ageing process is assumed to change, when the electric field is applied, are different from one model to the other. An assumption of a relationship between the applied field and the trapped space charge is made in the DMM model. The trapped space charge accelerates the ageing process through the electromechanical forces generated by the accumulation of charges. Whereas the Lewis model assumes that the applied field causes a macroscopic electromechanical stress that accelerates ageing process. Crine states that the electromechanical stress can rupture the bond and accelerate the ageing process when the electric field dependent energy is greater than the cohesive energy of the polymer. Lewis and Crine assumed that the existence of any space charge in the polymer must affect the macroscopic stress but this effect is not considered as a main effect on the model. Therefore, their models do not deal with space charge explicitly.

2.4.3 Limitations of the Electro-Thermal Ageing Models

The above electro-thermal ageing models can be used in describing the phenomenological way. They can be fitted to the experimental results to extract various parameters of the

models. These extracted parameters can be used along with lifetime models to expect other ageing conditions. This means that the ageing experiments can be carried-out on samples with high electric fields and temperatures, and the extracted parameters from these results can be applied for conditions that may take much longer time to be aged.

A general question can be asked: what is the purpose of these electro-thermal ageing models as long as they do similarly to the basic models (e.g. the inverse power law which have been used for many years to predict lifetime of insulation), with the advantage of only 2 parameters, compared with up to 6 for these models? A simple answer is that the electro-thermal ageing models in addition to predicting lifetime they can yield fundamental information about the ageing process such as the magnitude of the barrier in aged and unaged states. The additional insight is that the electro-thermal ageing models are often seen to fit ageing data better than basic ageing models (e.g. inverse power model) such as the threshold field which can be clear in the electro-thermal ageing models.

The ageing models parameters cannot be freely used for all sets of experimental data, as there are several factors that control the parameters. For example, DMM model parameters depend on space charge which is influenced by electric field, material type, the geometry and spatial dimensions of aged samples. The same issues can be distinguished for enthalpy and entropy magnitudes, submicrocavities dimensions for Lewis and Crine models.

2.5 Summary

As the major two affects to the ageing phenomenon are temperature and electric field, single factor ageing models is no longer used for investigating the life of the cables. Therefore, multi-factors ageing models are currently applied to develop the endurance of the polymeric insulation by understanding the causes of breakdown. In a simple way, Figure 2.7 describes the summary and the comparison of the famous multi-factor ageing models.

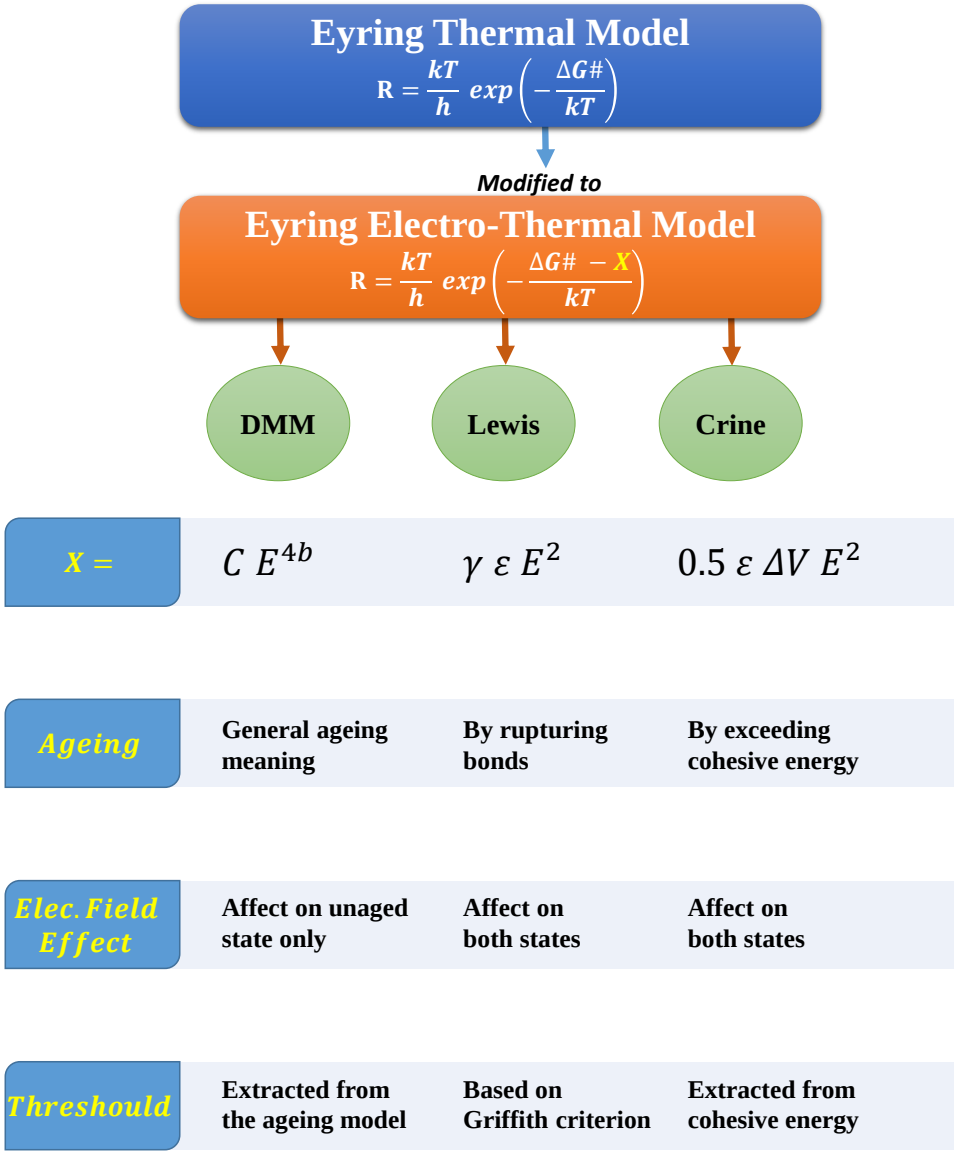

FIGURE 2.7: Summary of the electro-thermal ageing models.

Chapter 3

Developing Ageing Model

3.1 Introduction

In contrast to an ideal crystal, polymeric material in general does not retain indefinitely the nature that it possesses on first being manufactured. Over a period of time, both its physical morphology [47] and chemical composition [48] may change. In consequence, several of its properties may change, for instance its dielectric loss and conductivity may increase and its electrical and mechanical strength reduce. The material is said to age [9] and eventually it may not be able to perform its insulating function to the required standard. In this case, its service life is ended even though a catastrophic electrical breakdown may not have occurred. Ageing may therefore produce a limit to the effective service life of polymeric insulation even in the absence of an applied electric field.

With regards to electrical charge, they are present every where in insulating materials which are produced during material manufacturing, machining such as extrusion of polymers [49, 50], and their product usage (e.g.,cables, capacitors, etc.)[51, 52, 53, 54]. With the omnipresence of charges in the environment, it is of increasing importance to understand their real influence on the materials properties, on their ageing, and on our everyday life. Charging an insulator has been considered as a simple feature that is the consequence of which is the resultant internal electrostatic field produced. Then, technological solutions to treat any deleterious effects of the electric field consist of adapting the geometry of the high-voltage system such as insulator or capacitor [55].

As discussed widely in Chapter (2) about the influence of internal field, the recognition that the establishment of an electric charge distribution in dielectrics can have a profound influence on the degradation/ageing of the insulating materials. Therefore, some attempts of interpretations have emerged based on the applied field consideration. For

instance, the interpretation by Dissado et al.[30] for the effect of the internal electromechanical stress, that is produced by a charge distribution, into the developed life model for insulating materials.

Charge distributions in insulators are well known to affect and distort local fields around defects, interfaces, and localized changes in material properties. These effects are particularly well observed in the case of constant stress dc fields, as time then permits build-up of charge that is either injected at electrode-insulator interfaces, or possibly is a result of micro-discharges in voids (i.e., partial discharge (PD)). The development and utilization of several practical and non-destructive techniques of charge measurements have allowed quantitative analysis of charge distribution via measurement of an induced current that is directly proportional to the charge distribution profile [56]. This leads to further insight into the operating mechanisms by which charge distribution affects the pre-breakdown processes and take the insulation to failure state.

It is worth to mention that all partial discharges observed "in insulations or capacitors"are the ultimate feature of a process initiated by a few original charge carriers existing in insulations. The developed model in this thesis concentrates particularly on the study of charge distribution as the trigger for such discharges; more thorough charges at localized areas can result in macroscopically observed ageing/breakdown of the insulating material when these charges are released disruptively under specific conditions. Such a fundamental understanding supports design at the engineering stage to achieve the necessary life cycle reliability in practical insulation systems.

For several decades, failure of insulating materials was associated with 'macroscopic' reasons rather than to micro-structure. However, recent works are looking more carefully to the contribution of space charges to insulation damage [57, 58] which have acquired more interest. This is due to extra-clean and dry-cured materials that are now being used in insulation systems, especially for high-voltage cables, and the reduction of imperfection's level, which may be able to initiate degradation processes, is approaching the microscopic or submicroscopic scale.

3.2 Physical Basis of the Developed Ageing Model

The fundamental aim of the model is to describe quantitatively the effect of space charge on localized regions in a polymeric insulation upon the ageing mechanisms that limit the lifetime. In order to describe the ageing processes in a simple and general formalism, it has been assumed that the traps are uniformly distributed across the sample which can capture the injected electrons. These trapped charges are resulted from a competition between trapping and detrapping rates of $J(E,T,t)$ with a detrapping rate, where $J(E,T,t)$ is the current density at applied field (E), temperature (T) and a specific time (t).

The referred ageing models in the literature by Dissado, Crine and Lewis[30, 28, 29] have adopted Dakin's concept [16] of the polymeric material as a set of chemical and morphological moieties undergoing a local reaction. Dakin illustrated these local processes as reactions along a reaction coordinate $(x-axis)$ in which an energy barrier $(y-axis)$ has to be overcome. A further assumption made as only the forward reaction could occur. This means that once the products are obtained, they cannot reform the reactant state. In reality, this assumption is only valid if one or more of the products is separated either in space or phase from the other. However, reactions in solid materials that do not yield gaseous products cannot be expected to obey Dakins assumption. Thermodynamics, as Eyring considered [59], then forces to include the reverse reaction (i.e. product→reactant) together with the forward reaction (reactant→product).

In the same manner, the developed ageing model deals with trapping and detrapping process which can be equivalent to the two states in Dakin's model (reactant and product states). As represented in the other models that every single moiety undergoing a local reaction requires an energy to overcome from reactant state to product state, a similar situation exists here when a trapped electron needs necessarily an energy to overcome a trap depth energy. The life of a polymeric material is regarded as ended by a correlation with the presence of a critical amount of trapped charge that can release an energy causing molecular rupture damage and even fracturing in the bulk of the insulation or at the electrode-insulation interface[60, 61, 62]. Therefore, the degradation of polymeric materials such as polyethylene is largely related to the trapping of charges which the field enhancement produced by the accumulation of charges is the important feature of electric ageing, not the presence of trapped charges themselves. The consequence is that the presence of charges is not included in all ageing models, despite the fact that charge accumulation induces mechanical stress. This is precisely the ageing effect that the resulted mechanical stress has on the electrical ageing and breakdown which is discussed in this work.

3.2.1 Model in the Absence of Electric Field

In order to derive a thermodynamic expression for the trapping phenomenon in semi-crystalline polymeric materials, major parameters will be considered as they affect the trapping rate. The injected current is the first parameter which the trapping rate mainly depends on it as reported in the literature[63]. As the insulation is not entirely crystal in nature, traps in the amorphous regions partially capture the injected charge. Thus, the density of the traps is classified likewise as an affected parameter in the trapping rate. The other factor that has increased concern of charge trapping is the capture cross-section which can characterize the ability of the trap centre to capture the injected charges[64].

This model will be initially represented in the presence of temperature. Thereafter, the applied voltage across an insulation system is considered, and the model will be modified in furtherance of covering the effect of electric field . These modifications differ in the trapping and the detrapping processes. Trapping relates to the injection process from the electrode which can be classified as an external effect with regards insulation. On the other hand, detrapping is a bulk process and classified as an internal effect.

The trapping rate is considered to be similar to reaction rate in the literary models. Thus, it depends on the concentration of electronic charges which is, therefore, proportional to the injected current density. The dynamic of trapping rate can be written as:

$$\frac{dn_{T\rightarrow}}{dt} = K_T(N_T - n_T) \tag{3.1}$$

where N_T and n_T are the total traps and the trapped charges, respectively. The trapping coefficient, K_T, is given

$$K_T = \frac{J\sigma_T}{q} \tag{3.2}$$

where J is the injected current density, σ_T is the capture cross-section and q is the charge amount.

Charge carriers in solid dielectrics can be generated via charge injection from the electrodes and ionization within the material. For the purpose of simplification, the injected charge carriers from electrodes are only considered in the model. There are several injection mechanisms for injection process such as Schottky effect and tunneling[65]. To identify the appropriate mechanism in our system, it has been traced in Chapter (4) the values of currents density measured according to the electric field. It is given as:

$$J = AT^2 \exp\left(-\frac{\Phi}{kT}\right) \tag{3.3}$$

where A the Richardson's constant and Φ is the energy barrier height.

Once the electron has been captured, different mechanisms can cause its detrapping to occur[66]. These mechanisms are (1) photon assisted depopulation, which is negligible in the present study as the sample was not exposed to any light, (2) impact ionization and (3) tunneling which both take place at very high electric field, and also they are not considered in this work, (4) and thermal detrapping. Only thermal detrapping is considered in this model, and this occurs when the trapped charge carrier gains its energy for detrapping from the thermal lattice vibrations. The mathematical expression for the detrapping process can be described as:

$$\frac{dn_{T\leftarrow}}{dt} = -K_D n_T \tag{3.4}$$

where K_D is the detrapping coefficient. This coefficient was used for detrapping in the literature with good fitting results on different materials [67, 68, 69]. It is expressed as:

$$K_D = N_c v_{th} \sigma_T \exp\left[-\frac{E_T}{kT}\right] \tag{3.5}$$

where N_c is the effective density of states in the conduction band, v_{th} is the thermal velocity of the charge, E_T is the trap depth, k the Boltzmann constant and T is the absolute temperature [64, 70].

Based on the above assumption, the kinetics of trapping and detrapping process can be expressed as the sum of $(dn_{T\rightarrow}/dt)$ and $(dn_{T\leftarrow}/dt)$, it gives:

$$\frac{dn_T}{dt} = K_T(N_T - n_T) - K_D n_T \tag{3.6}$$

We can see that Equation 3.6 is a standard first order deferential equation. It can be solved if the initial condition is known. Before the injection takes place, the total quantity of trapped charges is zero $(n_T(x, 0) = 0)$. Therefore, the solution is:

$$n_T(t) = \frac{N_T K_T}{K_T + K_D}\{1 - \exp\left[-\left(K_T + K_D\right)t\right]\} \tag{3.7}$$

If we assume that the ratio of the trapped charges to the total traps can be described through a normalized variable X as:

$$X = \frac{n_t}{N_T} \tag{3.8}$$

then Equation 3.7 becomes:

$$X(t) = C\{1 - \exp\left[-\left(K_T + K_D\right)t\right]\} \tag{3.9}$$

where

$$C(T) = \frac{K_T}{K_T + K_D} = \left[1 + \frac{qN_c v_{th}}{A^* T^2} \exp\left(-\frac{E_T - \Phi}{kT}\right)\right]^{-1} \tag{3.10}$$

is the equilibrium value of X. From the definition of the variable X, all the traps are in initial state (un-trapped) at $X = 0$, and state of fully trapped charges at $X = 1$. At a fraction of trapped charges which is symbolized here as C^*, the released electromechanical energy from detrapping process is able to break the insulation bonds and terminates the lifetime. Therefore, the lifetime should never been terminated before the state of trapped charges reaches C^*. Regarding to Equation 3.10, the value of C^* is reached at a certain temperature as shown in Figure 3.1. This temperature is called threshold temperature T_{th} and given as:

$$C(T_{th}) = \left[1 + \frac{qN_c v_{th}}{A^* T_{th}^2} \exp\left(-\frac{E_T - \Phi}{kT_{th}}\right)\right]^{-1} = C^* \tag{3.11}$$

The lifetime equation can be expressed by setting $X(T)$ equals to C^* in the integrated equation, which gives:

$$t(T) = \left(K_T + K_D\right)^{-1} \ln\left[\frac{C(T)}{C(T) - C^*}\right] \tag{3.12}$$

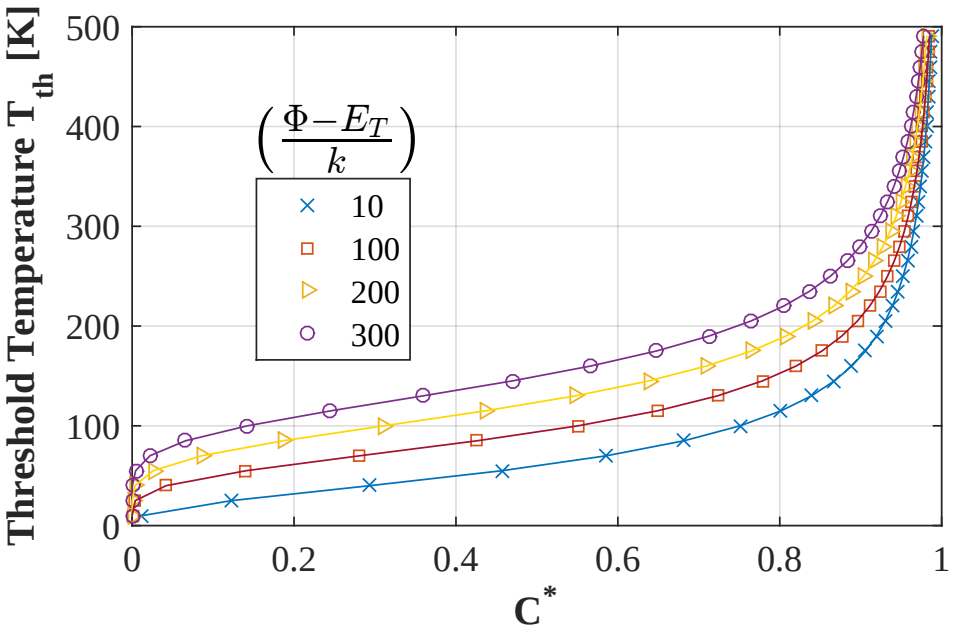

FIGURE 3.1: Plot of the relation between thermal threshold T_{th} and fraction of C^* according to Equation 3.11

3.2.2 Model in the Presence of Electric Field

In this section, the effect of electric field on trapping and detrapping process is considered. In trapping state, the minimum required energy to inject an electron into insulation (work function) is reduced as well as the energy of detrapping the captured electron. In each state (i.e., trapping and detrapping), the reduction term is based on a physical concept relate to the chosen mechanism.

According to Schottky injection in the trapping rate, the thermal work function is lowered by the effective work function ($\beta_s E^{1/2}$) in the presence of electric field as shown in Figure 3.2. Therefore, Equation 3.3 is modified to cover the effective work function as:

$$J = AT^2 \exp\left(-\frac{\Phi - \beta_s E^{1/2}}{kT}\right) \tag{3.13}$$

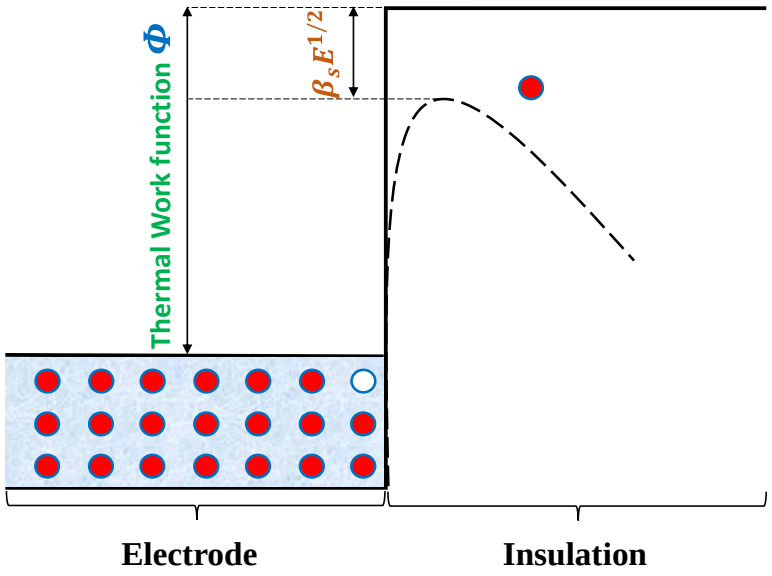

FIGURE 3.2: Mechanism of Schottky effect. The solid line represents the Coulombic barrier without electric field. The dashed line shows the effect of the applied field to the barrier, and its slope is proportional to the electric field.

Validity of the model can be examined by plotting $\ln(J)$ vs. $\sqrt{E}$. The slope of the experimental curve should lead to an estimated value of the dielectric permittivity in the term of $\beta_s = (q/4\pi\varepsilon_0\varepsilon_r)^{1/2}$. This was achieved profoundly in Chapter (4). Accordingly, the compatible injection mechanism for the trapping process in the developed ageing model is the Schottky mechanism.

When the electric field is applied, electrons are injected from an electrode to an insulation. These electrons travel to sites where they become trapped and form space charge. In a typical polymeric insulation, for example polyethylene, the distribution of trap sites will not be uniform. It was observed to be highly concentrated at the crystalline-amorphous interface [9]. Consequently, space charge is highly concentrated, in particular, around morphological defects, impurities and inclusions.

Generally, the electric field increases from the core (centre) of the cavity to its border. This causes an expansion of the charge distribution when the internal field reaches the critical field of detrapping (E_d). Figure 3.3 shows the influence of the internal field on the material morphology. The detrapping field differs from one insulation to another based on the relative permittivity ε_r of the material. This permittivity is higher in materials with lower strength field [71], and this is related to the lower depth of the trap which requires a small field to reach the detrapping field. Consequently, the required released energy from the detrapping process to break a bond decreases with increase in the permittivity ε_r and this triggers the breakdown. The released energy during the

discharge of the capacitor [60] is found to be sufficient to produce a mechanical force that can cause molecular damage in the dielectric materials, which eventually leads to the failure of the insulator. Several papers provide evidence that the degradation of polymeric materials is largely related to the trapping of charges [72, 73].

During application of the electric field, charges accumulate in the traps and electromechanical energy is localized around the traps. These electrons are highly concentrated in a small volume. It is reasonable to assume that a large fraction of the electromechanical energy released after detrapping contributes effectively to the triggering of breakdown.

To explain the expression of the electromechanical energy, the cavities are assumed to have a spherical shape of radius r_0 similar to Figure 3.4. Obviously, there are no polymer chains in the cavity, so only those on the surface of the cavity influence the electromechanical energy. Therefore, the stored energy strongly affects the thin shell on the skin of the surface of the spherical cavity. The relevant volume of the cavity can be expressed as the result of the surface area times the shell thickness λ. Thus, the effected volume is given as:

$$V = 4\pi {r_0}^2 \lambda \tag{3.14}$$

In order to calculate the electromechanical energy density, it is necessary to relate the internal field to its associated mechanical stress. This can be explained by using the electrostriction coefficient (α), which is a property of dielectrics that causes them to change their shape under the application of an electric field. It is approximately equal to $\varepsilon_0 \varepsilon_r$ [74]. The electromechanical stress is given as:

$$\sigma_{em}(r_0) = \frac{\varepsilon_0 \varepsilon_r E(r_0)^2}{2} \tag{3.15}$$

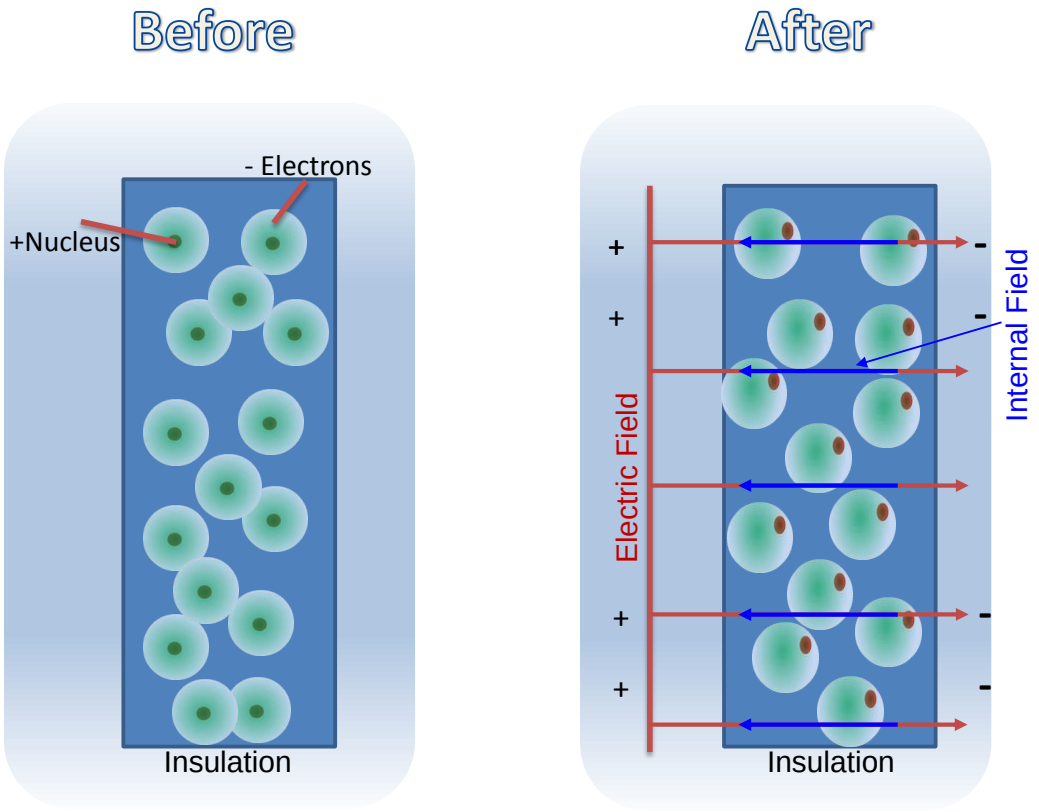

FIGURE 3.3: Effect of electric field on molecules of insulating materials with and without the electric field.

Therefore, the stored electromechanical energy in the spherical shell of a cavity can be estimated as:

$$W_{em} = \frac{\sigma_{em}(r_0)^2}{2\ Y} V \tag{3.16}$$

where Y is Young's modulus which is roughly equal to $1.5 \times 10^8 N/m^2$ for polyethylene.

As seen in Figure 3.4, an applied electric field directly effects the depth of the trap. This reduction is due to the resulting electromechanical energy from the accumulation of charge in the trap. Therefore, the coefficient of detrapping rate, in Equation 3.5, is modified by the electromechanical energy term in the presence of electric field as:

$$K_D = N_c v_{th} \sigma_T \exp\left(-\frac{E_T - W_{em}}{kT}\right) \tag{3.17}$$

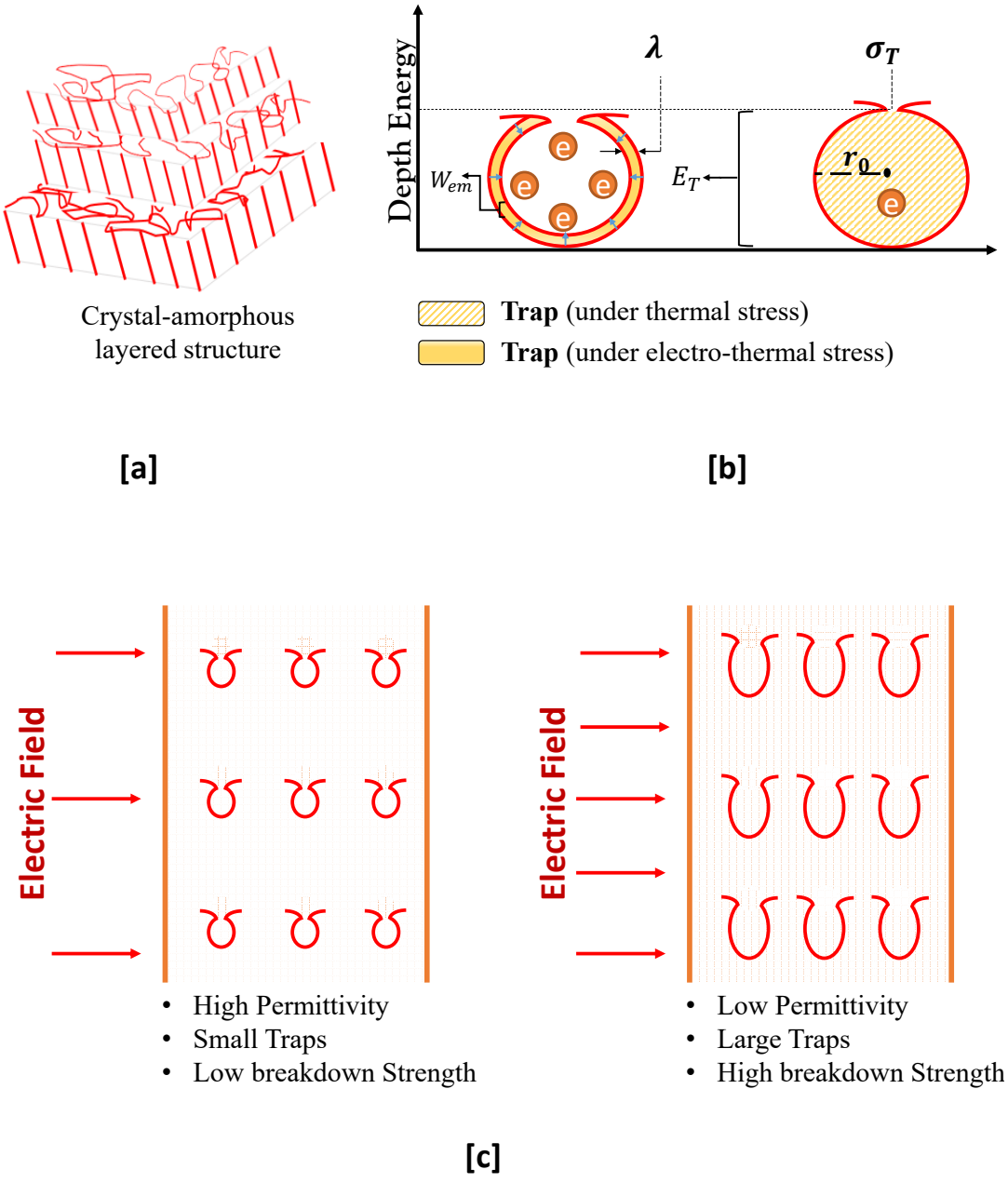

FIGURE 3.4: A single trap from a crystal-amorphous layered structure is shown with and without the effect of electric field.

According to the modifications on the work function of Schottky effect and the trap depth, the equilibrium value of C in Equation 3.10 in the presence of electric field will be modified as well as:

$$C(E) = \left[1 + \frac{qN_c v_{th}}{A^* T^2} \exp\left(-\frac{(E_T - W_m) - (\Phi - \beta_S)}{kT}\right)\right]^{-1} \tag{3.18}$$

With these substitutions, the electro-thermal life expression becomes:

$$t(E,T) = (K_T + K_D)^{-1} \ln\left[\frac{C(E)}{C(E) - C^*}\right] \tag{3.19}$$

Or, it can be written in other form as:

$$t(E,T) = \left[M \exp\left(-\frac{\Phi - \beta_s E^{1/2}}{kT}\right) + N \exp\left(-\frac{E_T - W_{em}}{kT}\right)\right]^{-1} \ln\left[\frac{C(E)}{C(E) - C^*}\right] \tag{3.20}$$

where

$$M = \frac{\sigma_T}{q} A^* T^2$$

and

$$N = N_c v_{th} \sigma_T$$

As a condition in determining the lifetime by substitution of the field independent variables by their field dependent counterparts, a fraction of the traps C^* has been filled. Once the internal electric field exceeds the detrapping field, the released electromechanical energy from the detrapping process leads physically to degraded regions and broken bonds. These regions are able to initiate a rapid breakdown of the material.

The next chapters deal with the experimental parts that are used to extract the ageing model parameters in Equation 3.20. Simply, three parts of experiments need to be perform in order to extract and calculate the model parameters. The first experiment is to detect the compatible mechanism for the injection process. It was investigated by using the conductivity measurements system. The second part is relate to space charge measurement which was performed by using the Pulsed Electro-Acoustic system (PEA). The last part is to check the validity of the model by compare the model expectation with the experimental result. This comparison is shown in Figure 6.13.

3.3 Summary

The developed ageing model dealt with here provides an appropriate answer to the increasing feeling about the existing space charges that steadily implemented into insulation could give a considerable contribution to polymeric material ageing under thermo-electrical stresses. The limitation of the model is precisely investigated under the effect of DC field. It is supported by a physical meaning that is related to the chemical defects 'traps'. One of the interesting feature of the developed model is that its parameters have physical meaning and, in principle, some of them could be determined by alternative ways of investigation, rather than life tests.

This model has a new concept of describing ageing process which is based on trapping and detrapping process. The effect of the released energy from detapping process was incorporated in the detrapping rate. On the other hand, the injection process was involved in the trapping rate and identified based on the insulating material. Regards to LDPE films, Schottky effect is the applicable mechanism for injection process.

Chapter 4

Deterministic Injection Mechanism

4.1 Introduction

This chapter contains a discussion of the conduction mechanisms in thin insulating films sandwiched between plane metal electrodes. Hence, the major concern is the high-field electrical properties of the films, as a small applied voltage will induce fields of the order 10^4 to 10^5 V/cm in the insulating films. Magnitudes of this order of fields are normally necessary in order to obtain observable current flow. With regards to conduction mechanisms, it is expected that the observed conductivity in thin insulating films is often due to extrinsic rather than intrinsic carriers. For instance, the current density in insulation is much higher than would be expected, and the activation energy associated with the conductivity is, rather than being equal to the gap energy, usually less than half the insulator energy gap [65]. It has been reported in literature [75, 76] that the source of the extrinsic conductivity is expected to be the inherent defective nature of evaporated chemical compound films.

When two points on an insulating material are subjected to a voltage V, an electric field exists as $E = -\Delta V$. Depending on the geometry of the electrode and some other factors, the electric field may be uniform (such as a sample sandwiched between two parallel electrodes) or may not (such as a sample placed between a needle and plane electrode). During the application of electric field, electrically-charged particles in the insulation will experience an electrostatic force in the direction of electric field. This force is equal to the product of their charge (in Coulombs C) and the electric field which can cause drift of the charge and transport through the insulation. The rate at which a charge is transported ($C \cdot s^{-1}$) is know as the electric current I, and its unit is amperes A. The electric current per unit area of cross section is know as the current density, J ($A \cdot m^{-2}$).

From the basic equation of Ohm's law, the current through a conductor due to drift is proportional to the voltage across it by this equation:

$$I = \left(\frac{1}{R}V\right) \tag{4.1}$$

where R is the resistance (in ohms Ω). By dividing both sides of Equation 4.1 by m^2, we can reach the Ohm's law in terms of the material properties (field E, and current density J) as:

$$J = \left(\frac{1}{\rho}E\right) = \sigma\ E \tag{4.2}$$

where ρ is the resistivity of the material and its unit is $(\Omega \cdot m)$, and $\sigma = (1/\rho)$ is the conductivity and its unit is $(\Omega \cdot m)^{-1}$. This implies that the mean velocity of the charged particles(drift velocity) in the direction of the field is proportional to the applied field.

The general form of the conductivity if related to the concentration of charge carrier n, is given by:

$$\sigma = n\ e\ \mu \tag{4.3}$$

where e is the electric charge (C) on each carrier, μ is the charge carrier mobility $m^2V^{-1}s^{-1}$. It is defined as the drift velocity ν_d per unit field which can be symbolically stated as:

$$\mu = \frac{\nu_d}{E} \tag{4.4}$$

4.2 Energy Band Structure

The basic concepts of band theory is described in this section as applied to covalent or ionic crystals. With regards to covalently-bonded crystal, silicon is a popular example that is used extensively in many electronic semiconductor devices. However, polymers are a type of molecular crystal, and therefore have very strong, covalent and intermolecular binding forces[9].

The electron energies of atoms are different in condensed matter from those of isolated atoms. Typically, atomic bonds can be classified into primary and secondary types. Primary bonds are the strong bonds with an energy value much greater than 0.5 eV, and secondary bonds are much weaker ($\ll 0.5eV$). Primary bonds can either be heteropolar (ionic), homopolar (covalent) or combination of both. Secondary bonds (van

der Waals)[77] are due to electric dipole-dipole interaction between nearby molecules or atoms. The energy of van der Waals bonds of polar atoms may be as high as $\sim 0.5eV$, and may be as little for non-polar atoms as $0.01eV$.

In ionic bonds, anions (ions with a negative charge) and cations (ions with a positive charge) are attracted to form stable units. The ionic bond is established from the coulombic attraction between different ions, since an ion can attract all oppositely charged ions in its vicinity. With regards to covalent bonds, atoms share pairs of valence electrons of opposite spin in a single joint orbital. Examples of covalent bonds and their energy value in electron volts are $C-C$ $(3.8eV)$, $C=C$ $(7.0eV)$, $C-H$ $(4.5eV)$ etc. To convert eV to $kJmol^{-1}$, the energy should be multiplied by 96.4 [9]. Figure 4.1 represents the various existing bonds between the atoms of the material.

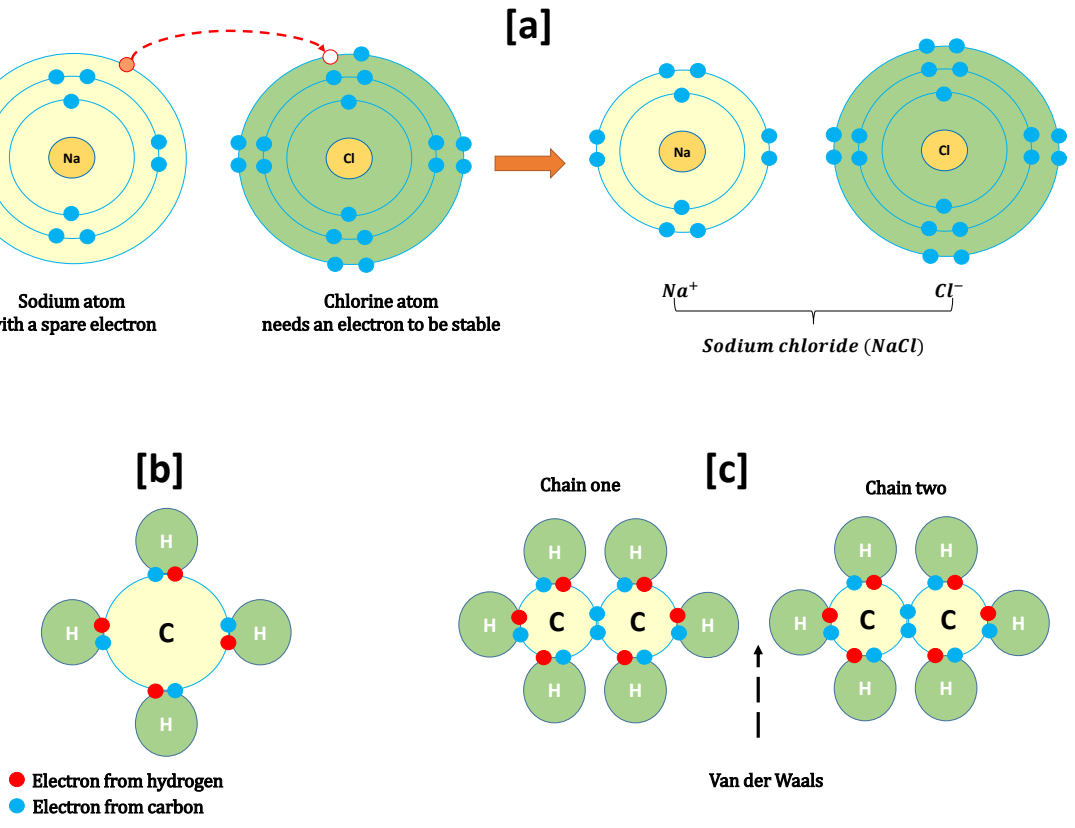

FIGURE 4.1: Schematic representation of atomic bonds; [a] shows the ionic bonding for sodium chloride (Na Cl), [b] for covalent bonding between carbon C and hydrogen H, [c] is the secondary type represented in Van der Walls as existing between two hydrogen atoms.

In high voltage cables, an insulation is contiguous with a conductor and, therefore, electrons will flow from one material to another until reaching a certain maximum level. This level is known as Fermi level. The probability, P, that an electron occupies an energy level with an energy, E, at a temperature, T, is given by the Fermi-Dirac distribution function as:

$$P(E,T) = \left[1 + \exp\left(\frac{E - E_f}{k_B T}\right)\right] \tag{4.5}$$

where k_B is the Boltzmann constant, and E_f is known as the Fermi energy level. At this level, the probability of occupation by an electron is exactly one half as shown in Figure 4.2. To calculate the Fermi energy, the electron density of the conduction band, $n = N_c \exp\left(-\frac{E_c - E_f}{k_B T}\right)$, should be in balance to the hole density in the valance band, $p = N_v \exp\left(-\frac{E_f - E_v}{k_B T}\right)$, as shown in the equation below:

$$N_c \exp\left(-\frac{E_c - E_f}{k_B T}\right) = N_v \exp\left(-\frac{E_f - E_v}{k_B T}\right) \tag{4.6}$$

where N_c and N_v are the effective density of states in the conduction and valence bands, respectively. The Fermi energy can be obtained from Equation 4.6 as:

$$E_f = \frac{E_c + E_v}{2} + \frac{k_B T}{2} \ln\left(\frac{N_v}{N_c}\right) \tag{4.7}$$

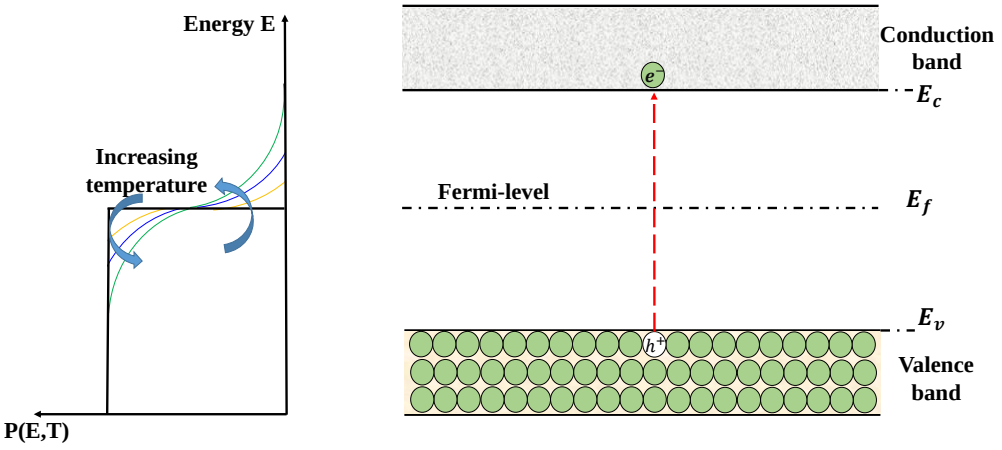

FIGURE 4.2: An energy-band diagram for a covalently-bonded energy crystal. On the left of the diagram, a representation of the Fermi-Dirac distribution indicating the probability of occupancy of an energy level as a function of temperature.

The electrons of a single, isolated atom occupy atomic orbitals at discrete energy levels of each orbital. When multiple atoms combine together to form a molecule, molecular

orbital will be formed as well that have discrete energy levels. Electrons can be freely moved in a band known as the conduction band, and in a fixed band (or in molecular orbits) known as the valence band. Figure 4.3 illustrates all the situations for the energy bands. Between the conduction and valence bands, there is a band gap or forbidden band which electrons need to gain energy to be released from the valence band to the conduction band. By using the Fermi-Dirac distribution function to calculate the probability of electrons to occupy the conduction band bottom, a small band gap range between 0 to 0.2 eV is observed in conducting materials. For semi-conductor, the band gap energy becomes slightly bigger which is 0.2 to 2.0 eV. The band gap in insulating materials has the largest energy[9].

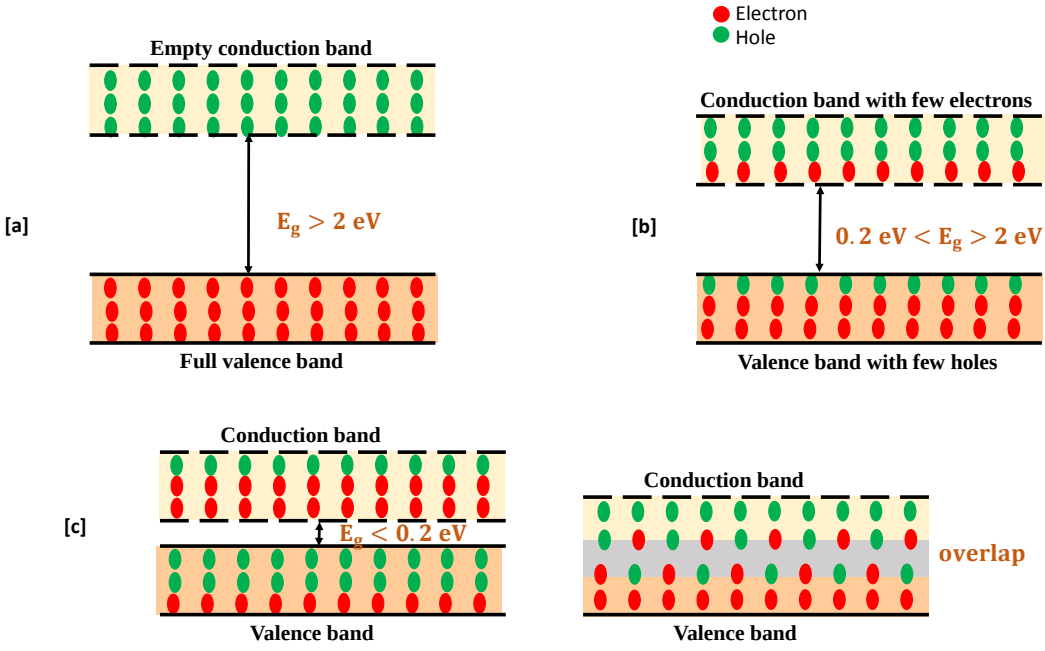

FIGURE 4.3: Diagrams of energy band of the materials in the three situations; [a] an insulator, [b] a semi-conductor, and [c] a conductor.

The question that should be asked is how do we determine the actual concentration of electrons within a given energy band such as the conduction band? In order to answer this question, the density of state needs to be known,$N(E)$, which gives the number of states per unit volume in a range of energy from E to $E + dE$. The concentration of electrons in the conduction band, as an example, is obtained by integrating the product of the probability of occupancy (Equation 4.5) and the density of state $N(E)$. To know the number of free electrons in the conduction band, n_c, the integration form will be written as:

$$n_c = \int_{E_c}^{0} P(E,T) \cdot N(E) dE \tag{4.8}$$

The results of occupied probability, free electrons and conductivity for the three cases of materials are represented in Table 4.1 including the range of each energy band.

Band gap (eV)	**Type**	**P(E)**	n_c	σ
0	Conductor	1	10^{29}	1.6×10^{7}
0.2	Semi-Conductor	1.8×10^{-2}	1.8×10^{27}	2.9×10^{5}
2	Insulation	4.3×10^{-18}	4.3×10^{11}	6.9×10^{-11}
∞		0	0	0

TABLE 4.1: Approximated results of conductivities, probabilities and concentrations in crystalline conductors, semi-conductors and insulations as reported in [9].

4.3 Charge Injection and Transportation

After a description of the energy band theory and an overview of chemical bonds through polymers, this section is to consider the movement of the released electrons in a more quantitative manner. In particular, the effect of high electric fields and other factors such as temperature are examined with regards to how charge is injected into an insulator, and the way in which the charge is transported through the bulk. The most popular mechanisms are shown in Figure 4.4.

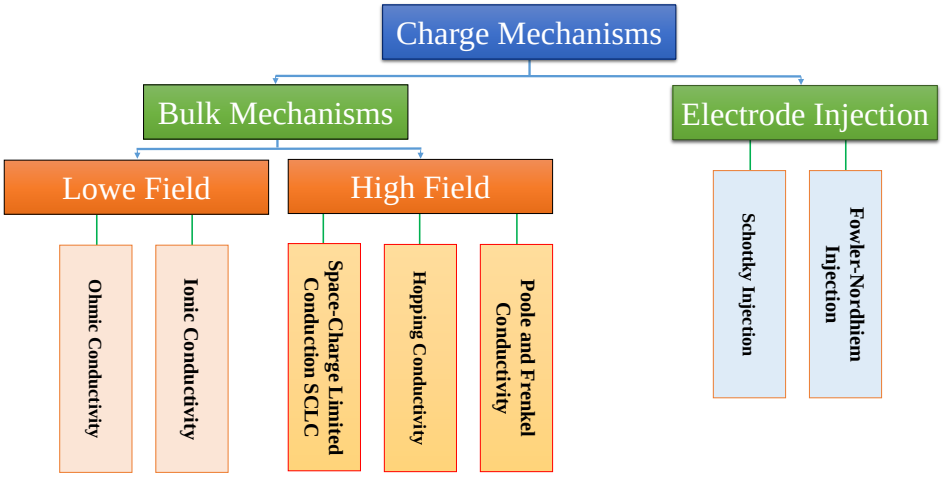

FIGURE 4.4: Charge transport mechanisms of electrode-insulator interface, and bulk.

4.3.1 Low-Field Conduction Mechanisms

4.3.1.1 Ohmic Conductivity

The relationship between the voltage and the current at low electric field tends to follow Ohm's law although verification of current at low electric field in an insulator is much difficult than in the high field. This is due to the small value of injected current and the high resistivity of an insulator. The conduction mechanism in this case is described as charge carriers, usually electrons or holes, and they acquire an average velocity proportional to the field. This concept was proposed to describe the movement of electrons in a crystal lattice, such as in a metal or semiconductor, which does not exist in insulators. The current density in such a material follows a linear relationship to the electric field as:

$$J = ne\mu E \tag{4.9}$$

However, the situation in polymers is different to the simple covalent or ionically bonded crystals of conventional solid-state physics. Most of the time, electrons and holes are unlikely to move freely. Even the ones which have sufficient energy to be released to the conduction band are likely to fall into traps located in the band gap. This is described as trap-limited mobility. Blythe [78] has verified this concept on polyethylene and this seems to be applicable to amorphous solids.

Trapping is interpreted, as shown in Figure 4.5, in terms of a modified band model[79, 80]. In the modified model, traps are localised in states belonging to molecules. Levels of these trap energies are influenced by the environment and will differ from one region to another. The depths of the traps are distributed unevenly and activation from the local state requires thermal activation.

4.3.1.2 Ionic Conductivity

Low-field mobility in polymers is frequently found to follow Arrhenius equation as:

$$\mu = \frac{ea^2\nu_0(T)}{kT} \exp\left(\frac{-\Delta G\#}{kT}\right) \tag{4.10}$$

where a is the distance between two traps, ν_0 is the attempt to escape frequency and ΔG is the Gibb's free energy. These are experimentally-determined values which are found to be constant over a given range of temperatures. The identification of carrier type is not an easy task. Several methods have been used to determine the type of the carrier [81, 82, 83, 84, 85, 86], which are summarised in Table 4.2, and have also been used to analyse the existence of ionic conductivity in polymers.

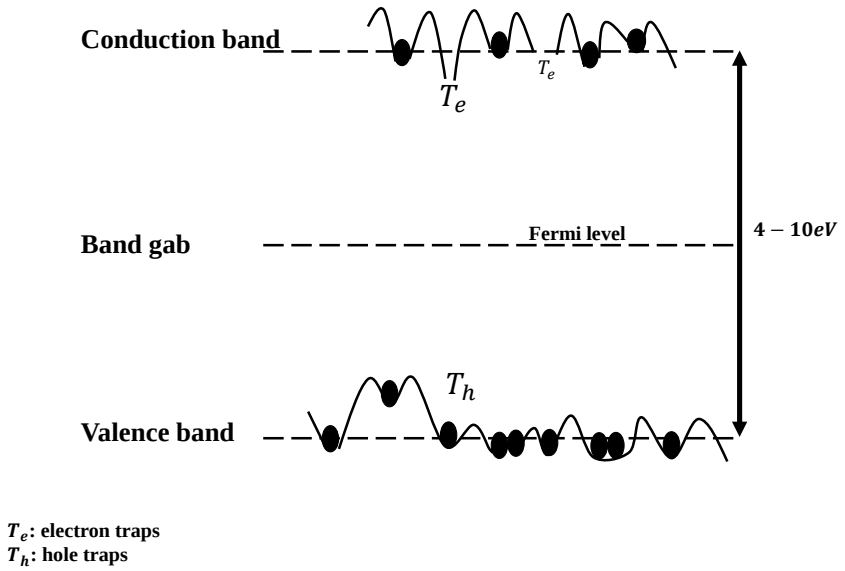

FIGURE 4.5: Energy diagram in polymers

Method	Ionic conduction	Electric conduction
Mass transfer	Yes	No
Pressure	Decrease	Increase
Glass transition $T > T_g$	Increase	
Melting point $T > T_m$	Decrease	Increase
Electrochemical reaction	Yes	No
Ionic impurity	increase	

TABLE 4.2: Property variations involved in ionic and electronic conduction.

If we consider electrons as the charge carriers instead, conduction will be different between crystal and amorphous material as shown in Figure 4.6. Based on a single crystal, movement of a charge in the conduction band will be trapped and de-trapped depending on the external stress. On the other hand, charges in amorphous regions can move by Brownian motion, tunnel-hopping, and thermally activated hopping may occur.

In addition, polymers have a large number of chains and electrons can move through the bulk of the insulation by conduction along the chain and by hopping to a neighbouring chain [87]. These electrons are located in wells, and are activated thermally which can be represented as hopping as shown in Figure 4.7. The potential barrier is reduced under the field application with respect to its direction. This will allow charge carriers to move between wells with a net flow in the field direction .

Since $\sigma = ne\mu$, the number density of carrier, n, is need to be calculated to obtain the ionic conductivity. It is likely to be temperature dependent. At least, it is reasonable to assume that the carriers are likely to be generated thermally. So the number density can be written as:

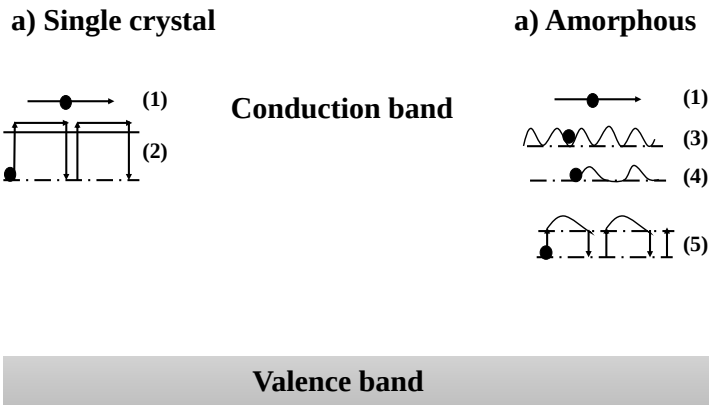

FIGURE 4.6: (1) Trap-free (2)Trap controlled band conduction (3)Brownian Motion (4) Tunnel-hopping (5) Thermally activated hopping [87]

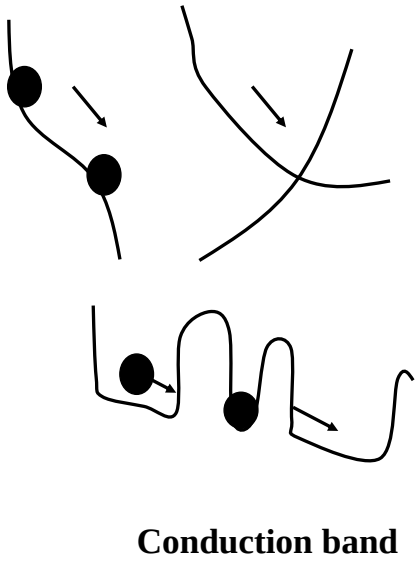

FIGURE 4.7: Movement of electrons in intermolecular conduction (Hopping to neighbouring molecules) [87]

$$n(T) = N \exp\left(-\frac{E_a}{k_B T}\right) \tag{4.11}$$

where E_A is the energy of formation and N is a concentration of possible formation sites. Now, we are able to write the final form of the ionic conductivity as:

$$\sigma = \frac{e^2 a^2 \nu_0(T) N}{k_B T} \exp\left(-\frac{E_a + \Delta G}{k_B T}\right) \tag{4.12}$$

4.3.2 High-Field Conduction Mechanisms

At high electric field, the current voltage characteristic deviates from Ohmic law and increases super-linearly with the field. Several mechanisms have been proposed in this section to explain the conduction observed at higher fields.

4.3.2.1 Space Charge Limited Current (SCLC)

Space charge limited current is generally observed in thin insulating films and found to be highly dependent on the thickness of the insulation. It has been suggested that if the contact between electrode-insulation is good, then more free charge may be injected. When the dielectric constant is high, this means that a high concentration of injected charges can build up within the insulation. Therefore, at least, initially more free charge may be injected than extracted.

Mott and Gurney proposed the theory of space-charge-limited current (SCLC) in solids [88]. To reach the conductivity form in space charge principle, we will begin from the general current density through the insulation:

$$J = q\ \mu_h\ n_h(x)\ E(x) \tag{4.13}$$

where μ_h is the mobility of free holes, n_h is the concentration of holes, and $E(x)$ is the electric field. The direction of x is orthogonal to the electrodes, or in other words, straight through the insulation and it is measured from the cathode surface at the origin. From Poisson's equation, the derivation of electric field in x-direction is given as:

$$\frac{\partial E(x)}{dx} = \frac{q\ n_h(x)}{\varepsilon} \tag{4.14}$$

So, we re-write the conduction current density and after substituting Equation 4.14 into Equation 4.13, then it becomes as:

$$J = \varepsilon \mu_h E(x) \frac{\partial E(x)}{dx} \tag{4.15}$$

By integrating Equation 4.15 and using the boundary conditions, we can get:

$$E(0) = 0 \quad and \int_0^d E(x)dx = V \tag{4.16}$$

where d is the specimen thickness and V is the applied voltage.

Then, the current density (which is also called the square law) is given by:

$$J = \frac{9}{8}\varepsilon\mu_h\frac{V^2}{d^3} \tag{4.17}$$

At low field, however, the current density does not obey the square relation with voltage. It is dominant with the ohmic conduction current given by:

$$J_\Omega = q\ n_0\ \mu_h\ \frac{V}{d} \gg \frac{9}{8}\varepsilon\mu_h\frac{V^2}{d^3} \tag{4.18}$$

The transition voltage, V_{trans}, from ohmic conduction to the space-charge-limited current comes when the injected space charge carriers exceed the thermally generated carriers, n_0, as illustrated below:

$$V_{trans} = \frac{8\ q\ n_0\ d^2}{9\varepsilon} \tag{4.19}$$

The above derivatives deal with trap-free insulations. However, the insulating materials usually consist of imperfections, such as structural disorders and impurities, which affect the trapping centres. These affect the transportation of charge carriers in the bulk of insulators. Hence, below is further extended work on SCLC with two extra parameters which are determine by traps[89].

$$J = \frac{9}{8}\varepsilon\mu_h\theta_a\frac{V^2}{{d_{eff}}^3} \tag{4.20}$$

where θ_a is the ratio of free carrier density to the total carriers density and ${d_{eff}}^3$ is the effective thickness due to the presence of traps. The transition voltage is given by:

$$V_{trans} = \frac{1}{\theta_a}\frac{8\ q\ n_0\ d^2}{9\varepsilon} \tag{4.21}$$

At a sufficiently high voltage, the injected charge-carrier number density is approximately equal to the number density of traps, N. At this stage, the trapped-field limited voltage V_{TFL} is reached and the current density rapidly rises. This voltage is given by:

$$V_{TFL} = \frac{q\ N\ d^2}{2\ \varepsilon} \tag{4.22}$$

To summarise the SCLC, Figure 4.8 shows all possible conduction pathways. At low

electric field, the space charge region will be built up to the transition voltage, and the current will be dominated by the ohmic relation with voltage. Above the transition voltage, the field of space charge will limit the current. As voltage increases, the injected charges will increase as well which lead to the movement of the Fermi level above the trap energy. This creates a sudden increment in the current density. Then, a new region of space charge is created with increasing voltage, see Table 4.3.

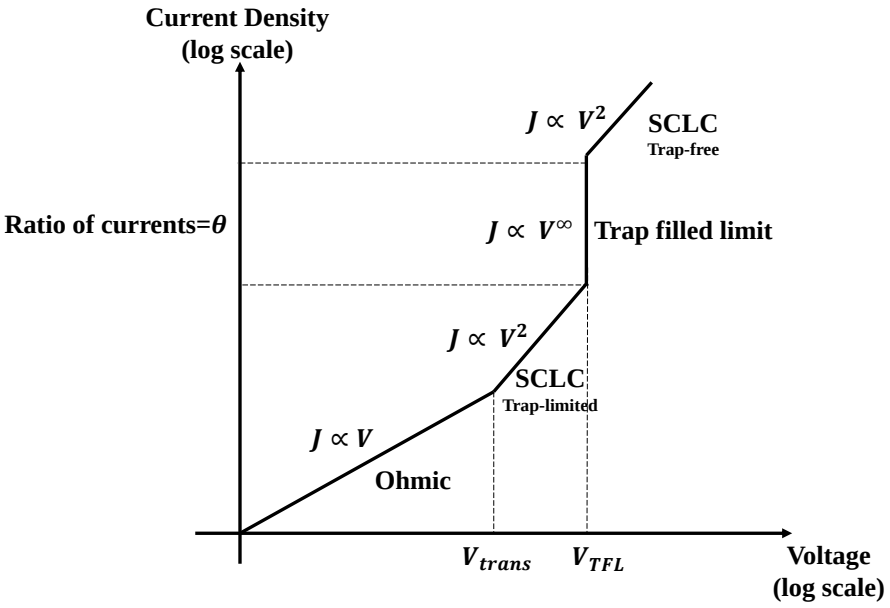

FIGURE 4.8: Schematic graph of current density vs. voltage in ideal case of space charge limited current.

Region	Voltage	Current Density	Slope
1	$0 < V < V_{trans}$	$J \propto V$	1
2	$V_{trans} < V < V_{TFL}$	$J \propto V^2$	2
3	$V = V_{TFL}$	-	∞
4	$V > V_{TFL}$	$J \propto V^2$	2

TABLE 4.3: The relation between voltage and current density as shown on the schematic $\log(J)$ versus $\log(V)$ in Figure 4.8.

4.3.2.2 Hopping Conduction

Due to the existence of traps in the forbidden band, the injected electrons are trapped within the bulk of the insulation. The unoccupied traps in the bulk can be described as empty potential wells. Once the charge has been trapped, the trap depth Φ, will have an effect on the charge and will inhibit its movement. In order to provide for the migration process through the insulation, a hopping mechanism is one of the conduction pathways that can take place in this situation to move the charge from one trap to another. The required energy to release the trapped charge, therefore, corresponds to the height of the trap. Figure 4.9 shows the hopping process through the bulk of a sample.

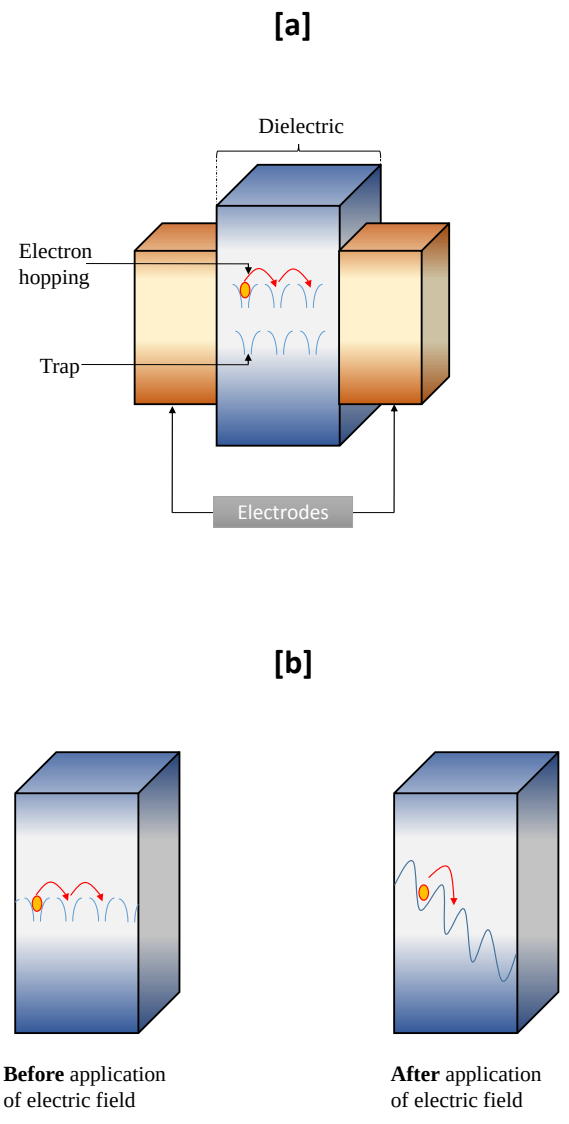

FIGURE 4.9: Hopping mechanism diagram where [a] shows the hopping process in a dielectric sample, and [b] represents an array of potential barrier before and after the application of electric field.

The traps in the bulk of insulation are individually separated by a distance a. Electrons can move in any direction in the absence of an electric field. The probability of a trapped charge [90] to move towards the right to the next trap is given by:

$$P(T) = \nu \exp\left(-\frac{\Phi}{k\ T}\right) \tag{4.23}$$

where ν is the escape frequency of electrons in order of 10^{12} to $10^{14} s^{-1}$.

During the application of an electric field, E, the potential barrier height will continue reducing in the forward direction with $\Phi - 0.5aEe$ and increasing in the backward direction with amount of energy equal to $\Phi + 0.5aEe$ to facilitate conduction as shown in Figure 4.9. The current density for a single trapping level is, therefore, a combination of the forward and backward as:

$$\begin{aligned} J =& \nu \exp\left[-\frac{\Phi + 0.5aEe}{kT}\right] + \nu \exp\left[-\frac{\Phi - 0.5aEe}{kT}\right] \\ =& \nu \exp\left(-\frac{\Phi}{2k\ T}\right)\left[\exp\left(\frac{aEe}{2k\ T}\right) - \exp\left(-\frac{aEe}{2k\ T}\right)\right] \end{aligned} \tag{4.24}$$

By using the hyperbolic sine function, $2\sinh x = \exp(x) - \exp(-x)$, Equation 4.24 can be rewritten as:

$$J = 2\nu \exp\left(-\frac{\Phi}{k\ T}\right) \sinh\left(\frac{eEa}{2k\ T}\right) \tag{4.25}$$

For a concentration of charges to be considered [91, 92], the current density takes the form :

$$J = n\ e\ a\ \left[2\nu \exp(-\frac{\Phi}{k\ T}) \sinh(\frac{eEa}{2k\ T})\right] \tag{4.26}$$

where n is the concentration of charge carriers.

From the previous discussion, however, the concept of 'hopping' is something of a misnomer since what actually takes place is a tunnelling effect as the trapped electron is not jumping over the top of a potential barrier [93, 94].

4.3.2.3 Poole and Frenkel Mechanism

The classical Poole-Frenkel (PF) emission [95] has a mechanism which is close to Schottky emission, in which a trapped electron is thermally-excited to be emitted from Coulombic (i.e., charged) traps in the bulk of a dielectric or semiconductor to the conduction band, under enhancement of electric field[96] . Therefore, it sometimes can be called as the internal Schottky emission[97]. By considering an electron in the centre of a trap, the Coulomb potential energy is reduced from one side of the trap when it interacts with an electric field, and this thereby increases the probability of the electron escaping from the trap. These Coulombic centres are considered as donors, although sometimes they can have acceptor centres which are directly included in the model [96]. Figure 4.10 illustrates the process of Poole-Frenkel mechanism. In the figure, Φ is the required energy for the trapped electron to escape the influence of the positive nucleus centre when there is no electric field. $\beta_{PF}E^{0.5}$ is the amount of energy that was proposed by Poole-Frenkel to reduce the barrier height of the trap. The quasi-conduction band edge means that the trapped electron at this level of energy is free from the effect of the positive nucleus. This term is often used when discussing amorphous solids[98].

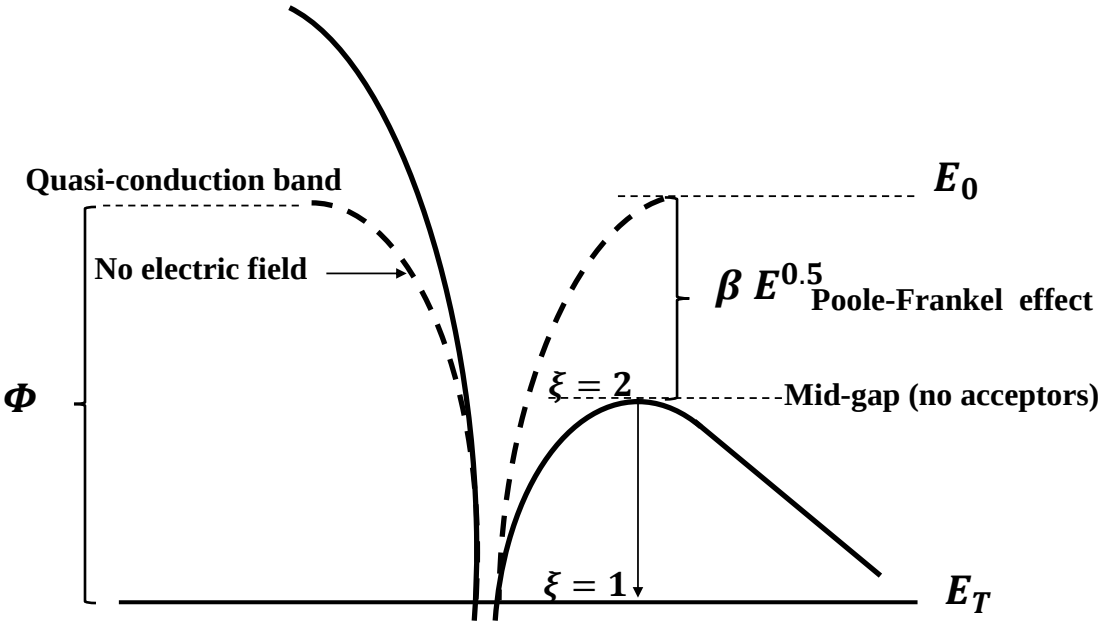

FIGURE 4.10: Coulombic potential well in the presence of a thermal (dotted line) and an electric field (bold line) illustrating the Poole-Frenkel effect.

For the Poole-Frenkel emission to occur, the trap should be neutral after trapping a charge and positively charged when the electron escapes [76, 99]. On the other hand, if the trap is charged when filled and neutral when empty, the concept of Coulombic attraction cannot exist as the Coulombic potential barrier is absent in such case.

Actually, the Poole-Frenkel concept was developed in order to explain the increment in electrical conductivity in insulating materials at high field and low mobility semiconductors before breakdown. According to Pool-Frenkel, the electrical conductivity, σ, is approximated to be proportional to the free carrier concentration in the quasi-conduction band [95]. This conductivity is due to the thermal ionization of Coulombic traps. The Fermi level is assumed to be located at the middle of the band gap ($\xi = 2$ in Figure 4.10). The conductivity, σ, can therefore be written as:

$$\sigma \propto \exp\left(-\frac{\Phi}{2\ k\ T}\right) \tag{4.27}$$

In the presence of an electric field, the trap barrier height will be reduced by an amount $\beta_{PF}E^{0.5}$ where

$$\beta_{PF} = \sqrt{\frac{q^3}{\pi\varepsilon}} \tag{4.28}$$

Therefore, the electrical conductivity as a function of electric field is modified and can be written as

$$\sigma(E) = C \exp\left(-\frac{\Phi - \beta_{PF}E^{0.5}}{2\ k\ T}\right) \tag{4.29}$$

where C is a proportionality constant. Equation 4.29 is Pool-Frenkel's first-order model of field-assisted thermal ionization of electrons from Coulombic traps. To reach the current density, J, from the conductivity, it is simply given by multiplying the conductivity by the electric field. This gives:

$$J = C\ E\ \exp\left(-\frac{\Phi - \beta_{PF}E^{0.5}}{2\ k\ T}\right) \tag{4.30}$$

This case has shown that this model is based on the Boltzmann approximation, and the Fermi level is assumed to be midway between the ground state of the trap and the bottom edge of the quasi-conduction band. Several authors [100, 101, 102] misquote the factor 2 in the denominator of the exponential in the current density equation. However, it has been proved that this factor can lie between one and two as shown in [99].

As discussed earlier, the current density was derived in the presence of electric field under the assumption that the level of Fermi energy exists midway between the ground state of the trap and the quasi-conduction band of the insulating material. This assumption of a 'mid-gap' Fermi level leads to a factor of 2 in the denominator of the exponential. The presence of deep level acceptors has an influence on lowering the Fermi level. Thus, the statistic involved in Equation 4.29 will be modified. When the acceptor concentration is so high, the Fermi level is at the donor trap level. This means $\xi = 1$, or in other word, $E_0 - E_F = E_0 - E_T$ as illustrated in Figure 4.10. Therefore, the current density in this case becomes

$$J = C\ E\ \exp\left(-\frac{\Phi - \beta_{PF}E^{0.5}}{k\ T}\right) \tag{4.31}$$

We can see Equation 4.30 and Equation 4.31 are limited cases, which depends on the acceptor sites in the insulation. Therefore, Pool-Frenkel can be generalized in an expression form that can take compensation into account. This equation is given as:

$$J = C\ E\ \exp\left(-\frac{\Phi - \beta_{PF}E^{0.5}}{\xi\ k\ T}\right) \tag{4.32}$$

where the factor ξ is a dominator factor of the exponential that varies between one and two depending on the acceptor compensation[103, 99, 104]. Most researchers who were not able to use the classical concept of Poole-Frenkel ($\xi = 2$) to interpret their data have employed Equation 4.31 and assume a significant number of acceptor sites[100, 102, 105].

We can see from the above model that the Poole-Frenkel reflects that the current density is proportional to the applied electric field. This is due to the effect of the ionization potential reduction, Φ, by $\beta_{PF}E^{0.5}$. To verify the mechanism to an insulation, a plot of $\ln(J/E)$ versus $E^{0.5}$ should yield a straight line as:

$$\ln\left(\frac{J}{E}\right) = \frac{\beta_{PF}}{\xi\ k\ T}E^{0.5} + \left(\ln C - \frac{\Phi}{\xi k\ T}\right) \tag{4.33}$$

The slope of the Poole-Frenkel plot, M, is proportional to β as:

$$M = \frac{\beta}{\xi\ k\ T} \tag{4.34}$$

It can be seen that the slope is a constant that depends on the material (from ξ) and the temperature (T).

4.3.3 Charge Injection

The electrode-insulator interface is complicated due to the presence of chemical and physical defects. These defects, such as chemical impurities and surface roughness, have a complicated energy-band which causes some sort of difficulty in interpreting the injection process.

The two of the most common mechanisms used for injection process are Fowler-Nordheim injection and the Shottky effect which are based on the development of Richardson-Dushman equation [106]. For electrons to leave a metal and enter an insulation, they require an energy Φ in the thermally-activated situation, or a reduction of Φ in the energy acquired from the electric field. These theories were initially developed for the injection of electrons from a metal into a vacuum in which the barrier height Φ is equal to the work function. However, the barrier height in the case of metal-polymer interface is modified by the local conditions based on the definition of the mechanism. Figure 4.11 shows an example of Schottky effect.

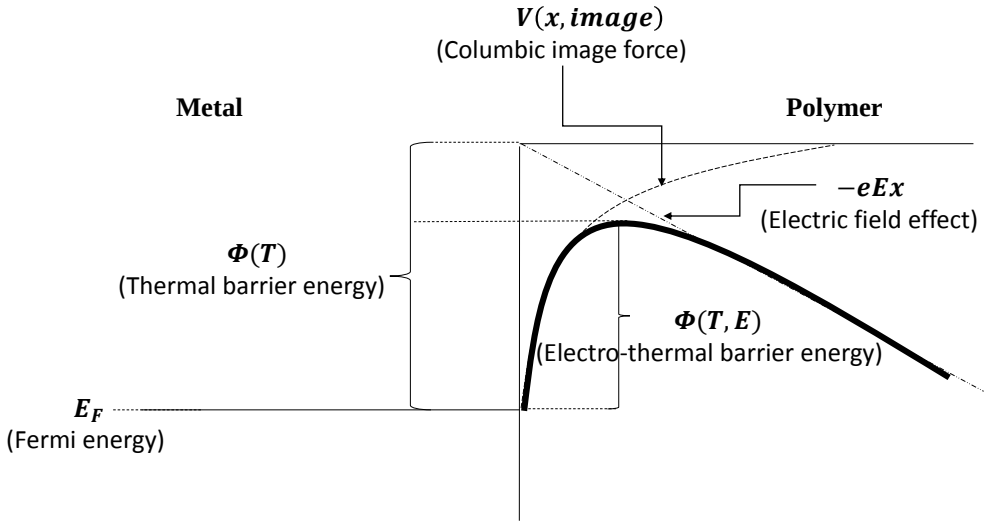

FIGURE 4.11: Diagram of an electrode-insulation interface represents the modification on the coulombic barrier in the presence of thermal and electrical fields.

4.3.3.1 Shottky Injection

Shottky injection is based on the development of electron emission as expressed by Richardson-Dushman principle, which is [106]

$$J = B_o T^2 \exp[-\frac{\Phi}{kT}] \tag{4.35}$$

where $B_o = 4\pi e m_e k^2/h^3$ which is equal to $1.20 * 10^6 Am^{-2}K^{-2}$. The first detected problem in Equation 4.35 is that the probability of an electron to be reflected back into the metal, instead of being emitted over the potential barrier, has not been taken into account. As the potential energy becomes very large, the injected electrons may be reflected and there is no emission. When Richardson took this into consideration in the equation, it takes the form:

$$J = AT^2 \exp[-\frac{\Phi}{kT}] \tag{4.36}$$

where $A = (1 - R)B_o$ is the emission constant and R is the reflection coefficient. Value of A in most of metals is about half of B_o, whereas in some cases it is less than the half as for some oxide coatings on Ni cathode which equals to $1 * 10^2 Am^{-2}K^{-2}$.

With regards to Equation 4.36, Richardson neglected the effect of electric field on the emission process which lowers the potential energy barrier Φ. However, Schottky considered this effect and applied this energy to Richardson equation. When a positive voltage is applied to the anode with respect to the cathode, the electric field at the cathode helps the thermionic emission process by lowering the potential barrier.

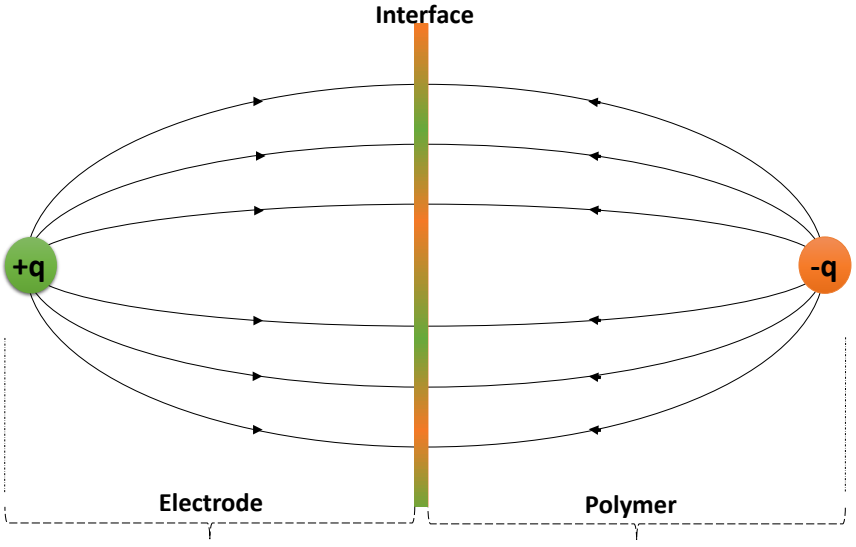

FIGURE 4.12: A charge placed in an infinitely conducting electrode which attracts an opposite charge on the polymer surface.

The electron outside the surface of the metal has to overcome the potential barrier to leave the metal and enter the insulation. Electrons are pulled by the effect of the positive charge left in the metal. This is represented by the theorem of image charges shown in Figure 4.12, which demonstrates that an electron is placed in a distance of x to the metal-insulator interface, and with the same distance to its new position in the bulk of the insulator. That is:

$$PE_{image}(x) = -\frac{e^2}{16\pi\epsilon_o x} \tag{4.37}$$

From Equation 4.37, potential energy has a reference level of zero at $x = \infty$. Schottky defines PE = 0 to be inside the metal. Therefore, this equation is modified to conform to the definition of zero PE as a reference.To do this, Figure 4.12 shows how the image PE varies with x. Far away from the surface, the PE is expected to be $(E_F + \Phi)$. So Equation 4.37 is modified to read:

$$PE_{image}(x) = (E_F + \Phi) - \frac{e^2}{16\pi\epsilon_o x} \tag{4.38}$$

From the definition of potential when a voltage difference is applied between the anode and cathode, there is a gradient of potential energy just outside the surface of the metal which is given as:

$$PE_{applied}(x) = -exE \tag{4.39}$$

where E is the applied field. The total PE(x) of electron outside the metal is therefore equal to the sum of Equation 4.38 and Equation 4.39 as sketched in Figure 4.12:

$$PE(x) = (E_F + \Phi) - \frac{e^2}{16\pi\epsilon_o x} - exE \tag{4.40}$$

Potential energy outside the metal cannot go up to $(E_F + \Phi)$. Once the electric field is applied, the potential barrier is effectively reduced to $(E_F + \Phi_{eff})$. This effective work function is therefore:

$$\Phi_{eff} = \Phi - \frac{e^3 E}{4\pi\epsilon_o} \tag{4.41}$$

This lowering of work function is known as Schottky effect. Therefore, the current density is similar to Richardson-Dushman but with Φ_{eff} instead of Φ. It is:

$$J = AT^2 \exp[-\frac{\Phi_{eff} - \beta_s E^{\frac{1}{2}}}{kT}] \tag{4.42}$$

where $\beta_s = [e^3/4\pi\epsilon]^{1/2}$ is the Schottky coefficient whose value equals to $3.79\times10^{-5}(eV/\sqrt{\frac{V}{m}})$ in the vacuum medium [106].

4.3.3.2 Fowler-Nordheim Mechanism

Due to the application of high electric fields ($10^8 - 10^9 V/m$), the interface potential barrier height becomes very thin and several mechanisms can describe this process. In classical mechanisms, a particle has to have an energy that is higher than the barrier potential energy to inject into polymers. However, particles, such as an electron, may pass through thin potential barriers and have a finite probability of existing in such regions [107], as the amplitude of electric field is increased. This is known as Fowler-Nordheim injection [108], and it is represented in Figure 4.13.

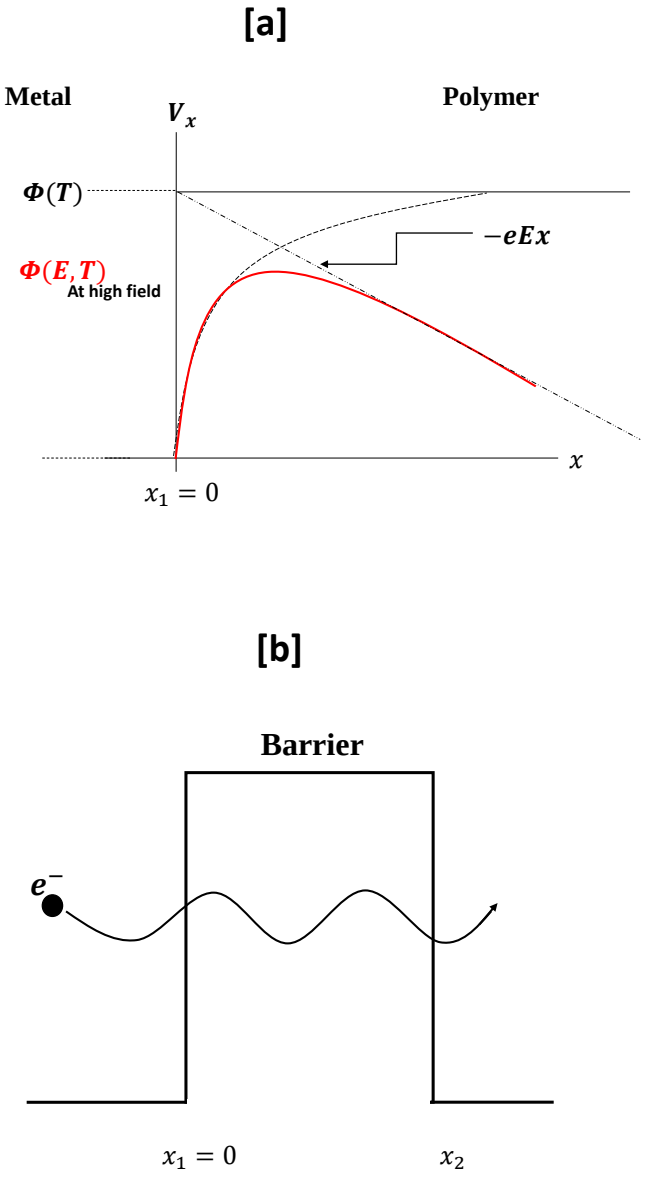

FIGURE 4.13: The Fowler-Nordheim concept; [a] the potential barrier shape used to calculate the current density, [b] electron wave travels through the barrier [106].

The calculation of current density in Fowler-Nordheim mechanism is based on the Wentzel-Kramers-Brillouin (WKB) approximation which was proposed by Wentzel [109], Kramers [110] and Brillouin [111] according to which the transmission of a potential barrier for a level of energy is applied. By using the WKB approximation, the current density, J, is given as:

$$J = \frac{4\pi mq}{h^3}\int_0^{\infty}(V_x-\Phi)\exp\left(-\frac{8\pi\sqrt{2m}{V_x}^{3/2}}{3ehE}\right)dV_x \tag{4.43}$$

where h is Plancks constant, m is the mass, E is the electric field , V_x is the top of the barrier height and Φ is the potential barrier height in eV [112].

By using Taylor expansion to expand V_x at the point Φ, the factor ${V_x}^{3/2}$ can be expressed in a polynomial of integer powers of V_x about any fixed value of V_x as:

$$J = \frac{4\pi mq}{h^3}\int_0^{\infty}(V_x-\Phi)\exp\left[-\frac{8\pi\sqrt{2m}\left(\Phi^{3/2}+\frac{3}{2}(V_x-\Phi)\Phi^{1/2}+...\right)}{3ehE}\right]dV_x \tag{4.44}$$

Apart from the first two terms of the Taylor expansion, the rest are negligible:

$$J = \frac{4\pi mq}{h^3}\int_0^{\infty}(V_x-\Phi)\exp\left(-\frac{8\pi\sqrt{2m}\ \ \Phi^{3/2}}{3ehE}\right)\exp\left(-\frac{4\pi\sqrt{2m\Phi}\,(V_x-\Phi)}{ehE}\right)dV_x \tag{4.45}$$

$$J = \frac{4\pi mq}{h^3}\exp\left(-\frac{8\pi\sqrt{2m}\ \ \Phi^{3/2}}{3ehE}\right)\int_0^{\infty}(V_x-\Phi)\exp\left(-\frac{4\pi\sqrt{2m\Phi}\,(V_x-\Phi)}{ehE}\right)dV_x \tag{4.46}$$

By solving the integration of the above equation, the final form of Fowler-Nordheim equation can be written as:

$$J = \frac{e^3\ E^2}{8\ \pi\ h\ \Phi}\exp\left(-\frac{8\ \pi\ \sqrt{2\ m}}{3\ e\ h\ E}\Phi^{3/2}\right) \tag{4.47}$$

4.4 Experimental Set-up

Test Specimens

For conduction measurements, low-denisty polyethylene LDPE was chosen as a sample. Some of the mechanisms discussed earlier were found to be highly dependent upon thickness. Therefore, the experiments were carried-out on two different thicknesses of LDPE $150\mu m$ and $180\mu m$. To avoid flash-over occurrence, the sample's diameter was chosen to be longer with a minimum of 20% of the electrode's diameter. The measurement was taken at a value when a specimen had the actual conductivity reading at the applied conditions (i.e. after approximately one hour).

Oven

The samples were tested at different temperatures as the temperature plays a significant role in the conductivity. However, validity of injection mechanism has been performed at different temperatures to keep the assumed mechanism much supported. The conductivity of insulations may be affected by the time of temperature exposure [113]. Therefore, the samples were placed in the oven for a period of 15 minutes to warm the samples to the desirable temperature. The experiments were performed at three different temperatures, which are 20 C^o, 40 C^o and 60 C^o.

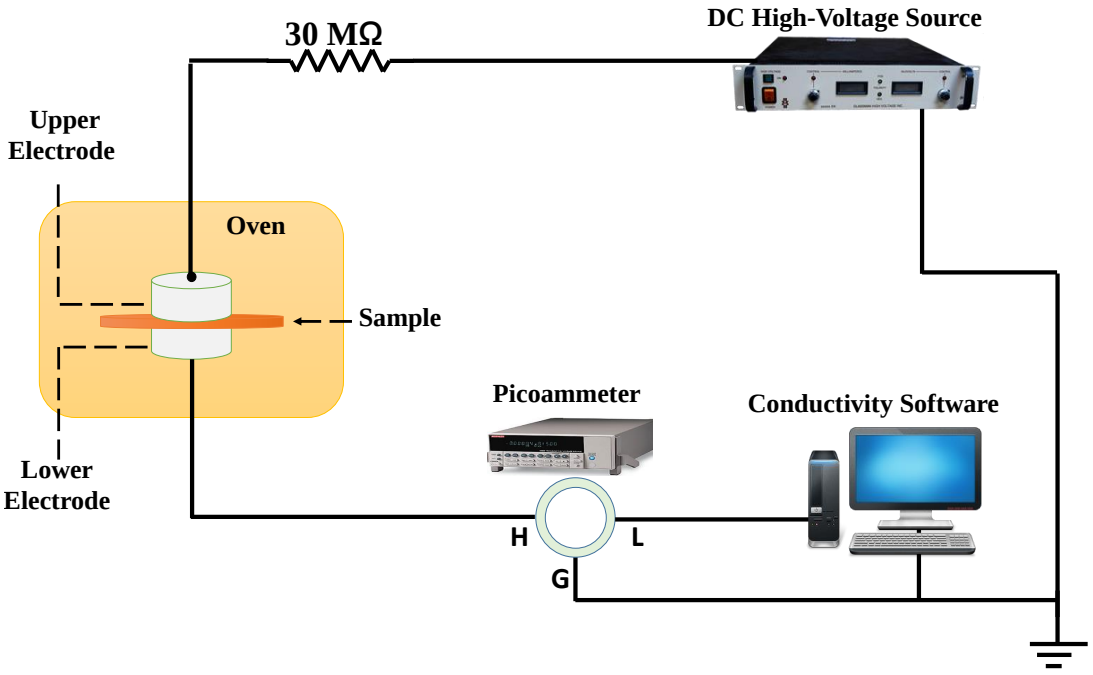

FIGURE 4.14: The conductivity measurment set-up.

Electrodes

The dielectric breakdown for a given specimen configuration may vary considerably, depending upon placement of the test electrodes and the geometry. Therefore, it is important to describe the used electrodes in the experiments. If the specified electrodes in standards (such as ASTM International standards[113]), or other electrodes are used, details of the electrodes should be described in the report for comparison. The electrodes surfaces should be in contact with the test specimen over the entire area, except for electrodes with rounded edges. In addition, it is important to keep the surfaces of the electrodes clean, smooth and free from projecting irregularities resulting from previous tests. If there are asperities, they must be removed. The type of electrodes for the conductivity measurements are in opposing cylinders with 22 mm in diameter and edges rounded to 3 mm radius.

High-Voltage DC Power Supply

The power supply, that is used in this experiment, is DC positive polarity which is provided by Spellman international company. It is connected to the sample's electrodes, and protected by a high value resistor in case the sample is broken down. The applied stress range for the test specimens were from 1 kV to 8 kV, with step-up voltage of 1 kV. Each step took 3600 seconds (60 minutes).

Picoammeter

The Keithley picoammeter is the one that was used for the experiments. It needs to be warmed, as stated in the manual, for at least one hour. It is then connected to the lower electrode to detect the current that passes through the specimens. This value is very small for LDPE specimens, which is in the order of 10^{-9} to 10^{-7} depending of the applied field.

Conductivity Software

Figure 4.15 shows the software that has been used for detecting the value from the picoammeter. This software has several functions such as setting the type of measurement (i.e. step-up voltage or voltage constant) , interval periods, calculating conductivity. In this experiment, we used the constant voltage by getting measurements at a specific time. The final reading in a period of one hour is chosen as a current reading of the given applied voltage.

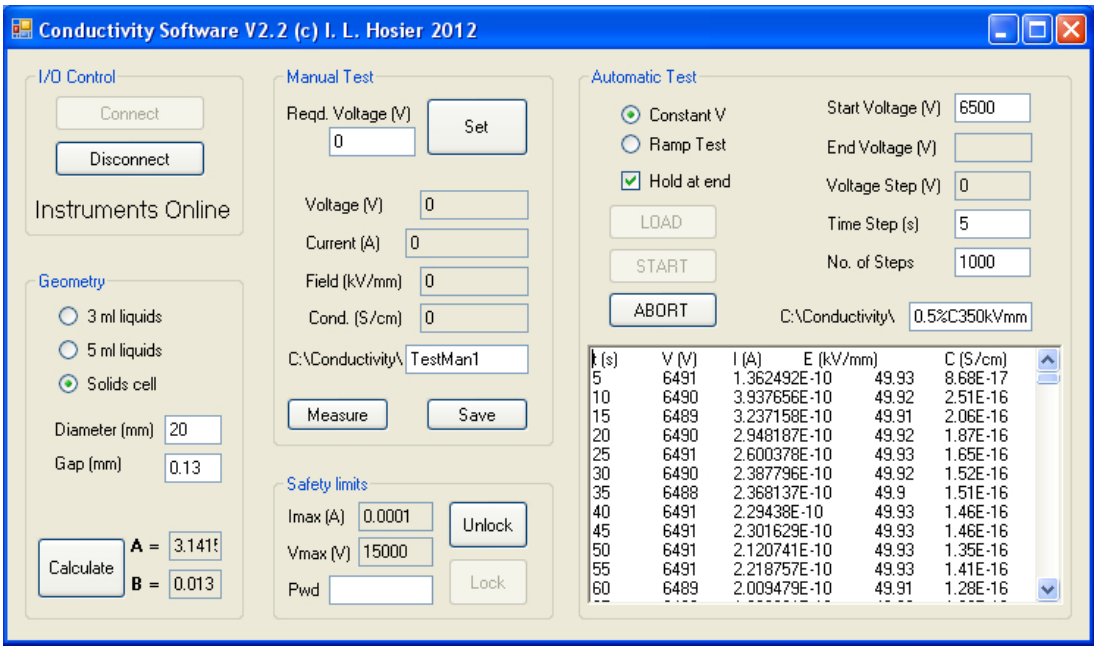

FIGURE 4.15: Conductivity Software.

4.5 Results and Discussion of Conductivity

Initially, the conduction current is necessary to be obtained at a value that is beyond the charging and absorption current levels. It should be measured after a specified period of time that can reflect the exact state in the insulation. In these measurements, the conduction current readings took 3600 seconds to be completed, and readings were taken for every 20 seconds. Although the applied field is very big, the current density is very small as clearly shown in Tables 4.4, 4.5, 4.6. For instance, the current density in a LDPE sample after being stressed by 6.67 MV/m for one hour at 20 C^o is 2.28×10^{-9} A/m^2. If the value of the current density at high electric field is very small, it can be imagined that it is so much lower at lower electric field.

It is well known that the applied electric field to an insulator can affect and distort local field around defects, interfaces, and localized changes in material properties. The effects are particularly well observed in the case of DC electric fields due to charge builds-up in an insulator. Obviously, these trapped charges are either injected from a conductor at electrode-insulator interfaces or possibly as a result of micro-discharges in voids/about defects (i.e., partial discharge (PD))[73]. Thus, the current-voltage characteristics should be analysed to know the compatible injection mechanism for LDPE samples.

4.5.1 Compatible Injection Mechanism

To check the validity of conduction mechanism for a specific material, the experimental results on current-voltage plot should yield the same relation between current and voltage on any applicable model. For example, the relationship between current and voltage in SCLC should follow the square relationship of the latter. On the other hand, mechanisms like Schottky and Poole-Frenkel need to be verified by two things; plot of $\ln(CurrentDensity)$ versus $\sqrt{ElectricField}$ should yield a straight line, and also by comparing the extracted permittivity from the slope Schottky and Poole-Frenkel with the exact relative permittivity of the insulation.

Whereas for this project the major concern was the trapping process, it is necessary here to clarify exactly which mechanism can be used for injecting electrons. The most popular mechanisms for injection process are tunneling (Fowler-Nordheim) and Schottky injections. Since the tunneling mechanism requires very thin film to occur and the current is relatively independent of temperature, it is surely not applicable for the electro-thermal aging model in the thesis. According to Schottky injection, the height of the barrier is adjusted by the applied field, and the current depends on temperature. Validity of Schottky injection mechanism has been performed on two different thicknesses of LDPE samples ($150\mu m$ and $180\mu m$), at three different temperatures (20 C^o, 40 C^o and 60 C^o).

The slope M of Schottky mechanism (Equation 4.42) is given as:

$$M = \frac{\sqrt{\frac{e^3}{4\ \pi\ \varepsilon_o\ \varepsilon_r}}}{k\ T} \tag{4.48}$$

As the slopes are given from the experimental results in Figures 4.17, 4.19, and 4.21, the relative permittivity of LDPE can be calculated from Equation 4.48, which are shown in Tables 4.4,4.5 and 4.6, as:

$$\varepsilon_r = \frac{e^3}{4\pi\ \varepsilon_o\ (M\ k\ T)^2} \tag{4.49}$$

The extracted permittivity from the experimental results is close to the LDPE permittivity (2.3). With regards to the Schottky effect (Equation 3.13), the value of Φ is calculated from the intercept term of Y-axis as:

$$Intercep\ \ of\ \ Y-axis = \ln(A\ T^2) - \frac{\Phi}{k\ T} \tag{4.50}$$

Alternatively, it can be extracted from the curve fitting of the developed ageing model in Figure 6.13 as it is close both way. The value of the work function Φ is 2.7×10^{-19} J, which seems to be in agreement with the literature [114, 115].

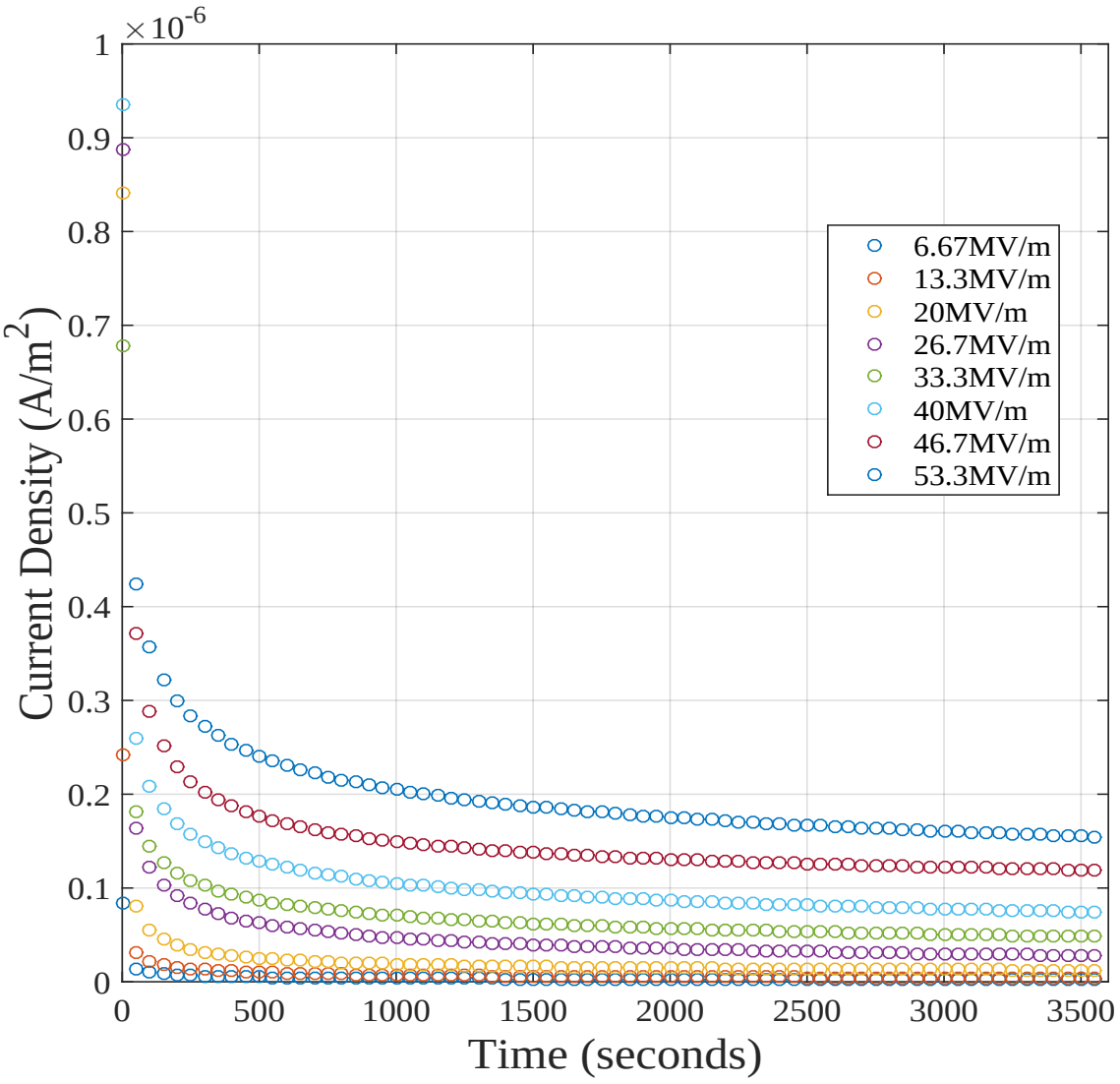

FIGURE 4.16: The current-time characteristic of LDPE at 1,2,3,4,5,6,7 and 8 kV at room temperature.

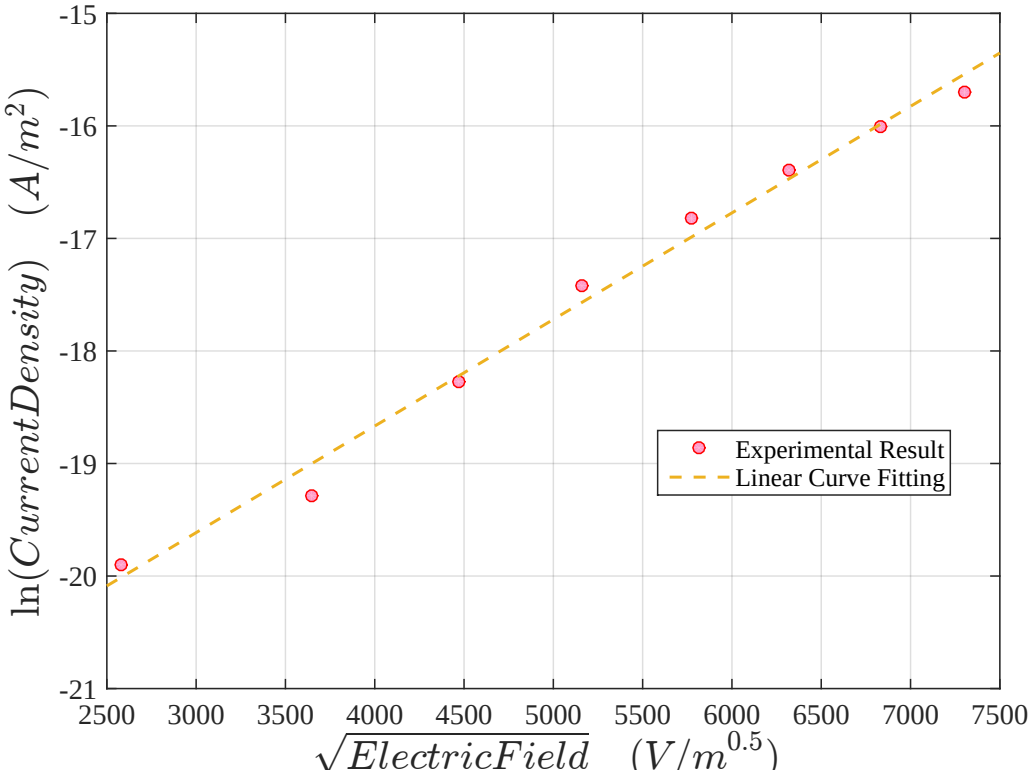

FIGURE 4.17: The curve of ln(J) vs. $\sqrt{E}$ for LDPE samples at room temperature.

Temperature [K]	**Thickness**[μm]	**Permittivity**
293	150μm	2.42
Electric Field [V/m]	**Current Density**[A/m^2]	**Conductivity**[S/m]
6.67E+06	2.28E-09	3.43E-16
1.33E+07	4.20E-09	3.15E-16
2.00E+07	1.17E-08	5.83E-16
2.67E+07	2.74E-08	1.03E-15
3.33E+07	4.97E-08	1.49E-15
4.00E+07	7.58E-08	1.90E-15
4.67E+07	1.12E-07	2.40E-15
5.33E+07	1.52E-07	2.84E-15

TABLE 4.4: The extracted permittivity at room temperature, and the current density and conductivity readings at different applied field.

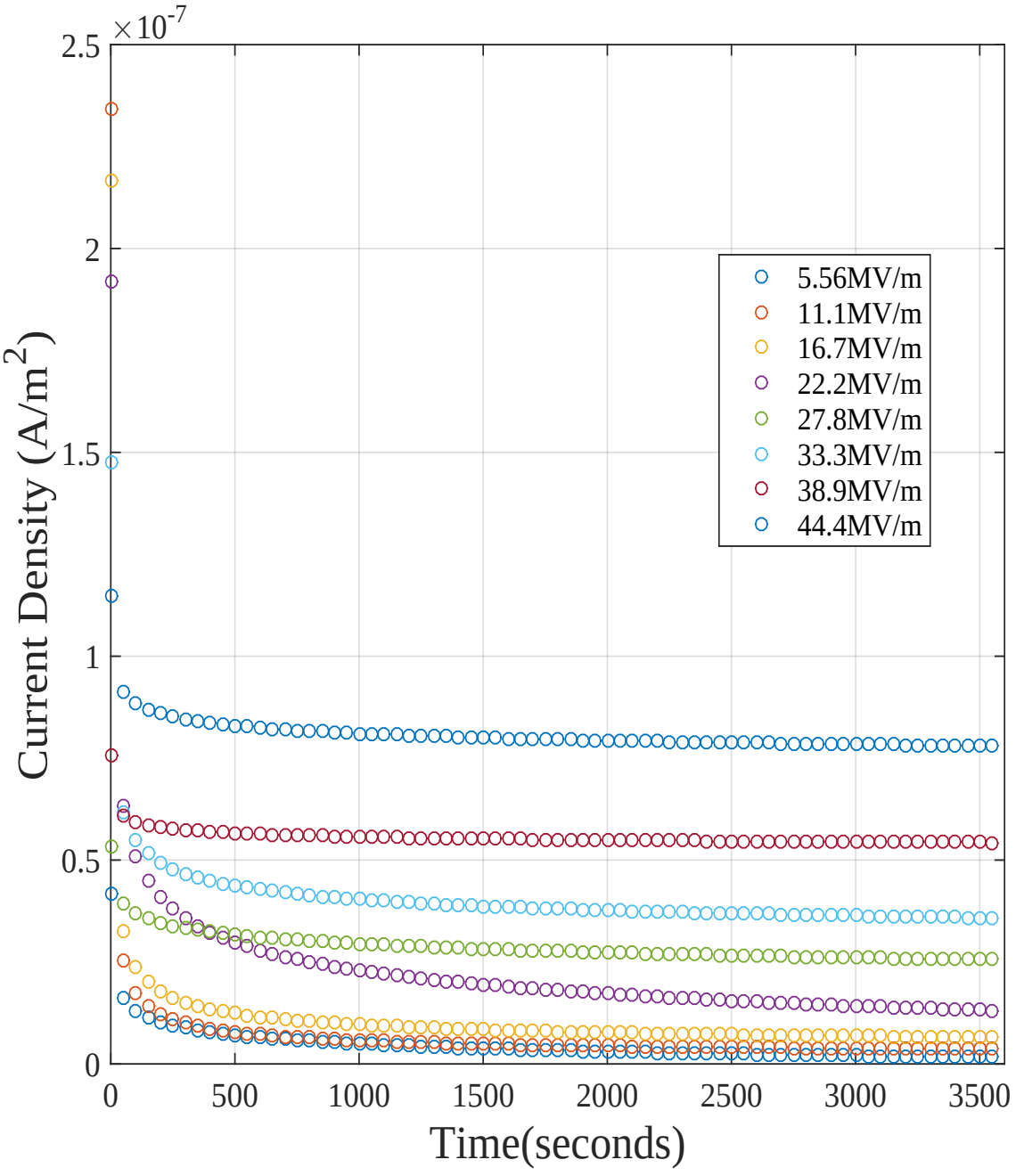

FIGURE 4.18: The current-time characteristic of LDPE at 1,2,3,4,5,6,7 and 8 kV when the temperature is 40^oC.

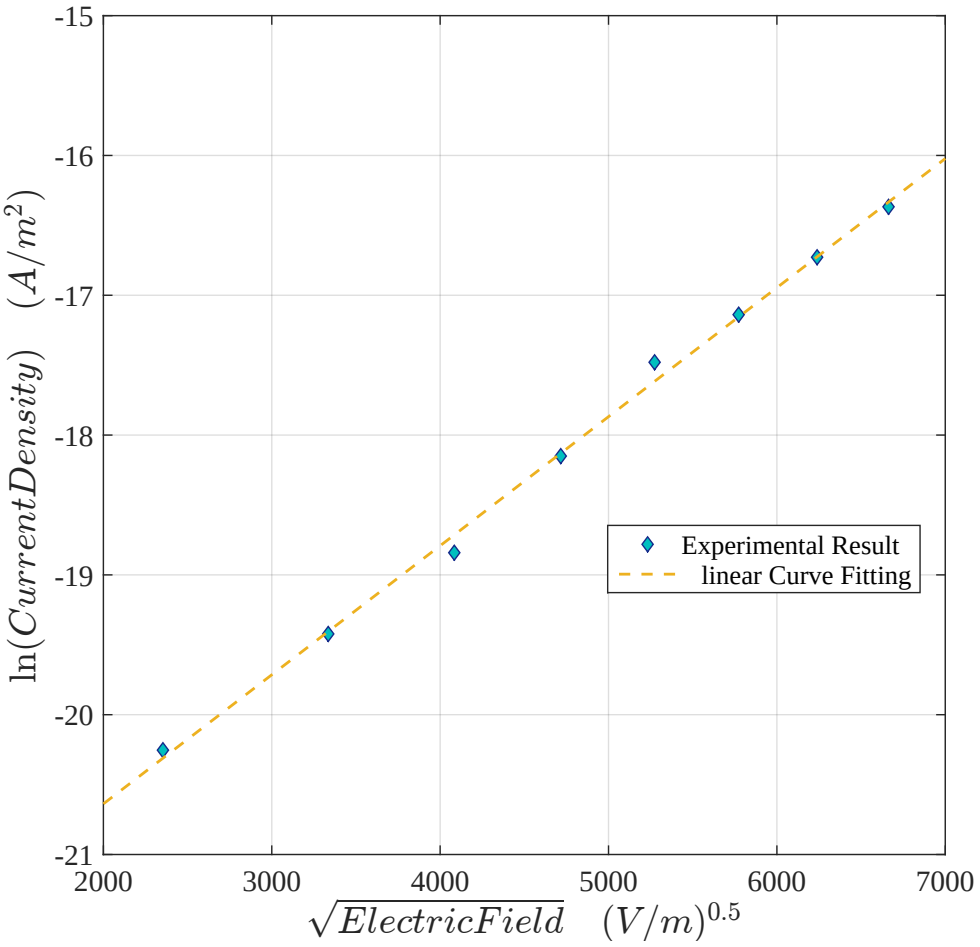

FIGURE 4.19: The curve of ln(J) vs. $\sqrt{E}$ for LDPE samples at 40^oC.

Temperature [K]	**Thickness**[μm]	**Permittivity**
313	$180\mu m$	2.33
Electric Field [V/m]	**Current Density**[A/m^2]	**Conductivity**[S/m]
5.56E+06	1.60E-09	2.87E-16
1.11E+07	3.66E-09	3.30E-16
1.67E+07	6.56E-09	3.94E-16
2.22E+07	1.31E-08	5.88E-16
2.78E+07	2.56E-08	9.20E-16
3.33E+07	3.59E-08	1.08E-15
3.89E+07	5.43E-08	1.40E-15
4.44E+07	7.80E-08	1.76E-15

TABLE 4.5: The extracted permittivity at 40^oC, and the current density and conductivity readings at different applied field.

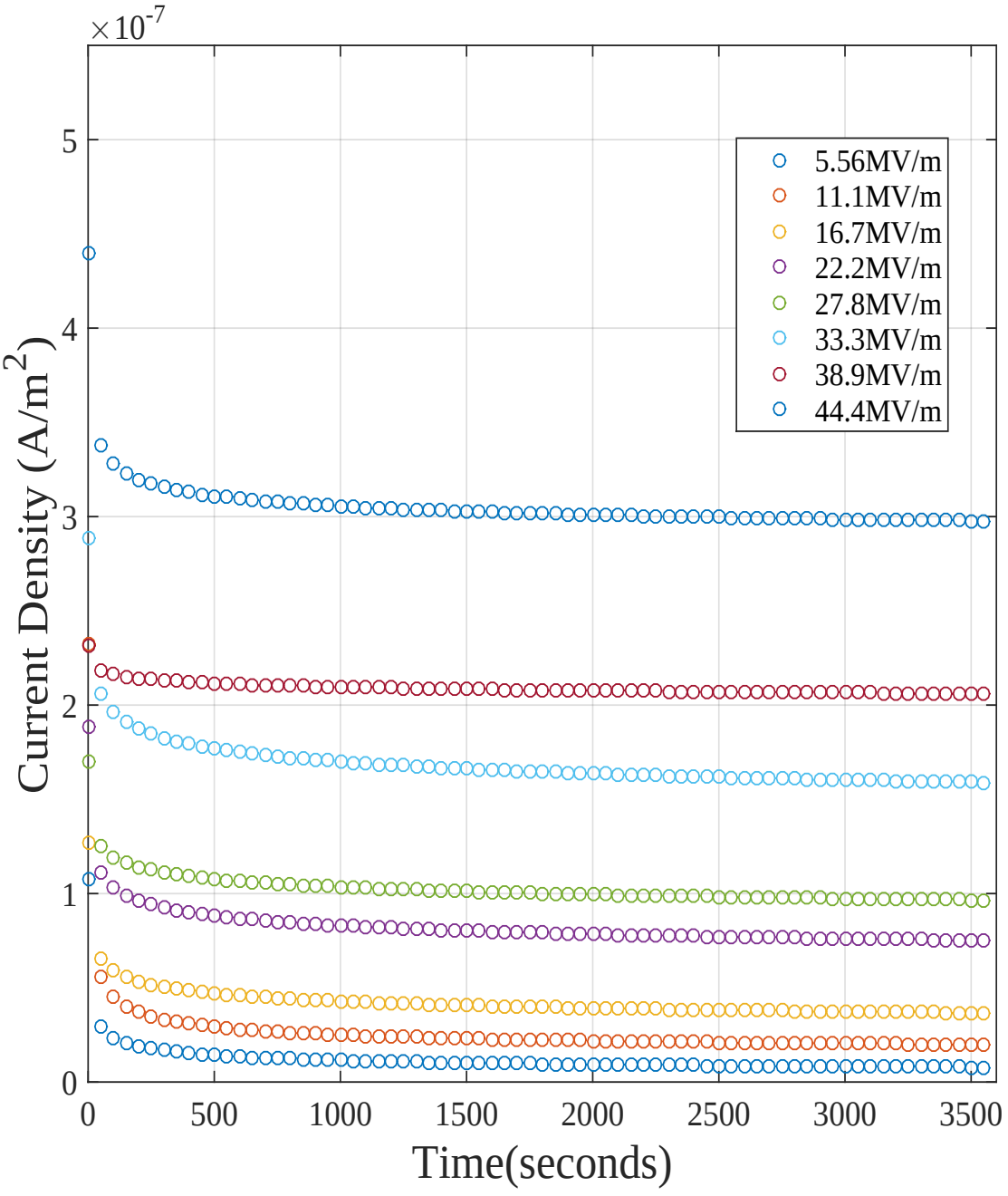

FIGURE 4.20: The current-time characteristic of LDPE at 1,2,3,4,5,6,7 and 8 kV when the temperature is 60^oC.

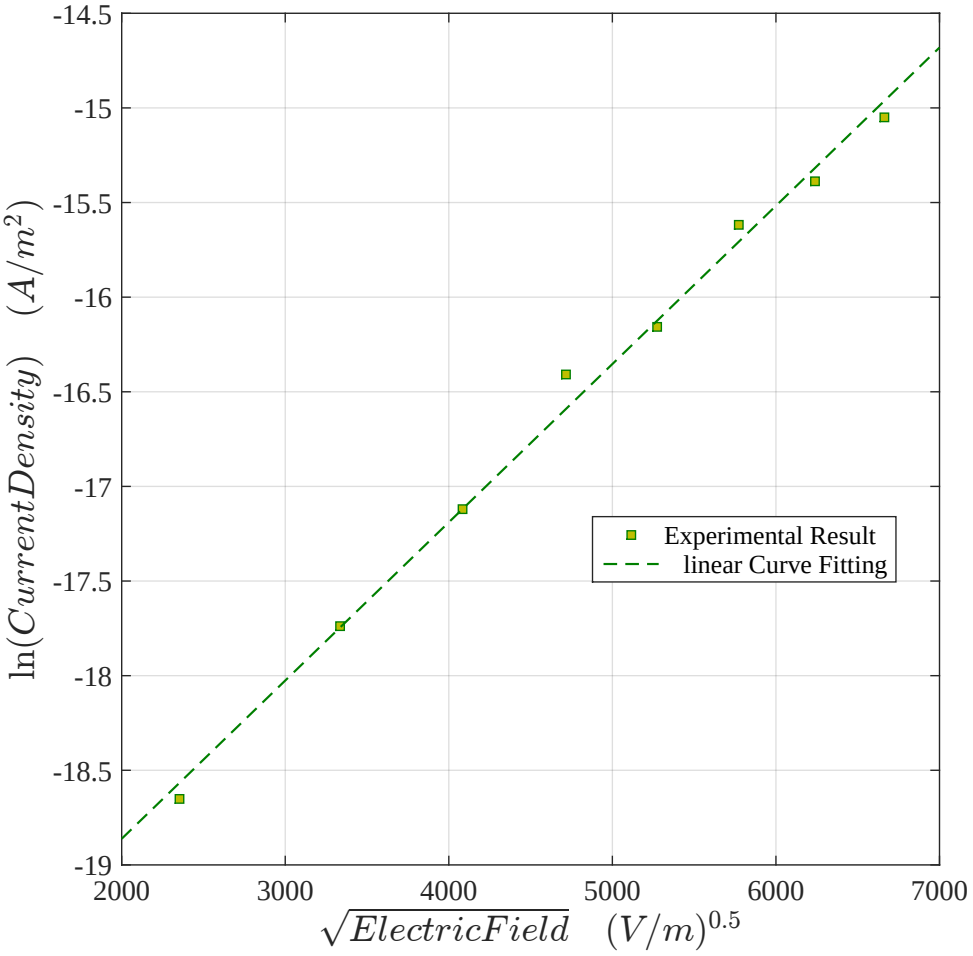

FIGURE 4.21: The curve of ln(J) vs. $\sqrt{E}$ for LDPE samples at 60^oC.

Temperature [K]	**Thickness**[μm]	**Permittivity**
333	$180\mu m$	2.4
Electric Field [V/m]	**Current Density**[A/m^2]	**Conductivity**[S/m]
5.56E+06	7.91E-09	1.42E-15
1.11E+07	1.98E-08	1.78E-15
1.67E+07	3.66E-08	2.20E-15
2.22E+07	7.50E-08	3.37E-15
2.78E+07	9.64E-08	3.47E-15
3.33E+07	1.64E-07	4.93E-15
3.89E+07	2.07E-07	5.33E-15
4.44E+07	2.91E-07	6.55E-15

TABLE 4.6: The extracted permittivity at 60^oC, and the current density and conductivity readings at different applied field.

The conductivity, σ, of LDPE samples can be calculated as the current density, J, and the electric field, E, are know by using:

$$\sigma = \frac{J}{E} \tag{4.51}$$

From the change in the curves of conduction current versus time that are illustrated in Figures 4.16, 4.18 and 4.20 , it is clearly shown that the current density generally decreases as expected, which is as a result of an insulating material under the effect of a DC field. When a DC high voltage is applied to the LDPE sample, the current density from the experiments will move rapidly from an initially high value to a value that is almost fixed. This is the situation of current when the voltage is applied across a sample.

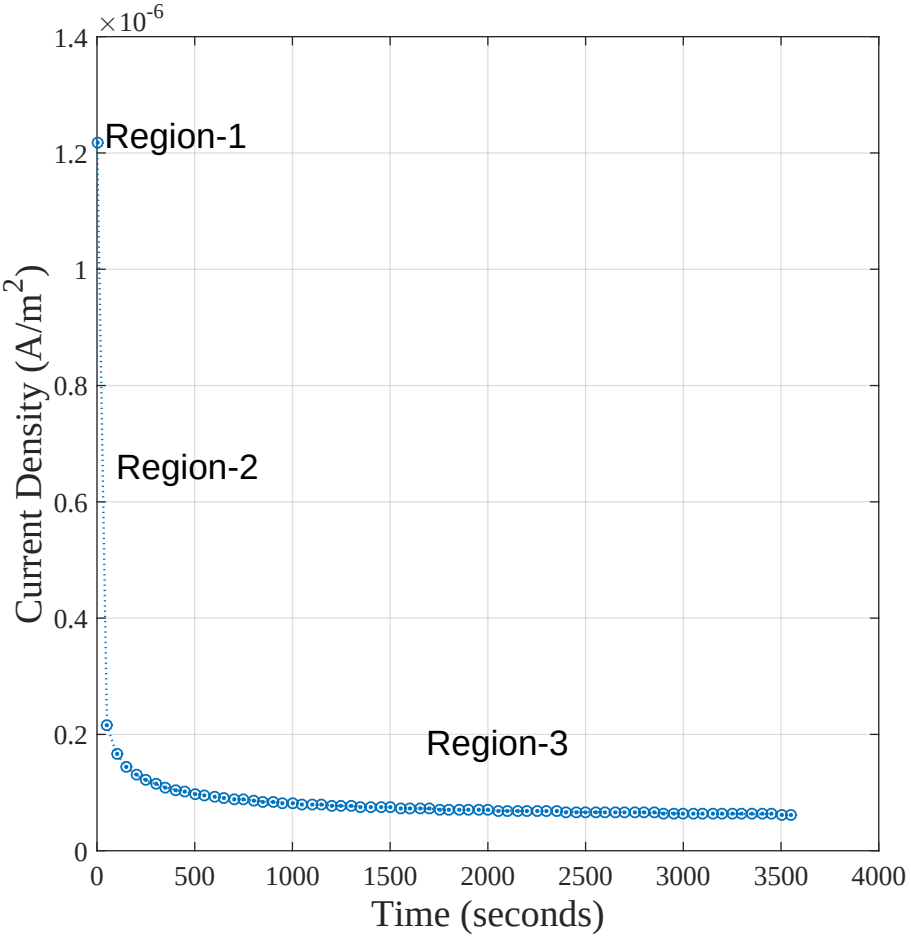

FIGURE 4.22: Representation of the current density parts during the application of electric field.

Generally, the current density versus time can be divided into three parts as shown in Figure 4.22. The first part is classified as a charging current, then a polarisation

current and the last one is a conduction current. In the first part, the charging current is required for charging the capacitance of the dielectric sample. This part starts from the first point of current density versus time on the figure up to the maximum value. Thereafter, the current value decreases rapidly with time. The measurement of the first two part charging current is not important to the exact conductivity measurements as it only distorts the electric current. The polarisation current is caused by the polarisation and accumulation of charges within the LDPE samples under the application of DC voltage. The period of the polarisation current is usually small and will also decrease rapidly with time. Both parts normally do not give the true reading of the electric current through a sample. However, the last part, which is the conduction current, is the selected part for detecting the reading and it is dependent on the applied DC voltage and the resistance of the LDPE sample.

4.5.2 Correlation of DC Conductivity with Space Charge

The curves of current density with time either at room temperature as shown in Figure 4.16, at 40^oC in Figure 4.18 or at 60^oC in Figure 4.20 show that the current density decreases with the duration of applied field. This reduction approaches a very narrow variation after about 3000 seconds. With consideration of this factor, the reading was continued for an additional 600 seconds.

When the DC applied field is increased, the amount of current density increases as well. The transient current from the polarisation stage to the conduction stage may take a little extra time when the DC applied field increases. In addition, the increment of current density becomes more obvious with the increment of the controlled isothermal condition as shown in Figure 4.20.

As shown in the experimental results, the electric current increases with the applied controlled temperature. Where the insulator is to be assumed similar to a capacitor with high resistivity between the two electrodes, the resistivity through the insulator will be affected and will have an inverse proportionality with the electric field and temperature. Due to the reduction in the resistivity, therefore, more electrons can accumulate and pass through the insulation sample which lead to an increment in the electric current value. Comparing Figure 4.18 which shows the conduction result at 40 ^oC and Figure 4.20 which shows the conduction result at 60 ^oC, it is clear to distinguish the effect of temperature on the sample once the electric field is applied. At 5.56 MV/m the current density is at 40 ^oC is 1.6×10^{-9} (A/m^2), while it is about five times the value at 60 ^oC, that is 7.91×10^{-9} (A/m^2). More examples can be extracted from Table 4.5 and Table 4.6. These increments in the conduction currents can be explained by the build up of charges by the injection of carriers from the electrodes to the LDPE samples.

4.6 Summary

Mainly, this chapter identified the applicable mechanism for LDPE samples. The Schottky effect can be applied as an injection mechanism. This process was checked by comparing the extracted permittivity from the experimental results at different thicknesses and temperatures with the normal permittivity. In all cases, extracted permittivity is in the range of 2.33 to 2.42. From this chapter, we can achieve the barrier height value from the intercept part of the linear equation of the Schottky principle.

Through the experimental results at different applied fields and temperatures, it was clear evidence that the conductivity of LDPE sample increases with increasing applied field and temperature.

As the resistivity of the insulation is reduced during the application of a DC field, the probability of successful charge injection and accumulation increase. This observation increases with increment of the controlled isothermal condition.

Chapter 5

Model Parameters Based on Space Charge

5.1 Introduction

Space charge is a concept in which excess electric charges, that are either emitted from the electrodes or ionized, are accumulated in an insulation. It occurs when the rate of charge accumulation is different from the rate of charge leaving the insulation by moving charges or trapped charges. The accumulated electrons may be injected electrons or ions depending on the mechanism of charge transfer. As electric field is a function of electrons, the local internal electric field will be modified and influenced by space charge. This affects the insulating behaviour and causes a faster degradation and premature failure of the material. Therefore, space charge accumulation in the materials is considered as one of the most affected parameters in determining the properties of an insulation system[116, 56].

Space charge is generally formed within an insulator by three main main processes as described in [117]. The first process is assumed when the dipoles are oriented in a homogeneous material and the accumulated space charge occurs only as two peaks near the electrodes with space charge-free in the bulk. The other case is described by immigration of ions when the electric field is applied. In this case, the positive charges migrate to the negative electrode while the positive electrode attracts the immigrated negative charges. As the mobility of the charge is not equal, an accumulation of negative space charge builds near the positive electrode while the contrary occurs when a global positive space charge builds near the negative electrode. This phenomenon of space charge is termed as hetero-polar charges (hetero-charges). The last case is the opposite one to the second case, which is defined as homo-polar charges (homo-charges). This type of space charge formations occurs when charges are injected at the electrodes generate a space charge with low mobility of charges, and the accumulation of charges near each

electrodes has the same polarity of the electrodes. Figure 5.1 shows the main formations of space charge in polymeric materials.

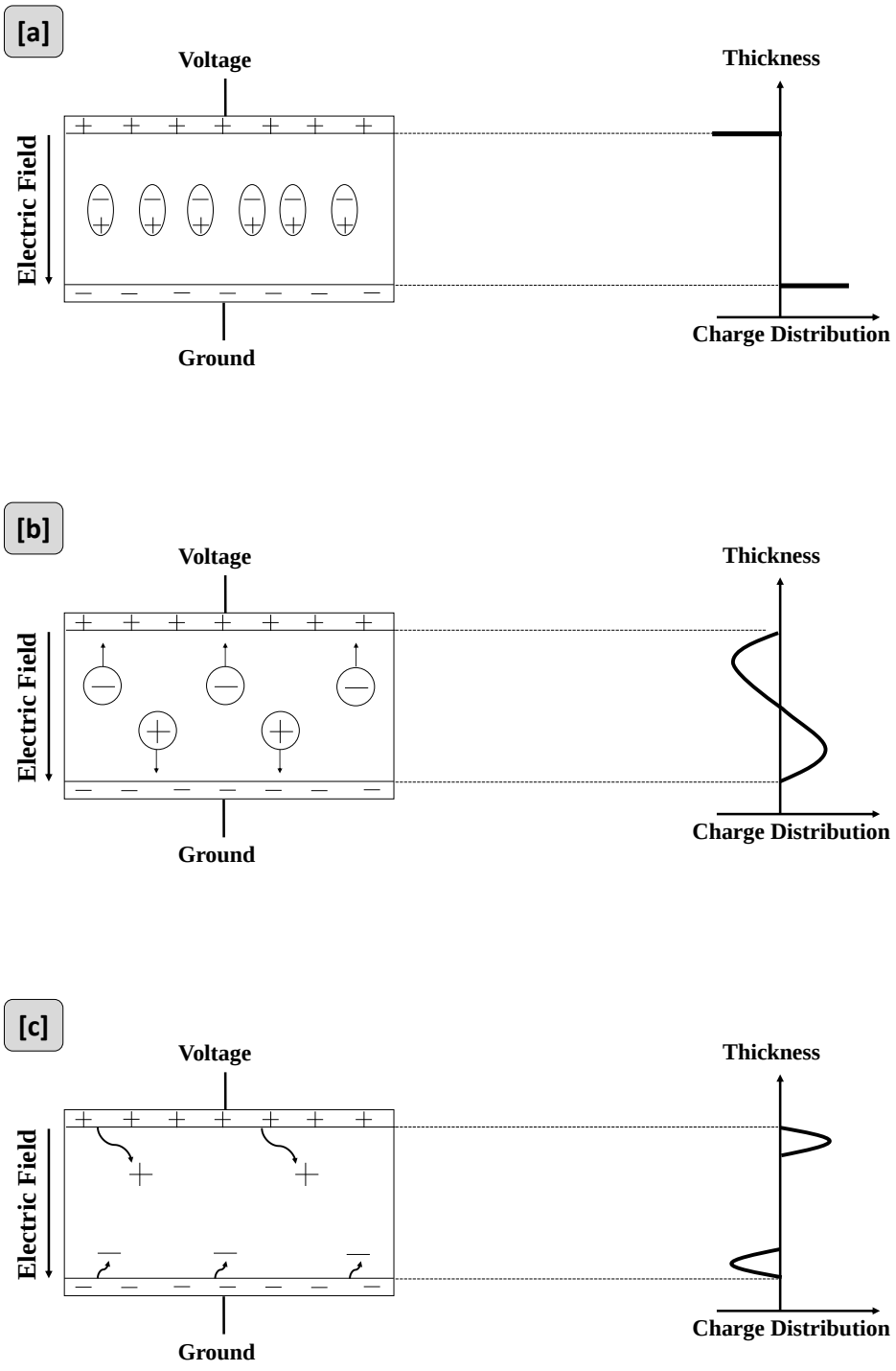

FIGURE 5.1: Space charge formations in an insulating material subjected to an electric field; [a] dipole orientation, [b] hetero-charges and [c] homo-charges.

In the past few decades, several techniques have been developed to measure the space charge distribution in insulating materials [118, 119, 120, 121]. Regarding to the history of space charge measurements, there are two classes of techniques that were recognised; destructive techniques and non-destructive techniques. The destructive techniques were initially used up to the 1980s, such as Dust Figure Method [122, 123]. These techniques have a principle that consists of cutting a test object into small slices, then the space charge is detected at the surface of the cut slice. Also, there are some other techniques that share the same detractive issue to charge distribution such as Thermally Simulated Current TSC [124, 125, 126], and Thermo Luminescence [127, 128].

On the other hand, the non-destructive techniques are more preferable as allow one to obtain a quantitative information about space charge. In the middle of 1970s, Collins [129] introduced a non-destructive technique for measuring space charge which the improvements of the current successful techniques are based on it. The common characteristic is a temporary, and non-destructive displacement of the space charge when a travelling disturbance such as thermal or pressure wave induced between the electrodes. It can be classified into three families; using thermal diffusion[130, 131], using elastic wave propagation [132, 133] or using electrical stress[134, 135].

The most commonly used technique is known as the Pulsed Electro-Acoustic technique PEA, which was developed initially by Takada and Sakai [136] and purified by many researchers. In the PEA system, both the high voltage and acoustic detecting circuits are electrically separated via the ground electrode providing damage protection to the amplifier and oscilloscope in the result of an electric breakdown. Therefore, the PEA system is regarded as the safest technique used for research measurement on cable samples through the application of high voltages. The principle of the Pulsed Electro-Acoustic is based on measuring acoustic waves generated by displacement of charge local regions when an electric pulse is applied to an insulator. Figure 5.2 shows the principle of the Pulsed Electro-Acoustic system [137].

When a voltage pulse is applied to an insulating sample, charge stored in the sample, $q(x)$, will be influenced and moved under the concept of the Coulomb force ($\vec{F} = q\ \vec{E}$). An acoustic wave $p(t)$ will be generated due to the movement of stored charges. The generated acoustic wave will be detected by a transducer which can transfer this signal to an electric signal, and $V_s(t)$ is the transducer output as a voltage signal. The amplitude of space charge is obtained from the wave profile as a function of time which is proportional to the local charge density. The resulted signal is fed to an oscilloscope to amplify it for further analysis. In order to prevent the reflection of the acoustic wave that may cause interference and distortion to the signal, an acoustic absorber is attached to the system to absorb the acoustic wave from the voltage pulse after being detected.

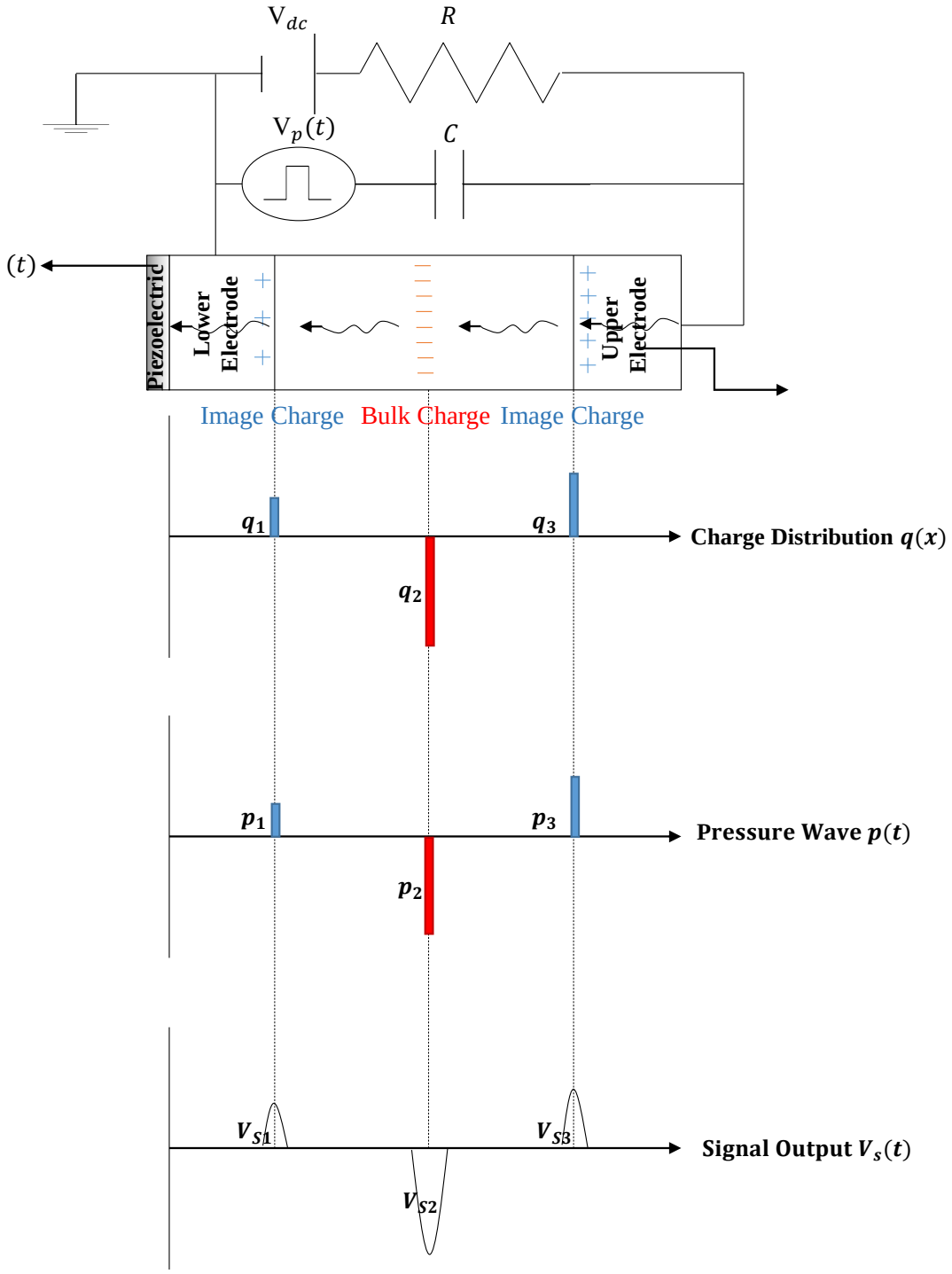

FIGURE 5.2: Basic principle of PEA technique.

5.2 Experimental Setup

The typical PEA system system is shown in Figure 5.3. The components of the system contain top stainless steel electrode, insulating sample which is low-density polyethylene LDPE, aluminium ground electrode, piezoelectric transducer and amplifier. Across the piezoelectric transducer (PVDF), an amplifier is placed there to amplify the signal from the transducer and then fed to a digital oscilloscope (DOS). Since the oscillations of negative and positive charge will be in opposite directions, the PEA system will only present the net accumulation of charge at any position.

A brief explanation about each individual component of the PEA system is described below:

• High Voltage Source:

There are two types of high voltage in the experiment. The first one is a high voltage DC source which is applied when the target of the experiment is to determine the injected charge at volt ON. A high voltage pulse source is the second type which is used to generate pulses to generate acoustic waves. Both sources are mounted in parallel across the two electrodes. In case of breakdown, a protecting resistor is connected in series to the DC supply and a coupling capacitor C is connected to the pulse supply to limit the current. Due to the excitation of space charge by a large pulse voltage, the experiment was performed at low voltage 600 V with a pulse width of 5 ns to generate an acoustic wave. Before any space charge measurement was taken, it is important to calibrate the the charge profile as it is quantifiable. Usually, a fresh sample contains very small amounts of charge existing in its bulk. Therefore, the application of a reasonable DC voltage in the calibration step at which no charge injection occurs and provides signals high enough to overcome the noise will give a charge profile though the bulk. In order to obtain the appropriate value at which charge injection starts for LDPE samples, a graph of applied voltage verses peak induced electrode charge can be obtained. The value of voltage at which the linear relationship starts to diverge is the calibrated voltage value for the test material. This value was observed in the literature by Dao[138] which is around 10 KV/mm.

• Upper and Lower Electrodes:

The electrodes are about a cylinder upper electrode which is connected to a coupling capacitor C and protective resistor R surrounded by a copper screen to avoid flash-over occurrence at application of high field. The lower electrode is flat Aluminium (Al) and its thickness is 10 mm. When an acoustic wave occurs across a sample, there is some reflections which cause distortion to the useful acoustic signal. To avoid these reflections, the considerable thickness of Aluminium plate in the lower electrode does the job. In addition to the previous purpose, the use of the defined Aluminium plat can create a

suitable delay time to avoid the disturbance caused by the firing of pulse source. This time delay is very small (in μs), and able to separate the electric vibration signal because of the pulse source with the useful electric signal representing the space charge in the sample through the digital oscilloscope. Between the electrodes, LDPE samples, that are supplied by GoodFellow Cambridge Ltd, are sandwiched at room temperature.

• Piezoelectric Device:

The most popular transducers, that are used for PEA systems, are Lithium Niobate (LiNbO3) or Polyvinylidenefluoride (PVDF). The purpose of using piezoelectric transducer in PEA systems is to convert the pressure that is produced from the acoustic signal to the electric signal. If the bandwidth of the transducer frequency is limited, then part of the frequency of the acoustic pulse will be lost and the detected output signal cannot obtained the right profile of the space charge in the insulating sample [139]. Although LiNbO3 transducer is sensitive to the temperature, the experiments were performed by this type as the measurements were taken at room temperature. The PVDF transducer has some advantages which make it more popular like easy to be cut, shaped and wide frequency range.

• Amplifier Device:

There are two amplifiers which are used in the PEA system. The first amplifier is connected across the piezoelectric sensor to amplify the converted electric signal,and the second one is to amplify the electric signal provided at the sensor. The amplified signal from the piezoelectric sensor is fed into the second amplifier before displayed onto a digital oscilloscope.

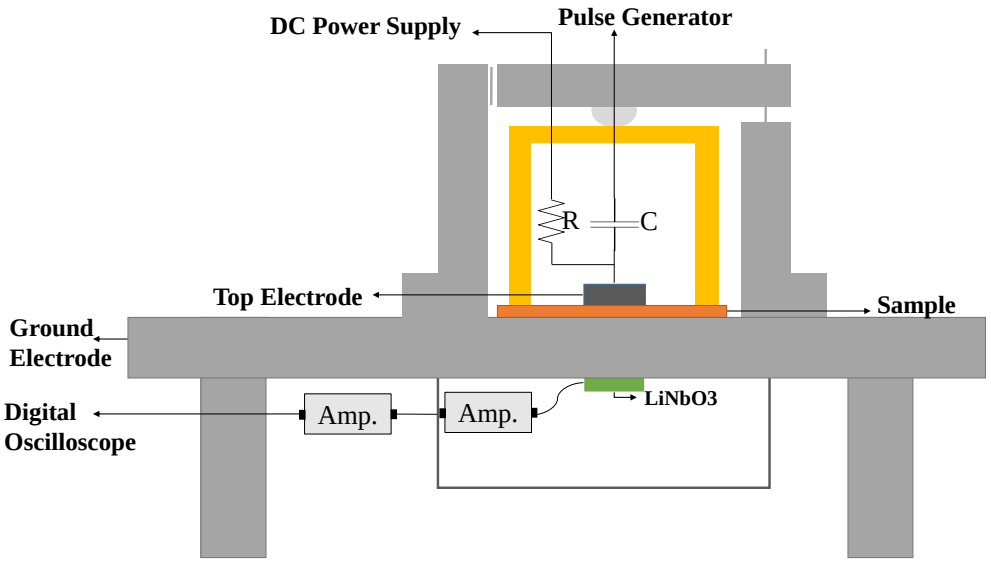

FIGURE 5.3: The PEA experimental setup.

5.3 Results and Discussion

5.3.1 Space Charge Profile

It is important to understand the necessity of finding a method to determine the constant of trapping and detrapping rate in the proposed model in Chapter 3. Therefore, the space charge measurements at decay stage are the most appropriate way to extract the detrapping rate constant, and thereafter calculating the trapping rate constant using two equations at different stressing times as described with more details in Section 5.3.3. Characterising the material parameters without extra unfavourable influences is slightly difficult task as the space charge can be easily influenced. These influences might be due to either the environmental impacts or due to the selected method of measuring the space charge as previously mentioned.

The used system for measuring space charge in this project is the pulsed electro-acoustic (PEA) method. As mentioned early, this method has advantage of being non-destructive which makes it possible for the condition monitoring of the insulating states of power equipments to be carried out conveniently. Figure 5.4 shows the space charge profile of a LDPE sample when the voltage is switched on. Clearly, the magnitude of the anode electrode is seen to be less accurate than the magnitude of the electrode closest to the piezoelectric detector located below the cathode electrode. This is due to the resolution of the PEA system which is limited.

The total injected charge in the material, Q, and the number of the trapped charges per volume, n, can be calculated by using the following equation respectively:

$$Q = \int_0^d |\rho(x)| \bullet S \bullet dx \tag{5.1}$$

$$n = Q/(S \bullet d \bullet q) \tag{5.2}$$

where d is the sample thickness, $\rho(x)$ is the charge density, S is the electrode area and q is the electric charge (1.602×10^{-19} C). The value of $\rho(x)$ is the area between the anode and the cathode which can be calculated using the space charge profile from the PEA results, the surface area S is $\pi \times r^2 = 63.585mm^2$ (radius of the electrode area is 4.5mm) and the sample thickness is d.

Based on the developed ageing model in the thesis, the only possible way of determining the model parameters is at the decay state after the removal of the applied voltage. In this case, the trapping rate is neglected as there is no charge injected. The two parameters that can be extracted from the space charge profiles at the decay are the trapped charge density $n(t)$ and the detrapping rate K_D. A numerical simulation was carried out in order to calculate them.

The kinetic equation becomes:

$$\frac{d_{n_t}}{dt} = -K_D \times n_t \tag{5.3}$$

and its solution is given as:

$$n_t(t) = n_0 \exp(-K_D t) \tag{5.4}$$

where n_0 is the initial condition which can be obtained from Equation 5.7 at the moment when the applied field is removed. Based on the definition of charge density from Equation 5.2, we can rewrite Equation 5.4 in another form as:

$$Q_t(t) = Q_1 \exp(-K_D t) \tag{5.5}$$

Now the solution becomes more easier to be solved through space charge measurements.

5.3.2 Curve Fitting

Curve fitting, also known as regression analysis, is used to find the best fit curve for a series of data points representing the total trapped charges with different times. The curve fitting will mostly produce an equation that can be used to find points anywhere along the curve with limited upper and lower ranges. In this case, it is about to find a curve

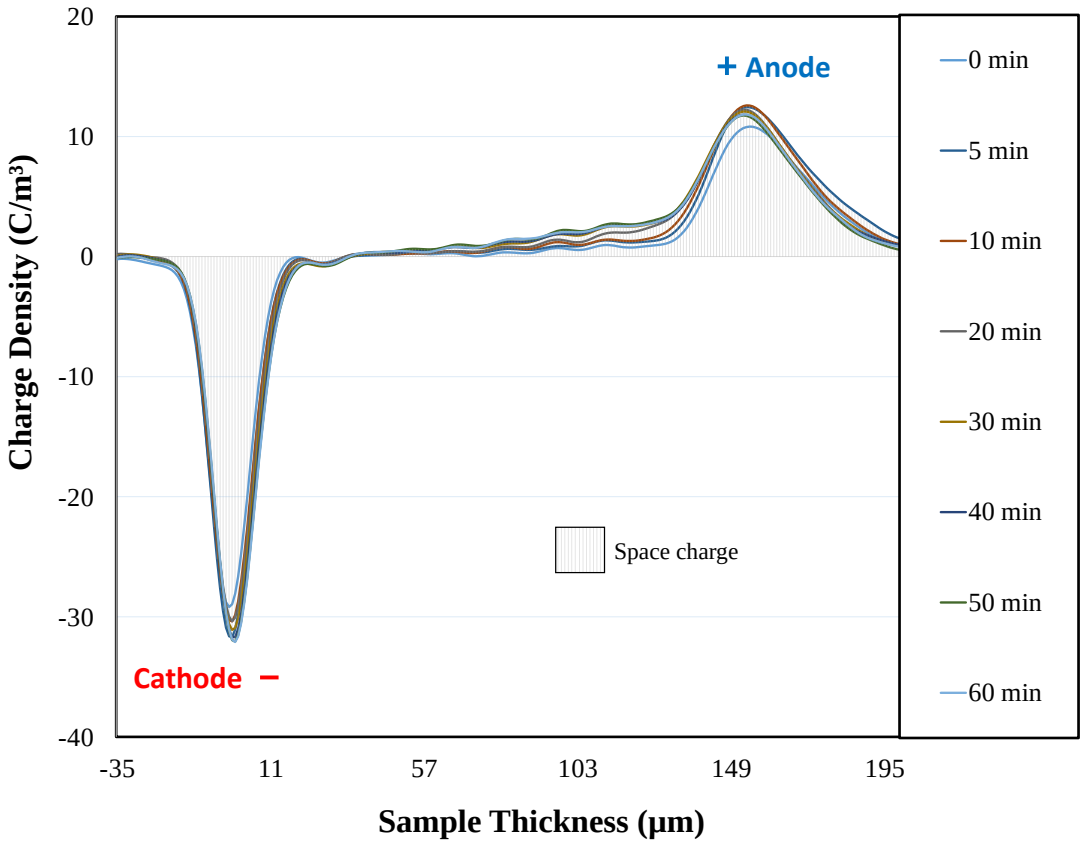

FIGURE 5.4: Space charge profile of additive-free LDPE sample under the application of electric field.

fitting equation similar to the kinetic equation so the values of the model parameters can be obtained based on the experimental results.

The most popular methods to fit data with time is the Least Squares which can minimize the square of the error between the original data and the values predicted by the equation. This method has the advantage of being relatively simple in terms of required computing power and of being well understood. However, the major disadvantage of the Least Squared method is that it is more sensitive to the outlier points in the experimental results. If a data point is widely different from the majority of the data, it can deviate the result of the regression. Therefore, the data should always be examined for precision before fitting.

There are five categories within the least squares fits; linear, polynomial, exponential, logarithmic, and power. The exponential equation was selected due to its similarity to the integrated form of the dynamic equation of the proposed model at the decay state

(Equation 5.5). This function fits a curve of the form:

$$y = a * \exp(-b * x) \tag{5.6}$$

where y represents the amount of charge remaining after a specific amount of time x passes. If the coefficient associated with b is positive, then y represents an exponential decay similar to the case of detrapping. On the other hand, when the coefficient is negative y represents an exponential growth such as trapping with time.

The exponential curve equation is generally used to fit data that increases or decreases at a high rate. The negative data or data equal to zero can not be fitted using the exponential equation. The curve appears as a straight line when plotted on a semi-log graph with a linear X axis.

5.3.3 Extracting and Calculating Model Parameters

From the space charge results in Figure 5.5, the total trapped charge Q and the detrapping rate constant K_D can be extracted by using the curve fitting. This has been done from the Trust-Region algorithm of fitting results in Figure 5.6 which shows the decay curve after being stressed for 20 mins and 25 mins, respectively. Once Q is determined, the trapped charge density n can be easily reached from Equation 5.2. In order to calculate the trap density N_T that exists in the kinetic equation, it is required firstly to perform the decay measurements at two different stressing times due to the two unknown parameters in the solution of the kinetic equation. Mathematically, this system of equations can be solved by substituting one of the equation in the other, and once one of these two parameters solved the second can be solved easily as well.

The total trapped charge density during the trapping and detrapping process for our proposed model is given by:

$$n_t(t) = Q(t)/(S * d * q) = \frac{N_T * K_T}{K_T + K_D}\{1 - \exp[-(K_T + K_D)t]\} \tag{5.7}$$

where S is the electrode surface area of radius equal to 4.5 mm and d is the sample thickness which equals to $150\mu m$. The equation for 20 mins stressing is given as:

$$4.10 * 10^{20} = \frac{N_T * K_T}{K_T + 2.41 \times 10^{-05}}\{1 - \exp[-(K_T + 2.41 \times 10^{-05})20 * 60]\}$$

and for 25 minutes of stressing with the same thickness and field is:

$$3.34 * 10^{20} = \frac{N_T * K_T}{K_T + 2.97 \times 10^{-05}}\{1 - \exp[-(K_T + 2.97 \times 10^{-05})25 * 60]\}$$

Parameter	Symbol	Unit	Value
Electric Field	E	MVm^{-1}	27
Trapping Rate Constant	K_T	s^{-1}	8.7×10^{-5}
Detrapping Rate Constant	K_D	s^{-1}	2.7×10^{-5}
Trapped Electron Density	n_t	m^{-3}	3.7×10^{20}
Trap Density	N_T	m^{-3}	4.3×10^{21}

TABLE 5.1: Results of the parameters of the kinetic equation solution based on the space charge measurements for LDPE additive-free samples of $150\mu m$ thickness.

By dividing the above two equations, the trap density will be cancelled and the solution simplifies as:

$$1.2 = \left(\frac{K_T + 2.97 \times 10^{-05}}{K_T + 2.41 \times 10^{-05}}\right) * \frac{\{1 - \exp[-(K_T + 2.41 \times 10^{-05})20 * 60]\}}{\{1 - \exp[-(K_T + 2.97 \times 10^{-05})25 * 60]\}} \tag{5.8}$$

Therefore, the trapping rate is calculated and then substituting it to reach N_T as the rest of the model parameters are detected. Table 5.1 shows the extracted and calculated parameters that based on space charge measurements.

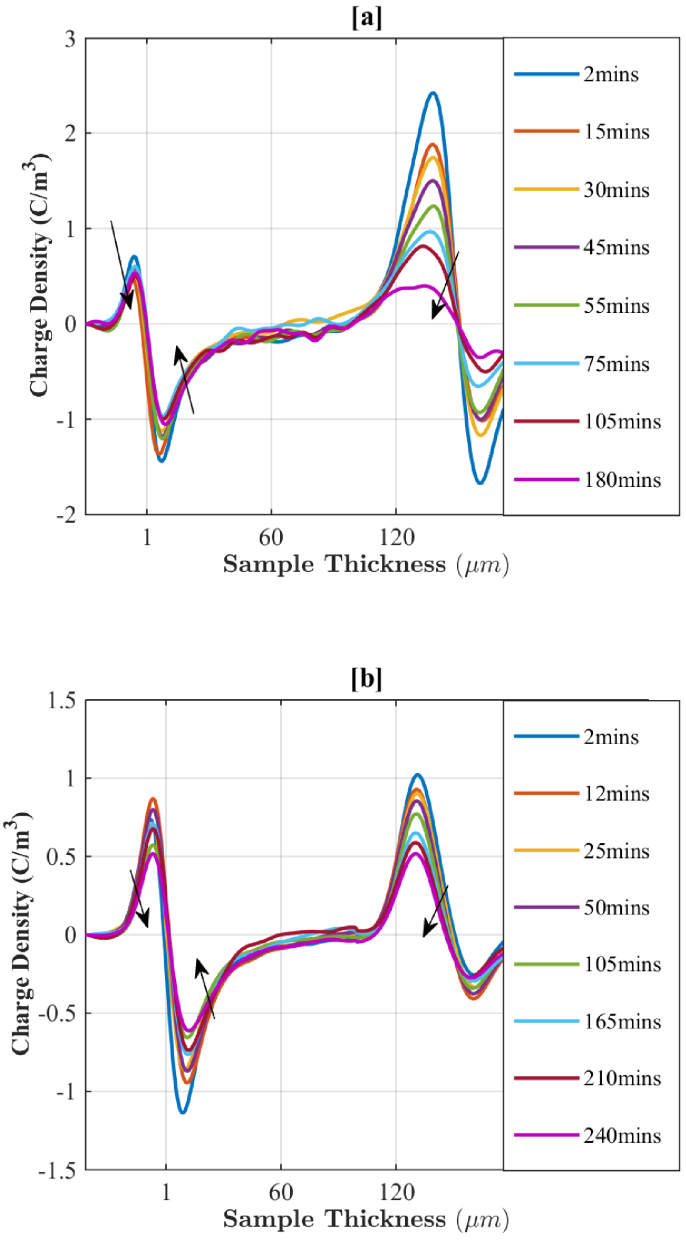

FIGURE 5.5: Space charge profiles after the removal of an applied voltage of 4kV for [a] 25 minutes, and [b] 20 minutes.

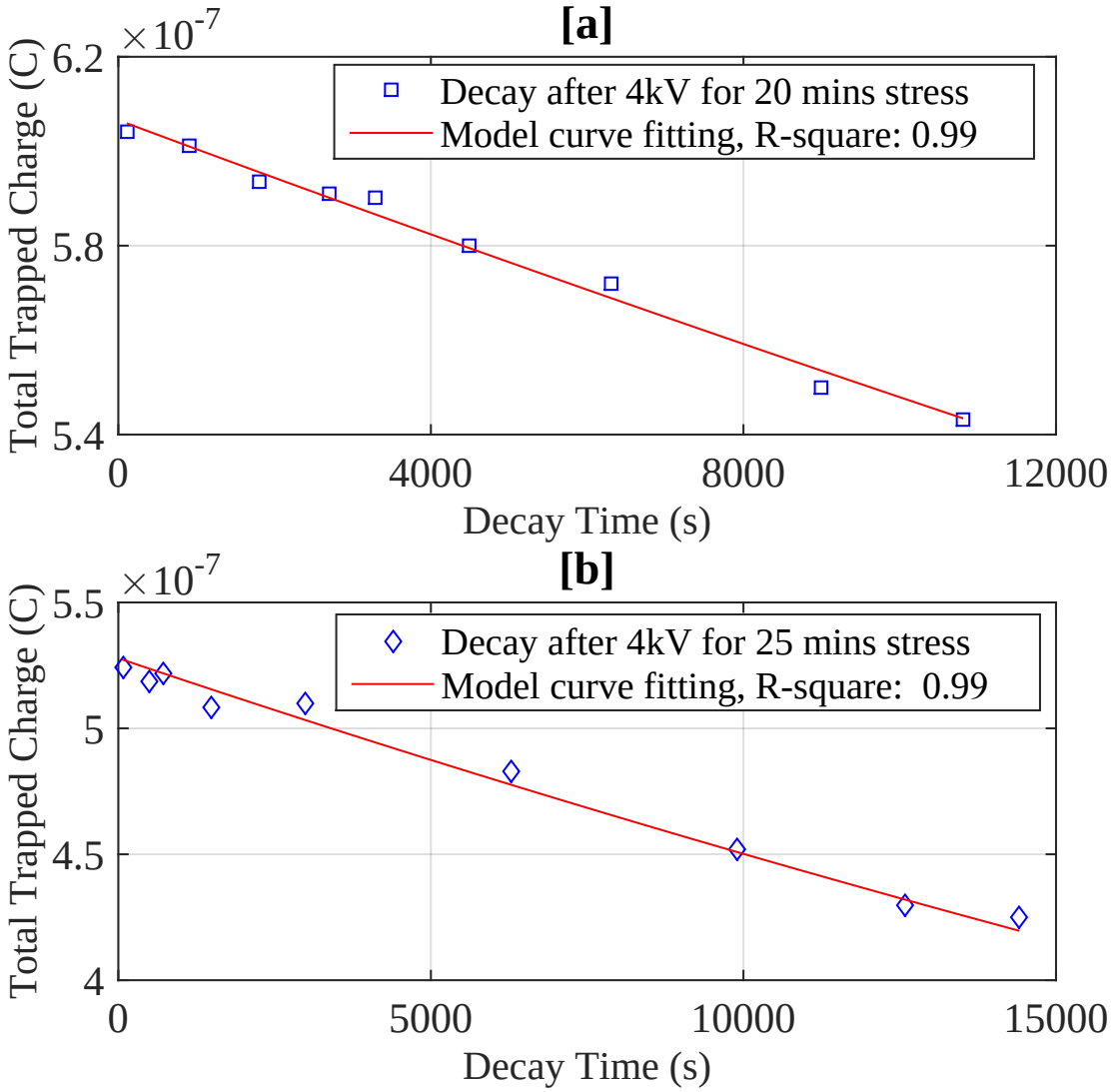

FIGURE 5.6: Decay of the total trapped charges with the exponential curve fitting after being stressed for [a] 20 mins and [b] 25 mins at 4kV.

The trap depth is the minimum energy required to free a charge from a trap. To understand the link between insulation structure and trapping characteristics, it is necessary to be involved in the model. According to Equation 3.17, the trap depth under electro-thermal stress can be determined as:

$$E_T = kT \ \ln\left(\frac{N_c v_{th}\sigma_c}{K_D}\right) + W_m \tag{5.9}$$

The effective density of states for electrons in the conduction band, N_c, is a constant and is equal to $2(2\pi m_e^* kT/h^2)^{3/2}$ where m_e^* is the electron effective mass which is roughly equal to m_e. Its value for polyethylene is in the order of $10^{23} \sim 10^{25} m^{-3}$ as was reported in the literature [140]. The thermal velocity, v_{th}, is a constant as well and is equal to $(3kT/m_e^*)^{1/2}$, which is in the order of $10^5 m/s$. Two parameters need to be estimated to find the depth of the trap: trapping-cross-section and mechanical energy.

Trapping cross-section σ_c, as mentioned above, is characterised based on the ability of trapping centres to capture injected electrons and can be calculated from Equation 3.2. It has been reported by Williams [64] that cross sections can be placed in three categories based on the initial charge state of the centre as: coulombic attractive, neutral or coulombic repulsive centres. The largest capture cross is related to the attractive centre which has a range from 10^{-16} to 10^{-18} m^2. The neutral centre has a range from 10^{-18} to 10^{-22} m^2. Then, the last centre is the repulsive centre which has a cross-section range from 10^{-22} to 10^{-25} m^2. Consequently, the cross-section can be estimated as all the parameters in the current density in Equation 3.13 are known. The value calculated of the cross-section, 6.55×10^{-16} m^2, is similar to the order of cross-section that is reported by Zhou et.al[70]. This trap centre can be classified as a coulombic attractive centre.

According to the induced electro-mechanical energy in an assumed spherical trap, a rough calculation for polyethylene shows that the energy density at 10^9 V/m can reach 2.4×10^5 J/m^3, which is about 1.5×10^{-5} eV per monomer unit. However, this energy is insufficient to disassociate individual monomer units whose strength is of the order of $3.5 - 4$ eV in polyethylene[28]. In order to solve this problem, Hageman et al. [141] have shown that free radicals and breaking bonds in polyethylene can be induced at modest mechanical stresses. The assumption is that c-c bonds strength value reduces to $30 - 40\%$ of the original value due to the relaxation of strained bonds when the stress is applied. The dissociation energy D varies with time and stress according to:

$$D = D_0 \exp\left(\frac{-t}{\tau}\right) \tag{5.10}$$

where τ is the lifetime under stress given by Equation 3.19. At breakdown, $t = \tau$ and $D_0 = 5.6 \times 10^{-19}$ J for (c-c) bonds. Thus, the required energy D to dissociate (c-c) bond is 2.06×10^{-19} J [14]. This energy would be acquired in a polymer chain occupying

a space charge centre with radius of 5 nm. This is close to the estimated value of trap radius that was previously reported by Mazzanti. et al[142]. The nano-cavities in insulation will be compressed by Maxwell stress induced by the electric field. These nano-cavities are much easier to be deformed compared to rigid molecular chains. As mentioned by Crine and Vijh in [28], nano-cavities near chain ends and in the amorphous phase are more likely to be firstly deformed. After detrapping electrons, the released energy entirely deforms the chains and causes chain scission. This leads to induced free radicals and the aging process is considerably accelerated.

These results, therefore, make the estimation of the trap depth easy as the trapping cross-section and mechanical energy is obtained. The trap depth is equal to 3.94×10^{-19} J. From thermodynamic considerations, the trap depth (in Equation 5.9) is in fact similar to the Gibbs free energy [69], which is used in the previous models[14, 28] as a parameter in the Eyring equation. This can be useful for comparison purposes between the developed ageing model in this thesis and the earlier models. The value of the trap depth is close to the activation energy barrier height in the Crine model[45].

5.4 Summary

Despite the pulsed electro-acoustic measurement has advantage of being non-destructive which makes it possible for the condition monitoring of the insulating states of power equipments to be carried out conveniently, the accuracy of the anode magnitude is seen to be less than the magnitude of the cathode which is closest to the piezoelectric detector.

The curve fitting can be achieved either when the power voltage is switched on or off (decay). The curve should yield the exponential regime; growing-up with time at volts on measurements, or decaying with time when the power supply is switched off. Based on the usage purpose, a decision can be made to select the appropriate type. In this research, the decay measurement is the possible method for reaching the model parameters. From the pace charge profile, the detrapping rate constant K_D and the trapped charge n_T can be extracted which assist of reaching the rest of the model parameters.

The anode and cathode charge profile could be classified as hetero-charge, homo-charge or mixed. Existing of home-charge (charges with similar polarity of the electrode) may refer to charge that injected from electrode. On the contrary, hetero-charge occurs due to ionization process in the insulation. Depend on the experimental results, the injection process is the dominant charge to low-density polyethylene samples.

Chapter 6

Electro-Thermal Ageing Experiments

6.1 Introduction

The dielectric breakdown strength also known as electrical breakdown strength is a topic with both great academic and technological interest in electrical insulating materials. The electrical breakdown strength of a specific insulating material is defined as the ability of the material to resist deterioration under the application of electrical stress, since the insulation at this stress can no longer maintain its integrity. In many cases, the breakdown strength will be used as the determining factor in the design of the devices in which the insulation is to be used. The breakdown strength is usually expressed as the applied voltage stress per the thickness of the stressed insulation as kV/mm or in standard unit v/m.

In the literature, the concept of intrinsic strength has been discussed. It is defined by the characteristics of the insulating material itself when it is pure and defect-free. However, this situation cannot be experimentally accomplished due to the impossibility of insulation to be defect-free. In laboratory work, a thin sample is used and there is a small chance for defects to exist in the sample. It is noteworthy that there are other external factors that can cause some effects to the measurements of breakdown strength of an insulating material. In this regard, several theories associated with breakdown mechanisms that may contain thermal, electrical and mechanical as well as chemical parameters have been proposed [143, 144].

There are wide variety of different testing methods and electrode geometries that are used in laboratory for testing the breakdown performance of insulations. The comparison of breakdown strength can be performed between two results under the same conditions

once the manner of testing is known. There are two types of testing methods that are commonly used; the constant-stress test and the progressive-stress test.

The progressive-stress test is popular with the advantage that the results can be obtained in short time. Furthermore, it has been found that the variation in the breakdown results is less influenced when compared to the constant stress [145]. This type of measurements is more popularly used in insulations that have additive nano-composite to compare the breakdown strength within the same material (additive-free), or others [146].

Despite the long-time that is needed for the constant-stress test, it is still the appropriate method of measurement for ageing mechanisms in insulations. It has been used to verify the ageing models of polymeric material[13, 29, 30] and one of its disadvantages is it requires a critical control of electric field as a little variations in the applied field may lead to a significant variation in the time to breakdown.

In regards to the electrode geometry, the needle plate arrangement is continuously use in experiments due to its ease of implementation. At the tip of the needle, electric field enhancement may cause a premature failure to the sample. In addition, the needle electrode could lead to voiding problems when the needle is inserted into the sample. In this case, the measurements of breakdown strength could be related to the effect of the geometry type more than the properties of the insulation itself. However, parallel plate electrodes can be used for breakdown strength, but the problem is that the enhancement of electric field at the edge may lead to a flashover[147]. In order to avoid this problem, an electrode arrangement that can reduce the effect of edges, such as two ball-bearings, can be used provided that the ball-bearing curvature radius is much greater than the sample thickness. Therefore, flashover at the edge of the sample is reduced as the edges of the electrodes are away at a great distance from the sample. This is much better than the case of the needle electrodes.

6.2 Breakdown Categories

6.2.1 Thermal Breakdown

When an insulation is subjected to an electric field, there is an electrical power dissipation that causes heating to a part of the insulation. At above a critical temperature, a catastrophic failure may occur directly or indirectly in the insulation, and this is known as a thermal breakdown.

As the current flows partially through an insulator, electrical power will be dissipated which, therefore, leads to an increase in its temperature. In case the breakdown has not occurred, then the increment in temperature will continue until the steady-state heat flow is set up when the cooling of the insulation 'i.e. self-control' is equal to the

electrical power dissipation. Once the breakdown occurs in any part of the insulation, this can be related to either the physical changes in the insulating structure which reduce the breakdown strength below the applied field (such as melting the insulation); or the conductivity of the insulation that increases its electrical power dissipation, hence causing a further increment in temperature which leads to thermal runaway. The first case is referred to as destructive breakdown, and the second is thermal instability [148]. This is clearly shown in Figure 6.1; [a] represents power versus temperature at three different applied voltages $V_1 < V_2 < V_3$. The straight line on the graph illustrates the rate of heat loss from the insulation system as a function of temperature. This is assumed to be Newton's law of cooling which is given as:

$$\frac{dT_{insulation}}{dt} = -C\ (T_{insulation} - T_{ambient}) \tag{6.1}$$

.

When V_1 is applied at the ambient temperature, T_0, there is no cooling to the system. Therefore, the electrical power dissipation after a period of time can cause an increment to the system's temperature. At temperature, T_1, the electrical power dissipation is equal to the rate of cooling and thus the steady state is reached. The system would cool down as the cooling rate exceeds the electrical power dissipation. If the critical temperature (breakdown temperature) is less than T_1, then the breakdown would occur after applying the voltage, V_1, and before reaching the steady state. This corresponds to the destructive breakdown. However, if the breakdown did not occur at this temperature and voltage V_2 is applied, then the stabilization temperature would be higher at T_2. This temperature is metastable, and the power dissipation would increases faster than the cooling rate when the temperature was increased and lead to thermal runaway breakdown and this corresponds to the thermal instability. T_2 refers normally to the highest temperature that irreversible damage could occur. The V_3 is always classified as unstable voltage and, therefore, temperature remains continues to increase until breakdown level is achieved.

From Figure 6.1 [b], the steady state temperature of the hottest part of the insulation is illustrated at various voltages corresponding to Figure 6.1 [a]. If the hottest part at T_1 exceeds the critical temperature, then destructive breakdown occurs. If, however, the breakdown does not occur, then the voltage will increase up to V_2, and consequently temperature increases as well to T_2. When the voltage V_2 increases even slightly to $V_2 + \partial V$, then the temperature increases unlikely until breakdown occurs (thermal instability)[149]. There is no steady state at V_3.

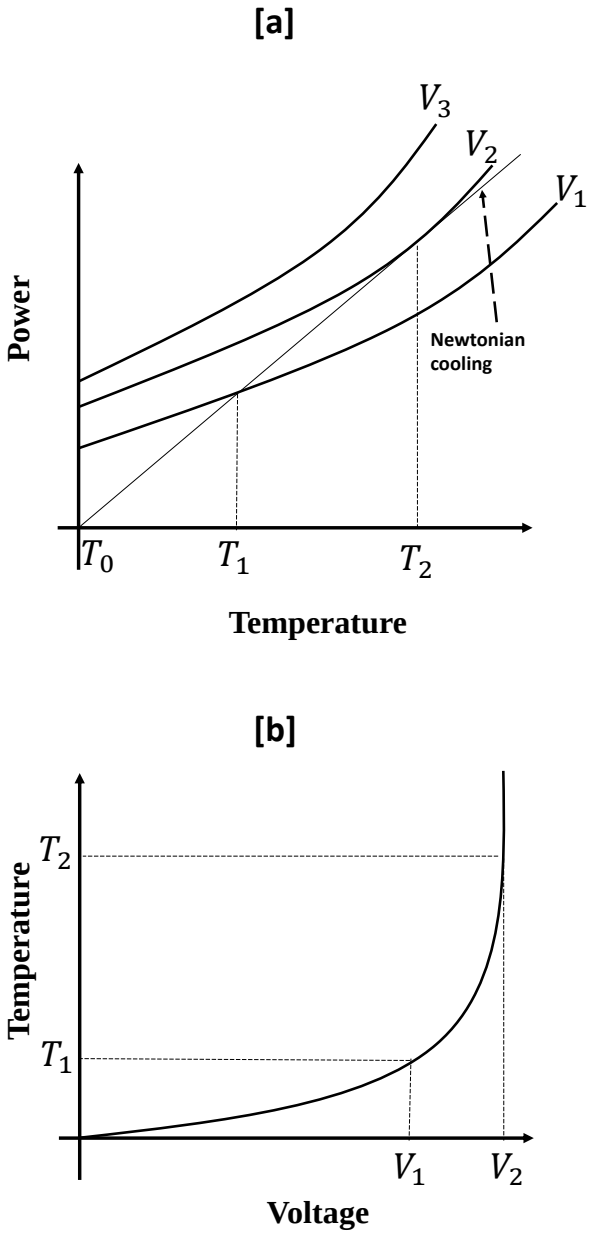

FIGURE 6.1: [a] A representation graph of heat input rate versus temperature under the effect of three different voltages, [b] shows the variation of steady state temperature with voltage at the hottest part of the insulation.

6.2.2 Electromechanical Breakdown

A notice on breakdown strength has been detected by Stark and Garton [150] that was dropped off when temperature was increased for many thermoplastic materials. They speculated that this reduction was due to a mechanism which is known as electromechanical breakdown. It occurs often when the mechanical compressive stress on the insulation that is resulted from the electrostatic attraction of the electrodes (or more precisely by electrostriction) exceeds a critical value of the dielectric elasticity. From

these two stresses for the equilibrium situation, the electromechanical breakdown voltage between two parallel-plates dielectric slab can be evaluated as:

$$\begin{gathered} electrostatic \quad compressive \quad stress = opposing \quad elastic \quad stress \\ \frac{\varepsilon_0 \varepsilon_r}{2} \left(\frac{V}{d}\right)^2 = Y \ln\left(\frac{d_0}{d}\right) \end{gathered} \tag{6.2}$$

where Y is Young's modulus of elasticity, d_0 is the initial thickness of the insulation, and d is the reduced thickness when the voltage, V , is applied.

The general form of the electromechanical breakdown voltage, V_m, is:

$$V_m = d_0 \left[\frac{Y}{2.72\ \varepsilon_0 \varepsilon_r}\right] \tag{6.3}$$

The electromechanical breakdown is likely to be common mechanism in polymers such as polyethylene, in which hot spot formation through Joule heating has been observed in [151]. As thermal runaway process does not occur in some polymer, it is likely that the reduction in Young's modulus could rise the chance of the electromechanical breakdown to occur. Another study [152] suggested that the breakdown may be combined between thermal and electromechanical. The local field could lead to increase the local temperature and consequently reduces Young's modulus.

6.2.3 Electronic Breakdown

With regards to electronic breakdown, the applied field to an insulator causes unstable magnitudes of either the number or the energy of the electrons. Eventually, this cause destruction to the lattice which can cause breakdown. This category can be divided into two types; intrinsic, and avalanche. At a very high stress field, a large number of electrons can cross the valance band to the conduction band. If this stress remains for a while, then huge electrons will be available in the conduction band. Thus, the conduction current caused by these electrons increases rapidly and leads to which is known as an intrinsic breakdown.

Avalanche concept was initially developed for a polar crystal insulation. When electrons at the cathode acquire sufficient energy from the internal field, then will be able to collide with other atoms/molecules and lead to produce more electrons and holes. Assume these electrons produced further electrons, an avalanche of n electrons will be produced in n generation. This process will be repeated until the propagation of electrons is built across the insulation. It is represented in Figure 6.2.

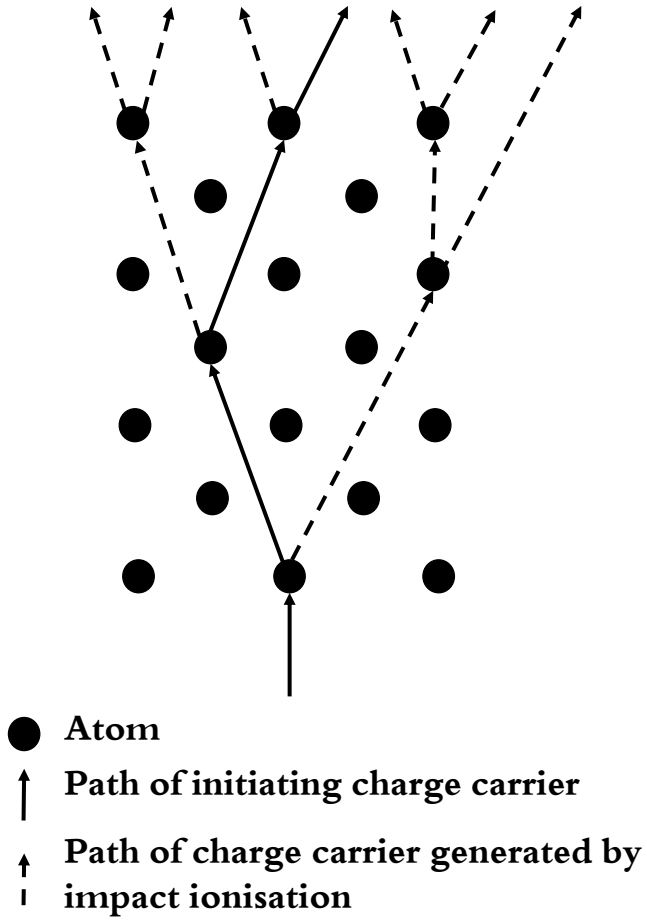

FIGURE 6.2: Scheme of avalanche breakdown.

6.3 Weibull Distribution Analysis

The endurance of insulating materials can be described usually by applying the two-parameter Weibull distribution function which is also known as the extreme-value distribution. It is commonly used in the data analysis for both types of breakdown measurements (i.e. time-to-breakdown from constant voltage or breakdown voltage from progressive-stress tests)[153]. The cumulative distribution of the two-parameter Weibull function is:

$$F(x) = 1 - \exp\left[-\left(\frac{x}{\alpha}\right)^{\beta}\right] \tag{6.4}$$

where x is the measured variable which is usually time to break down or the breakdown voltage, $F(x)$ is the probability of failure at a voltage or time less than or equal to x, α is the scale parameter and it is positive, β is the shape parameter and it is positive as well. The probability of failure, $F(x)$, is zero when $x = 0$. Furthermore, this probability increases continuously as x increases, and eventually reaches certainty

at $F(x) = 1$. In regards to the scale parameter, α illustrates the time to break down or the breakdown voltage at the cumulative failure probability of 63.2% (that is 1 – $1/e$ where e is the exponential constant). This value is analogous to the mean of the Normal distribution[154]. The unit of α is similar to the the unit of x. The spread of time to break down or voltage data is represented by β. The large value of β means that there is a small variation in the range of the data.

To use the two-parameter Weibull distribution on a probability graph paper, the measured data is plotted on the horizontal axis which is scaled logarithmically. On the other hand, the probability of breakdown is plotted on the perpendicular axis which is also non-linear. The axes are scaled so the plotted data should yield to follow a straight line. The data needs to be ordered from the smallest to the largest value, and the cumulative probability of failure, $F(x)$, has to be performed at each point. By using the Maximum Likelihood Estimation (MLE), we can fit a straight line through the data points to give better estimations for α and β. The used program for the analysis of this study is ReliaSoft Weibull 7++ and Matlab. The data of breakdown were represented between the two-sided 90% confidence bounds.

Ross [155] achieved a good, simple, approximation for the most likely probability of failure. It is:

$$F(i,n) = \frac{i - 0.44}{n + 0.25} \times 100\% \tag{6.5}$$

where i is the progressive order of failed tests and, n is the total test number of breakdown times or voltages in order from smallest to largest. This method has been proven as the best approximation of cumulative failure probability [156]. There are alternative methods that can also be used such as the mean rank method, where:

$$F(i,n) = \frac{i}{n+1} \tag{6.6}$$

and symmetrical cumulative distribution function method, which is given as:

$$F(i,n) = \frac{i - 0.5}{m} \tag{6.7}$$

However, the expression 6.7 has significant systematic errors into graphical probability estimations of the distribution's parameter and, in addition, is not consistent with the technique of the MLE. Figure 6.3 shows an example of a Weibull plot with clearly explained the upper, lower and best fit lines.

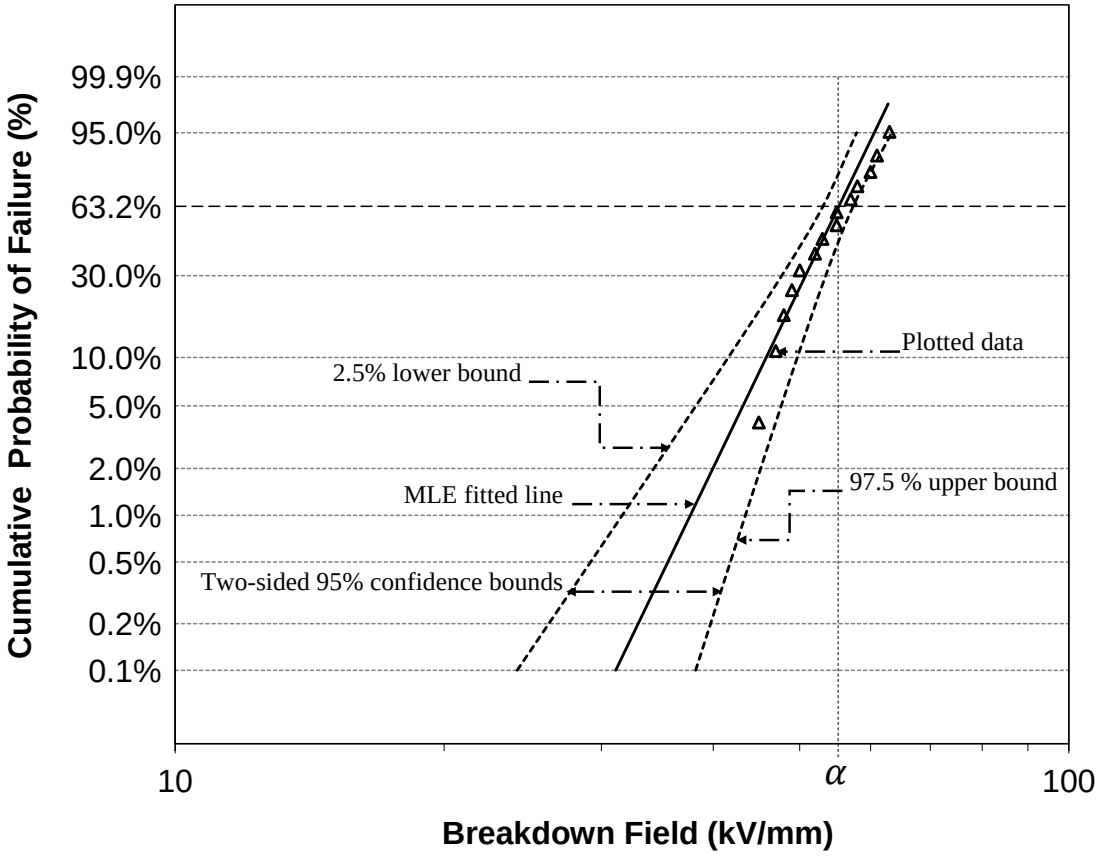

FIGURE 6.3: An example plot of Weibull of MLE fitted line and two-sided 95 % confidence bounds.

6.4 Experimental Procedure

Low-density polyethylene samples of $150\mu m$ were used to investigate the breakdown time at 80^0C as a fix ambient temperature with variant fields from 60-140 MV/m. The required time to break samples has to be considered when the voltage is applied to the samples. In addition, because of only one power supply was available, a novel approach has to be applied so the samples can be stressed at different electric fields at the same time. Therefore, a new breakdown system was built for this purpose which involves the concept of voltage divider of three roofs; each roof has 10 test cells stressing under the same electric field.

The available electrodes for the long-time measurements of multi-test cells under the effect of temperature, are the upper and lower cylindrical electrodes with diameter of 15 mm and 24 mm respectively. Both electrodes have edges rounded to 3 mm. As mentioned earlier, this type of electrodes can cause flash-over at the edges and becomes more obvious in the presence of high temperature. To avoid this problem, it has been considered that a limit of applied voltage that can keep the measurements in the safe-side. When the breakdown occurred through a sample, either one or both electrodes may have a black spots which could affect the next measurements from the same electrodes. Therefore, both electrodes were cleaned and polished once a test-cell has a broken sample.

A Spellman power supply which can generate up to 60 kV was used. A stop-clock was connected to the power supply to monitor the time to breakdown for the samples. This clock starts calculation once the power supply is ON, and stops at breaking a sample as there is no voltage supplied. When a sample is failed, the high voltage tester is the method that used to detect the failed sample. Figure 6.4 shows the breakdown system that has been used for these measurements.

At the beginning, the oven needs to be closed to heat the system up to the experimental temperature. By using a sensitive temperature measurement, the ambient temperature can be reached in maximum of 15 minutes. At this stage, the electric field is applied to the samples. When the failure state occurs to any sample in the oven, the power system is switched-off. In order to detect the failed sample, a High-Voltage Tester is used after disconnecting the ground from each test-cell. One of the High-Voltage Tester terminal is connected to the top electrode and the second is grounded. At each time of a test-cell investigation, the test cell is grounded. If the sample is broken, then the high voltage in the Tester is drop-off to zero. This means this investigated sample is failed. Once the time-to-failure for the broken sample is recorded, the electrodes are polished and cleaned to be ready for a new investigated sample.

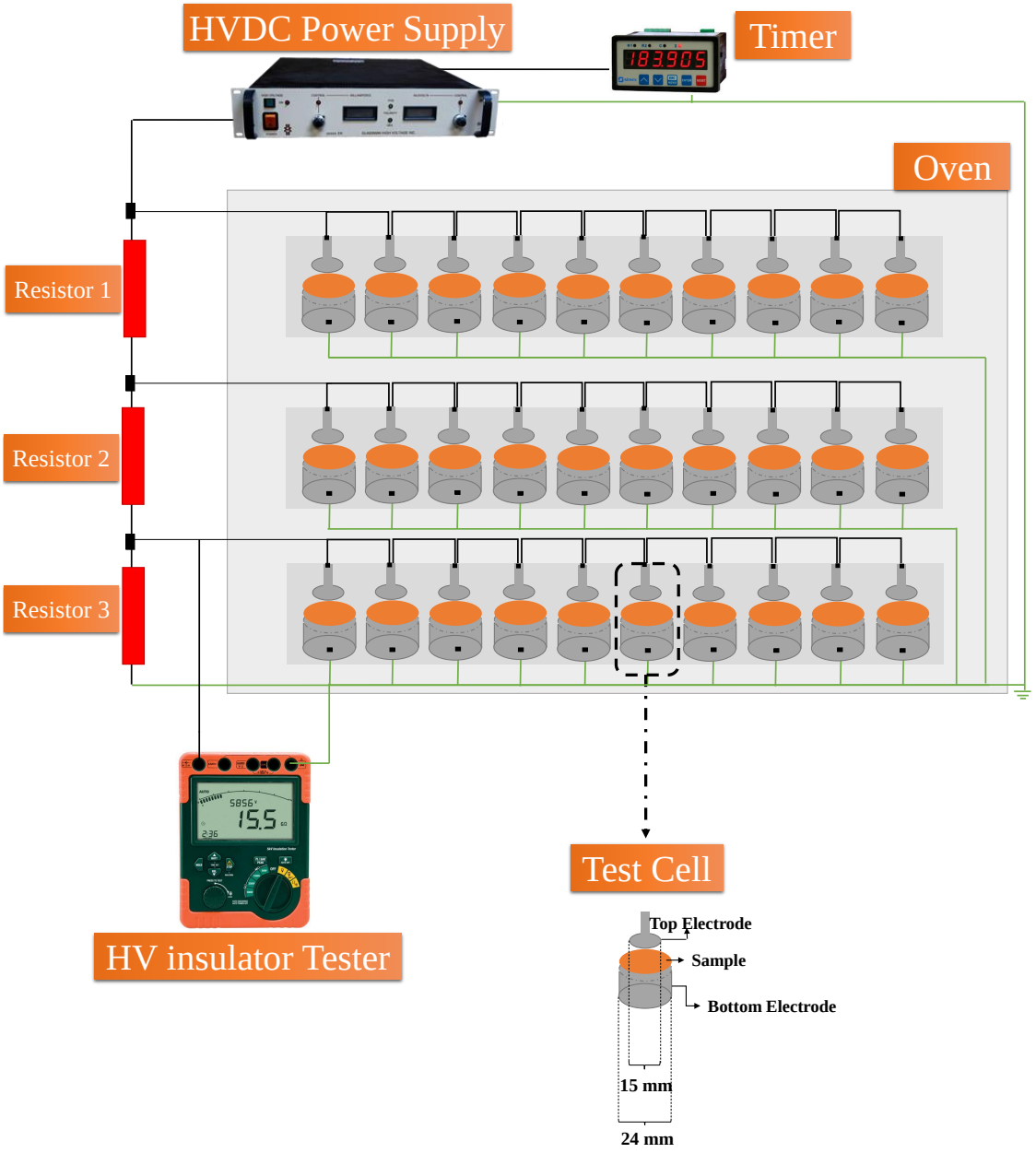

FIGURE 6.4: The developed breakdown system which is designed based on voltage divider principle

6.5 Results and Discussion

6.5.1 Weibull Distribution Analysis

The plots of the probability failure, $F(i, n)$, versus the time to breakdown for all different fields are represented in Figures 6.6-6.12. The scale parameter of the Weibull distribution function can provide the characteristic lifetime at the applied field, and is estimated from these plots. The best fit lines (bold line) are drawn in the figures with the value of 95% confidence intervals for each measurement.

Looking to the scale parameter of the time to breakdown,α, it increases gradually when the applied field is reduced. For instance, the characteristic lifetime to break a LDPE sample at 140 MV/m is around half day while it is approximately the double at 120 MV/m. Therefore, a longer lifetime requires lower fields and vice versa.

It seems to be complicated to decide what mechanism the sample was failed from the Weibull distribution analysis since there is no physical parameters behind the Weibull function. However, the developed model in Chapter 3 is proposed to explain the ageing mechanism, and the results in this chapter are mainly to compare the model expectations with the experimental results under the combination of electrical and thermal stresses. It is worth to mention the cause of space charge to breakdown which was reported by the authors like Fukuma et. al. [157] as is assumed to be a cause in the developed model.

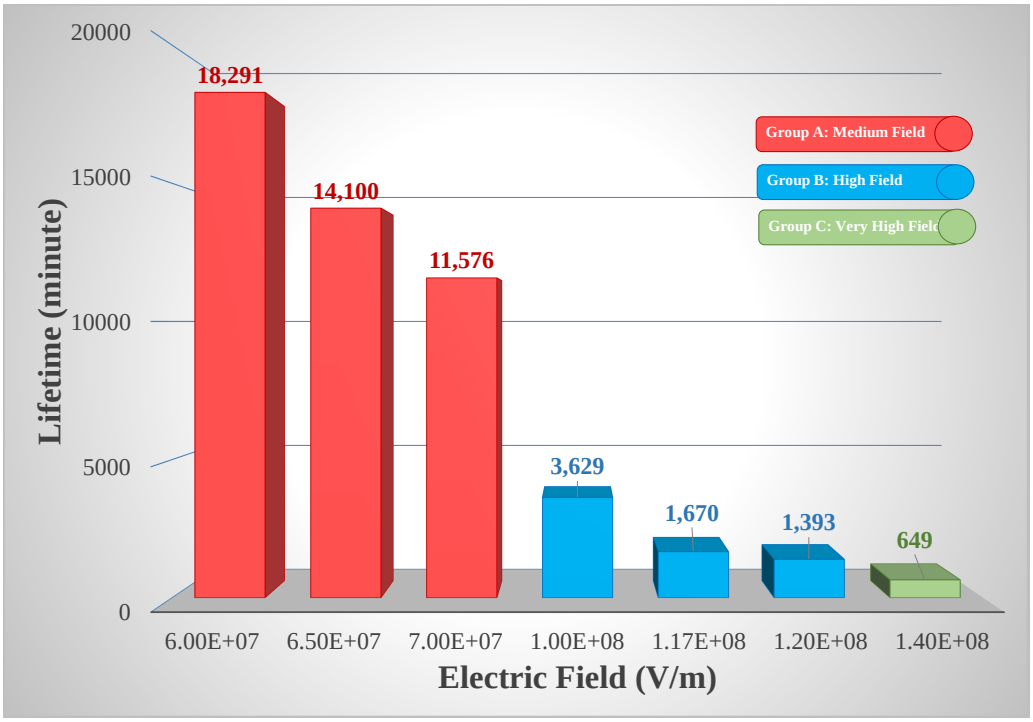

FIGURE 6.5: Comparison of the lifetime of LDPE samples under different applied fields.

The measurements were split into three groups; group A medium applied field from 60-70 MV/m, group B high applied field from 100-120 MV/m and group C very high applied field at 140 MV/m and above. In each group, the voltage divider principle is applied to get three different levels of electric fields together. Figure 6.6 shows the Weibull distribution of LDPE samples under the highest effect of electric field. In reality, the reachable value in the experimental set-up conditions (i.e. in the closed oven to stabilize the applied temperature around the samples) was 140 MV/m. However, this value of electric field can be much higher if the samples are immersed in a liquid that can assist avoiding the occurrence of flash over during the ageing process. The reason behind taking a reading without immersing the samples is to accommodate the normal conditions of insulating cables. Due to the long period of getting data at low electric field (roughly a year or more), the last set of electric fields were considered to be from 60 MV/m to 70 MV/m.

Certainly, several measurements at the same field of every single level in the oven were taken for the purpose of Weibull analysis to represent the characteristic value of the lifetime at this field. Continuing the measurements of the lifetime endurance, the second group 'high field' has three levels; 120 MV/m, 116 MV/m and 100 MV/m respectively. The distribution of Weibull function at these fields and under the same conditions are illustrated in Figures 6.7-6.9.

Electric Field $[MV/m]$	**Temperature** $[^oC]$	**Breakdown Time** $[min]$
140	80	648
120		1.4×10^3
116		1.7×10^3
100		3.63×10^3
70		1.2×10^4
65		1.4×10^4
60		1.83×10^4

TABLE 6.1: The charecterisc lifetime for different applied fields at 80 ^oC.

Table 6.1 shows the characteristic value of the lifetime for each applied field. The required time to break a sample that stressed at 140 MV/m is approximately half of the time at 120 MV/m. The second group 'B' lifetime lies between 1 day and 2.3 day. A massive time can be distinguished at the medium electric field since the lifetime begins from 8 days up to 12 days. Figure 6.10-6.12 shows the distribution of the lifetime at the medium applied electric field group.

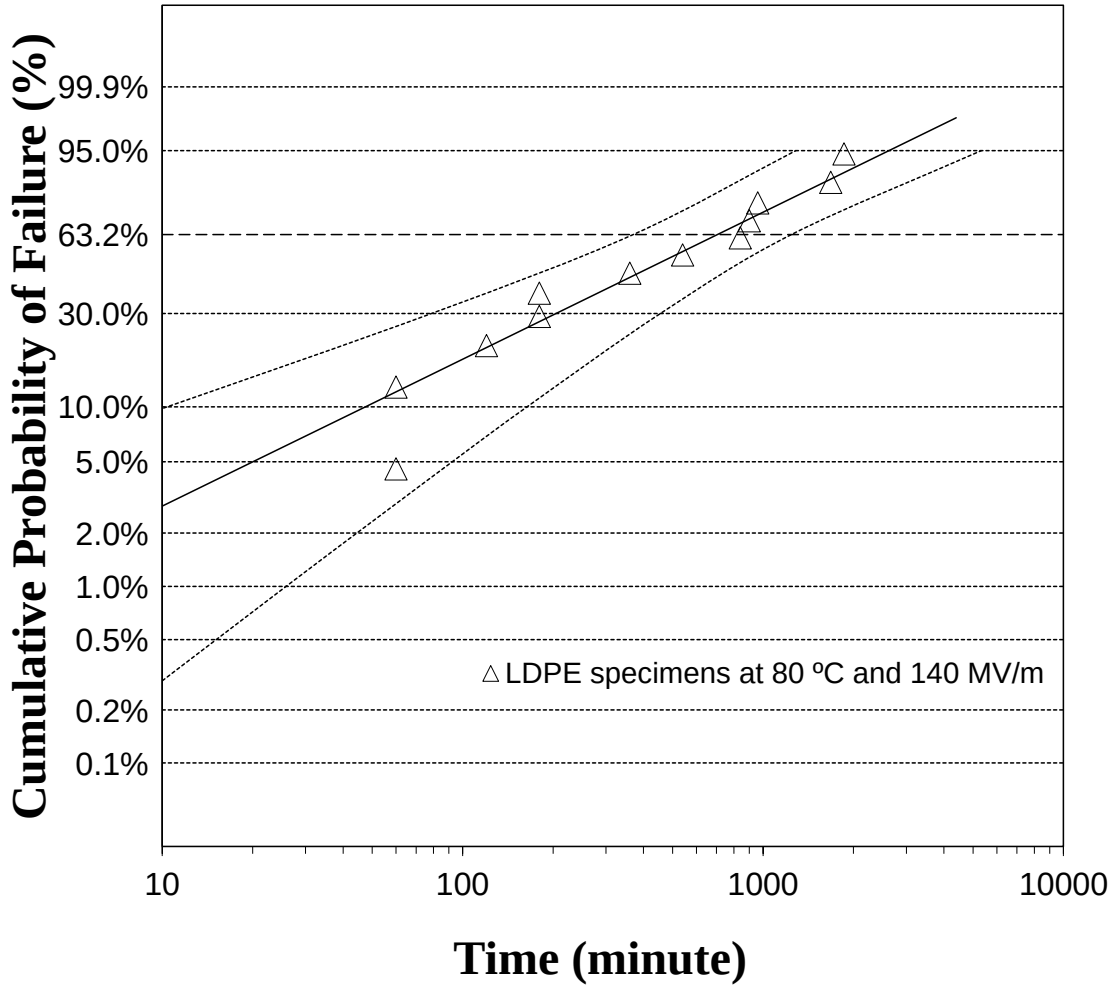

FIGURE 6.6: Weibull plot of time-to-fail under DC field of 140 MV/m at 80 ^oC.

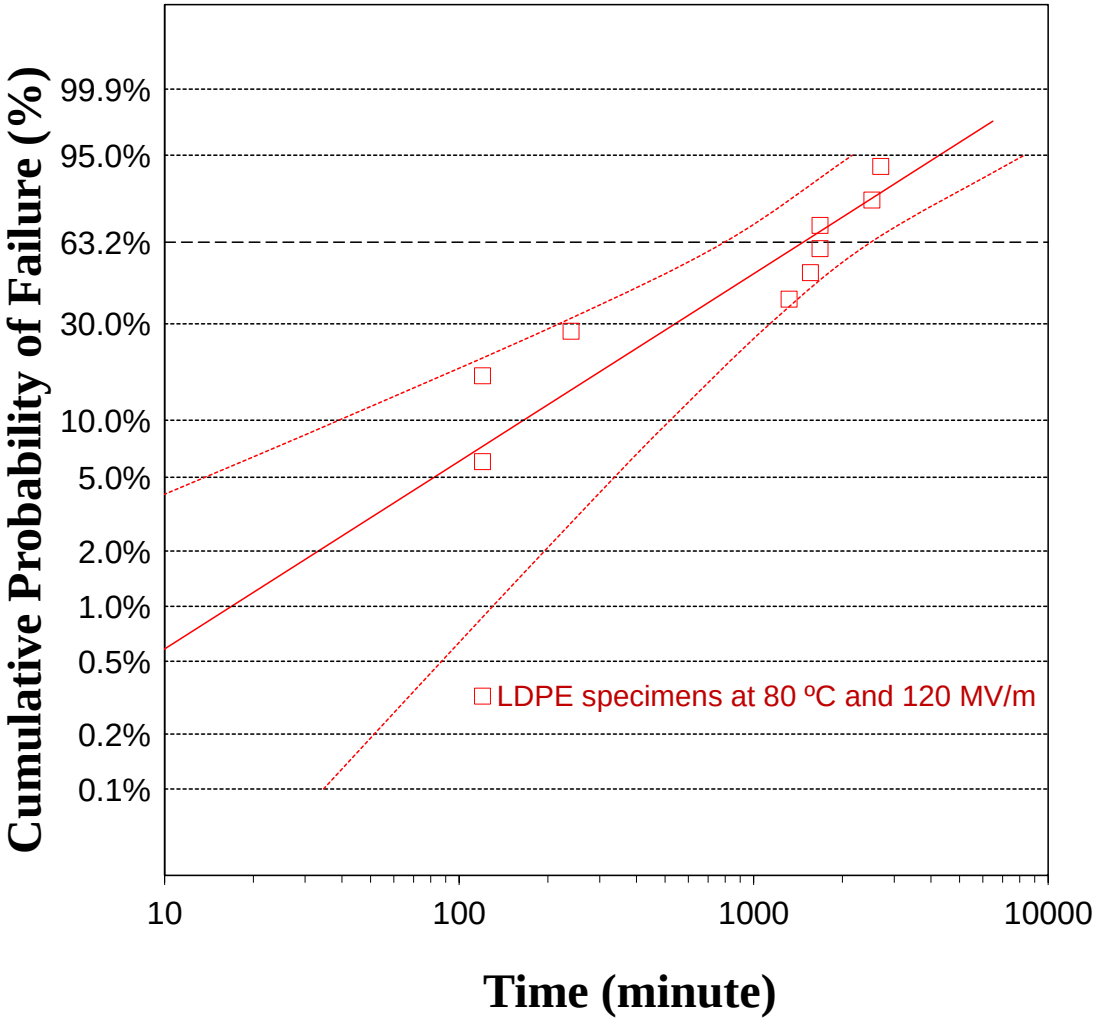

FIGURE 6.7: Weibull plot of time-to-fail under DC field of 120 MV/m at 80 C^o.

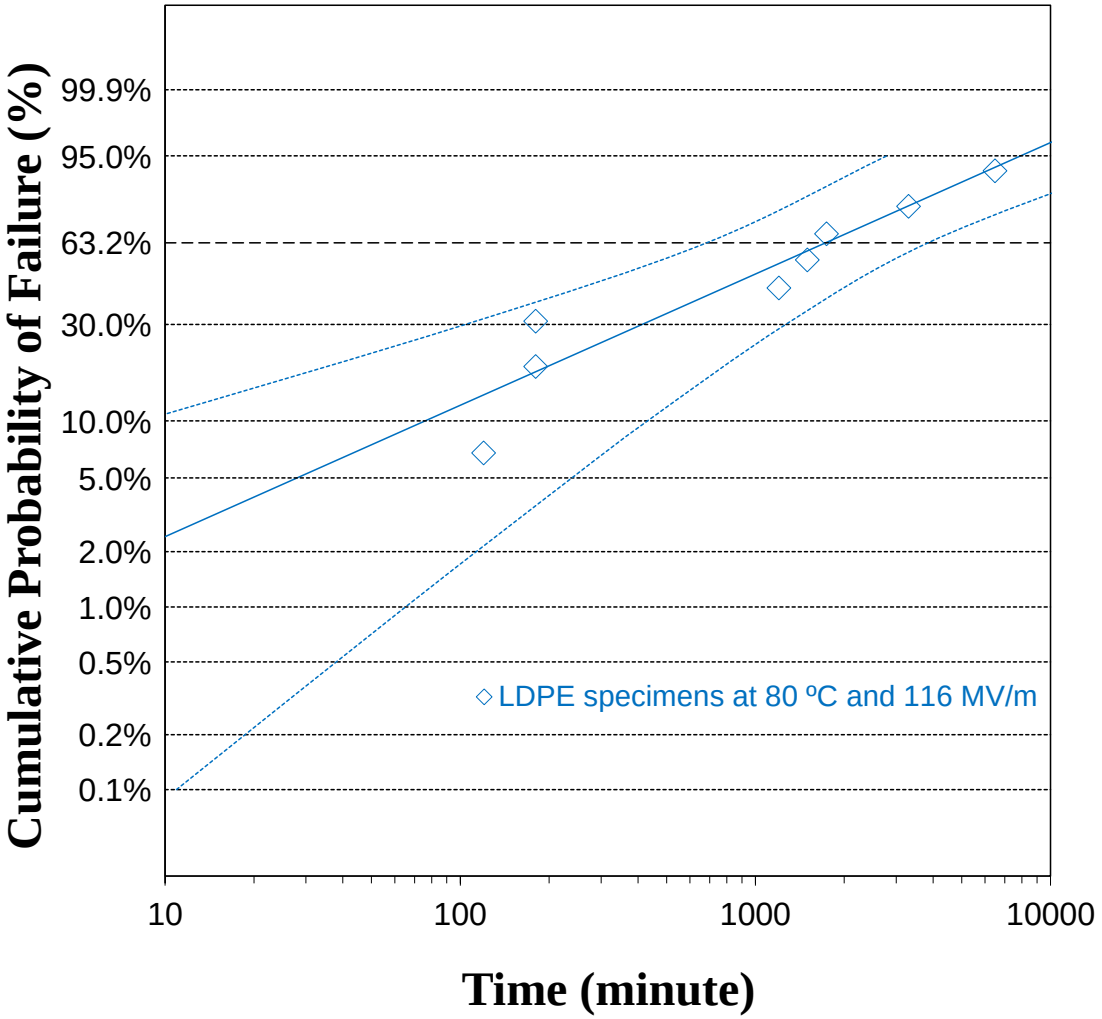

FIGURE 6.8: Weibull plot of time-to-fail under DC field of 116 MV/m at 80 C^o.

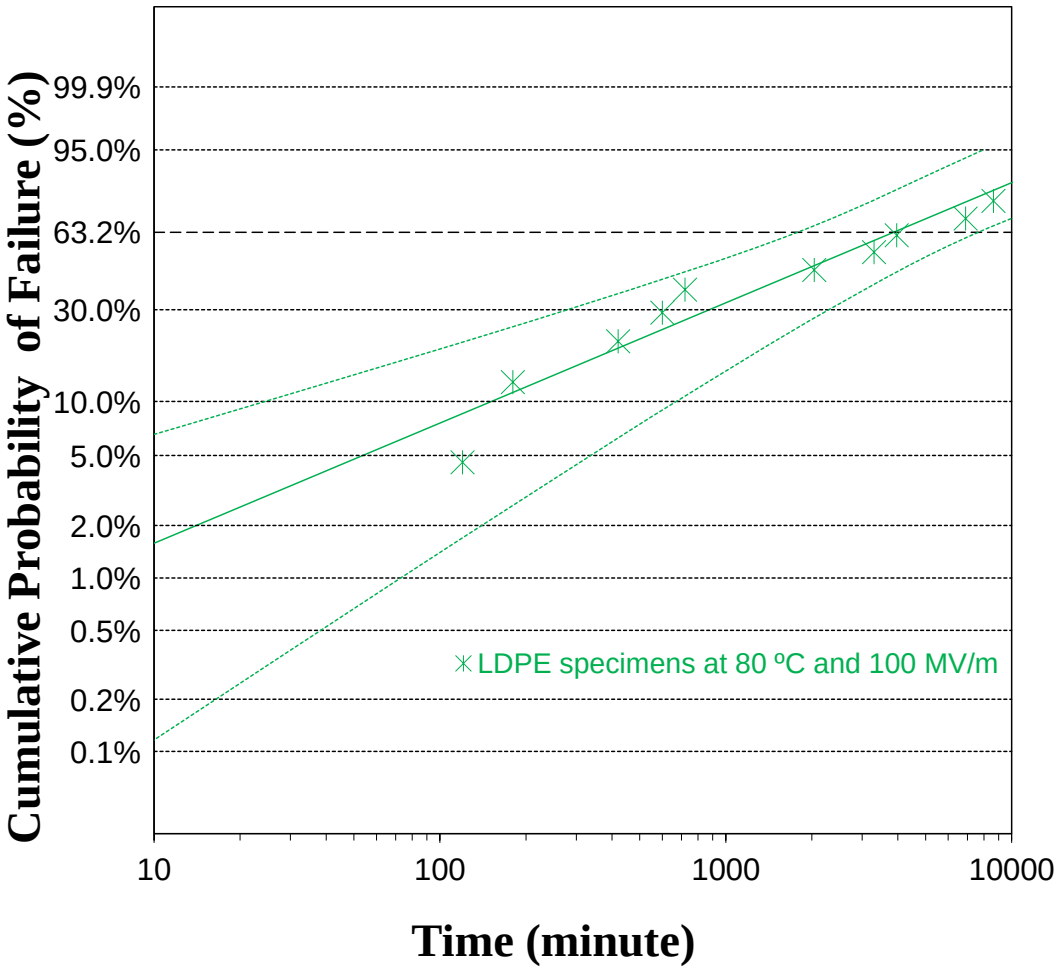

FIGURE 6.9: Weibull plot of time-to-fail under DC field of 100 MV/m at 80 ^oC.

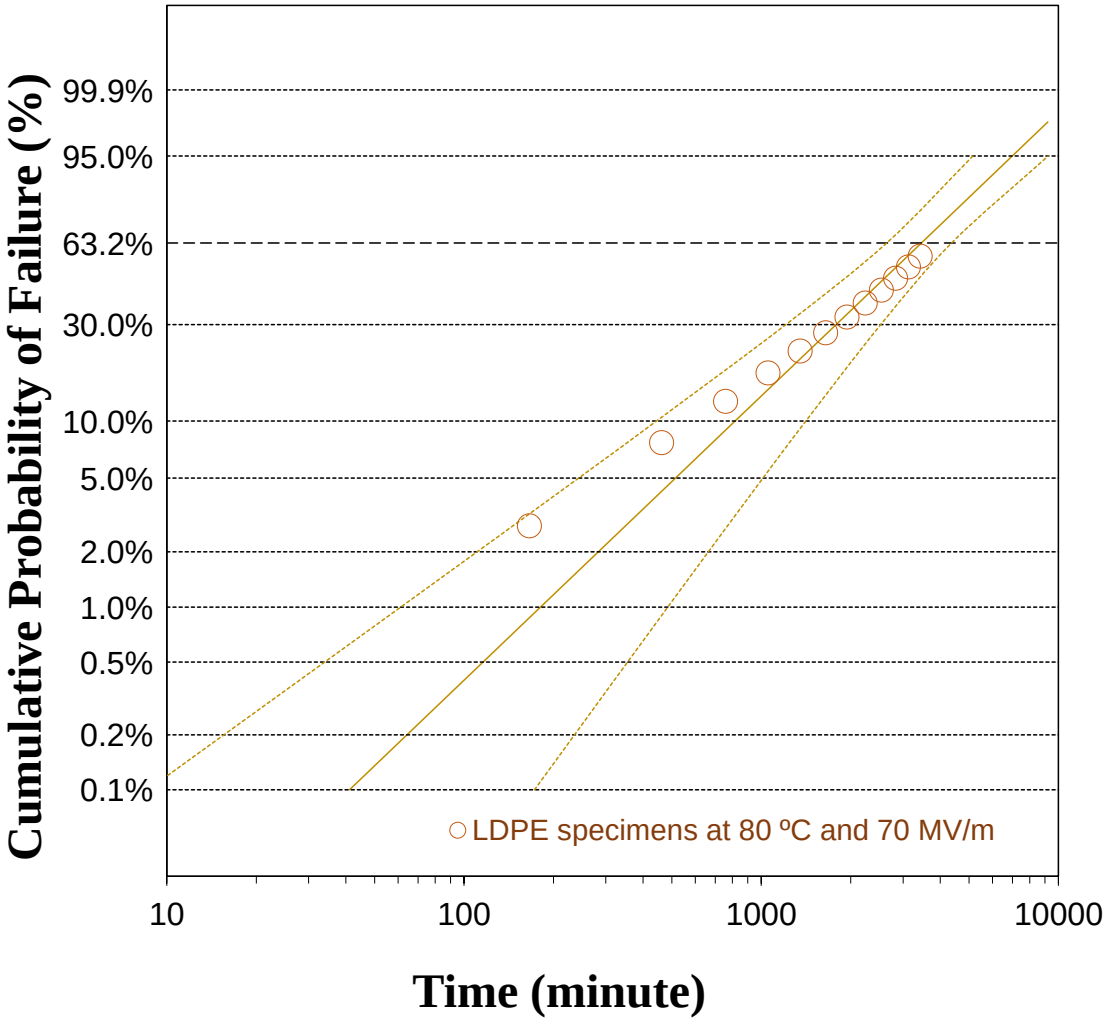

FIGURE 6.10: Weibull plot of time-to-fail under DC field of 70 MV/m at 80 ^oC.

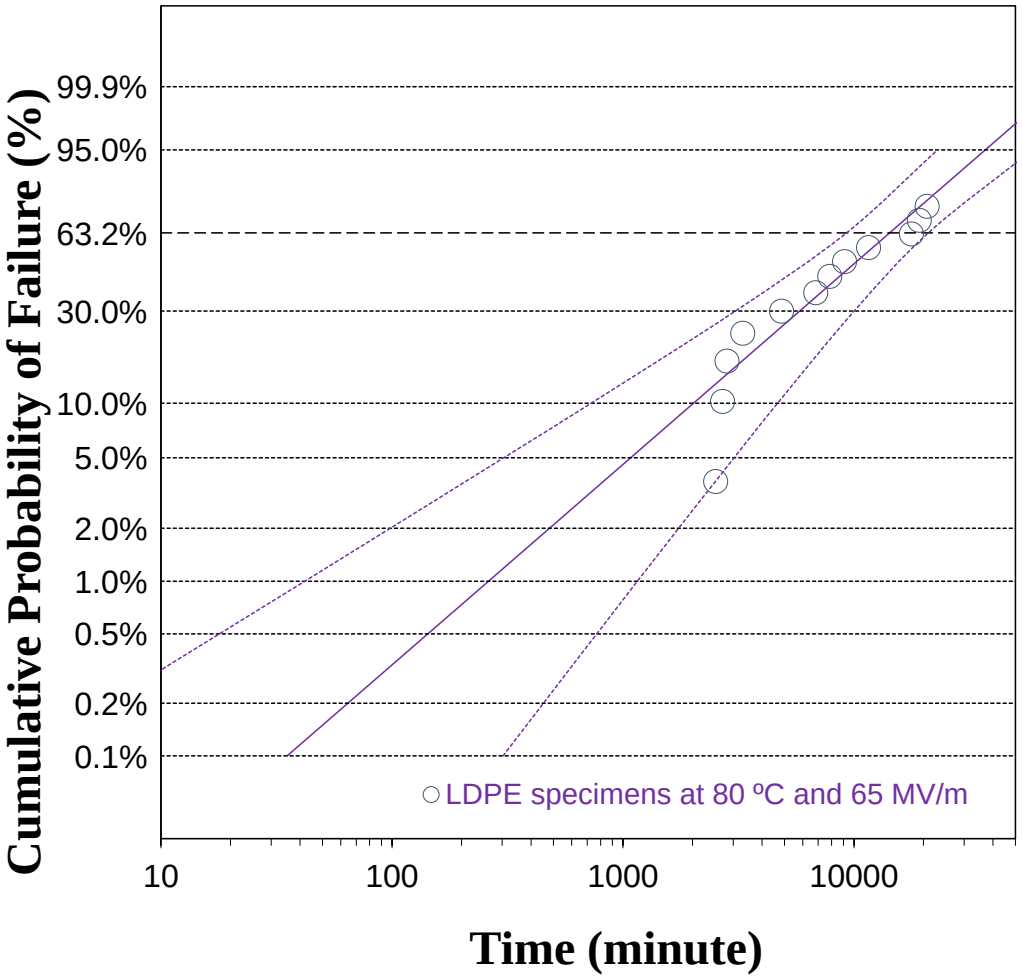

FIGURE 6.11: Weibull plot of time-to-fail under DC field of 65 MV/m at 80 ^oC.

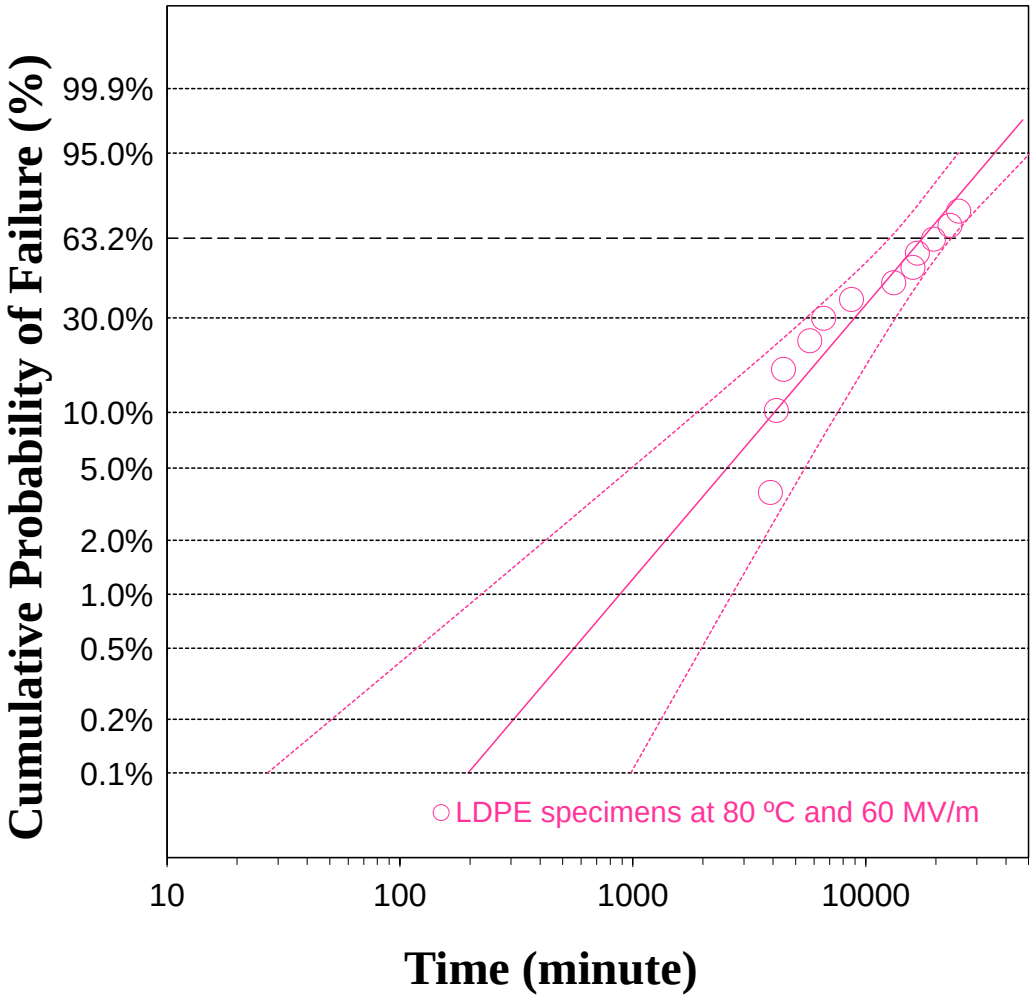

FIGURE 6.12: Weibull plot of time-to-fail under DC field of 60 MV/m at 80 ^oC.

6.5.2 Extracting the Critical Fraction C^*

The value of C^* is the only parameter in the developed model that has not been obtained. Some of the parameters are based on the space charge results, and other can be achieved from the conductivity measurements. The excluded parameter that cannot be directly measured but is rather extracted from the experimental results of the breakdown is C^*. This value was obtained by applying the ageing model in Equation 3.19 to the experimental values of the breakdown expressed in Figure 6.13 and its extracted value is 0.34. This value is in accordance to that reported in the literature wherein the DMM model was applied to polyethylene-terephthalate samples[14].

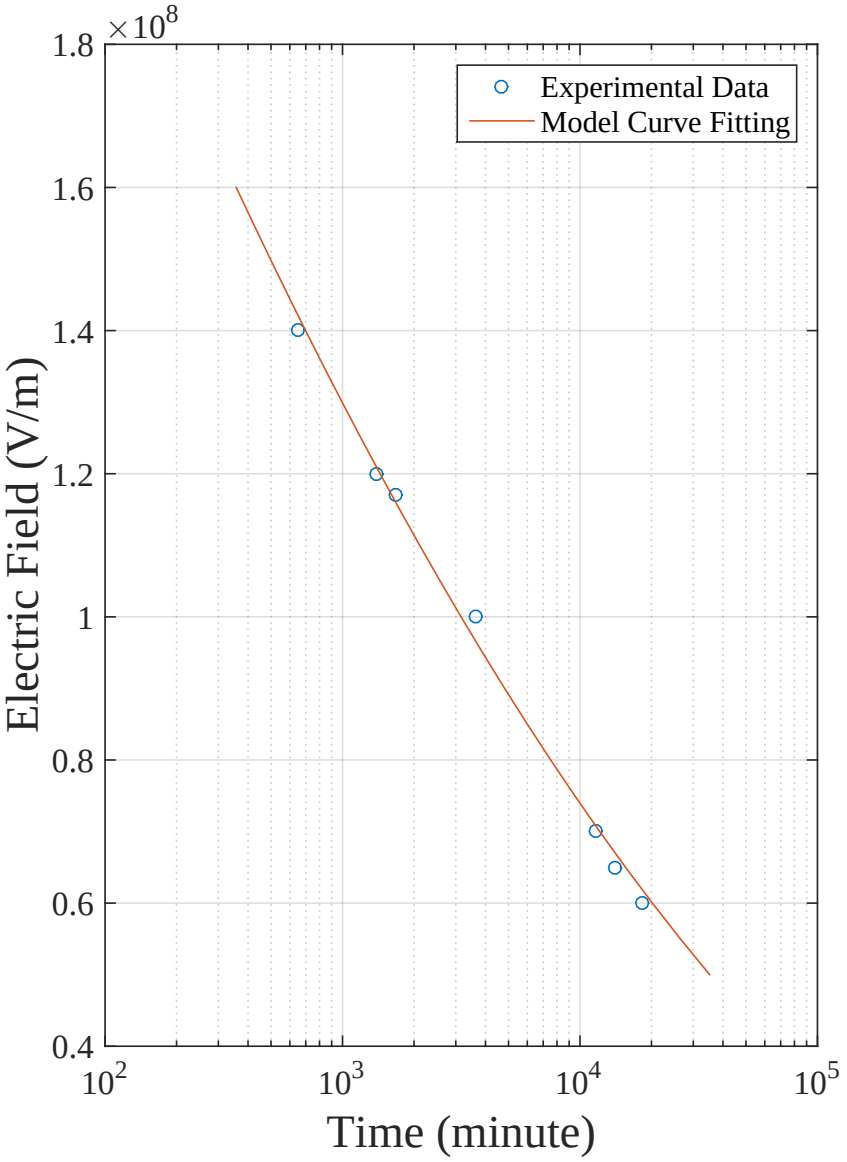

FIGURE 6.13: Electrical life line (solid line) obtained by the model, fitting dc experimental data on LDPE samples in oven at $80C^o$. The life points (circles) are relevant to 63.2%.

6.6 Summary

Although there are several mechanisms for describing the breakdown phenomenon, it is not easy task to determine the appropriate mechanism for a specific material. The applied conditions to the tested samples could vary the mechanism from type to other such as temperature, electrodes geometry, and type of test which is either the constant-stress test or the progressive-stress test.

The Weibull function is a statistical analysis of distributed results. Therefore, it cannot be a predictable method for the insulation lifetime. The α values increase gradually when the applied field is reduced. This means more time is required at lower electric fields. With regards β, the time-to-breakdown measurements are normally below 2 as shown for the previous measurements. It is in agreement with the reported results in [14] for Polyethylene-Terephthalate PET samples.

As the purpose of this project is to investigate the ageing process of insulations based on trapping and detrapping process, this chapter was significant in order to apply to the model results to be compared with the experimental results. Also, the critical fraction of the trapped charges C^* can be extracted based on the curve fitting of the model to the experimental results.

Chapter 7

Two-Dimensional Ageing Model Simulation

7.1 Introduction

The presented model in this work investigates the ageing process without describing the growth of breakdown path. Generally, it was considered that during the ageing process, the molecule dissociation contributes changes to the structure of polymer such as changes in morphology leading to the final breakdown[158, 30, 34]. In a homogeneous material, molecule dissociation seems obvious to take place randomly in the insulating material, and the final breakdown could occur due to the accumulation of the deteriorated regions with molecule dissociations. Some of the authors used percolation process to describe the accumulation of deteriorated regions as shown in [159]. Other simulation models for mechanical failure considered that the crack development during ageing was not only due to the growth of itself, but in addition to the accumulation of damage regions[160, 161]. However, because the failure was assumed to be due to the formation of percolation path through the insulation, these models are not suitable for use in electrical ageing process in which the breakdown strength has to be gradually decreased with the time of ageing process.

However, it is important to mention that the insulation below a critical value of stress should survive forever. This is the definition of deterministic breakdown theories [9]. In the developed ageing model in this thesis, the insulation systems below such critical values are considered as well. Thus, the risk to its integrity is reduced as the local fields that lead to rapid premature failure are eliminated.

A great deal of attention over many years has been paid to study ageing of polymeric insulations but without explicit agreement among them as to what physical mechanism is involved (as discussed previously in Chapter 2). One of the main concerns is regarding

the model's parameters. Every single parameter of the ageing models has a range of values while only the characteristic or average value is used in the model to extrapolate an insulation life. It is difficult to do the calculations at every single value in the parameter's range. The other obstacle is to find a suitable way of figuring the insulation lifetime based on these calculations. However, it is convenient to study the effect of the model parameters by representing the insulator as a grid whose bonds are identical capacitors. Each individual capacitor can have a different random number within the range of the upper and lower values of the model's parameter. For example, electric field in some regions are higher based on the concentration of charges in these regions, also spatial location of chemical structure within the polymer is different which causes variations in the depth of traps. These considerations will not only affect the rate at which a single defect grows up but also to defect amalgamation during cluster generation and the formation of the breakdown path. Figure 7.1 shows an example of breakdown path through siliconized SiC under the application of electro-thermal stress[162].

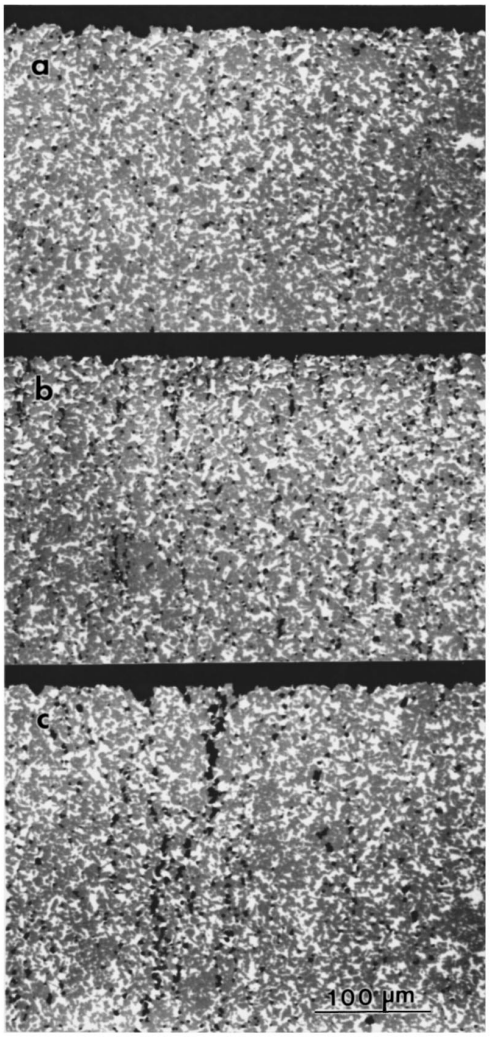

FIGURE 7.1: Evolution of cavity damage in siliconized SiC at 1300 ^oC. This figure obtained from S. Wiederhorn [J. Am. Ceram. Soc. 79, 977 (1996)].

7.2 Flowchart and simulation steps

The flowchart, which is shown in Figure 7.2, represents the steps of simulating the ageing model to illustrate breakdown path through an insulation sample. This simulation is performed by using Matlab program in 2-dimension. Initially, the model parameters can be split into two groups regarding to parameters of each bond in the grid. The first group has fixed values and requires the user to enter them once at the beginning such as the boundary conditions, applied temperature and thickness of the sample. The rest of the parameters have a range of values that differ from one bond to another in the mesh such as trap depth and cross-section.

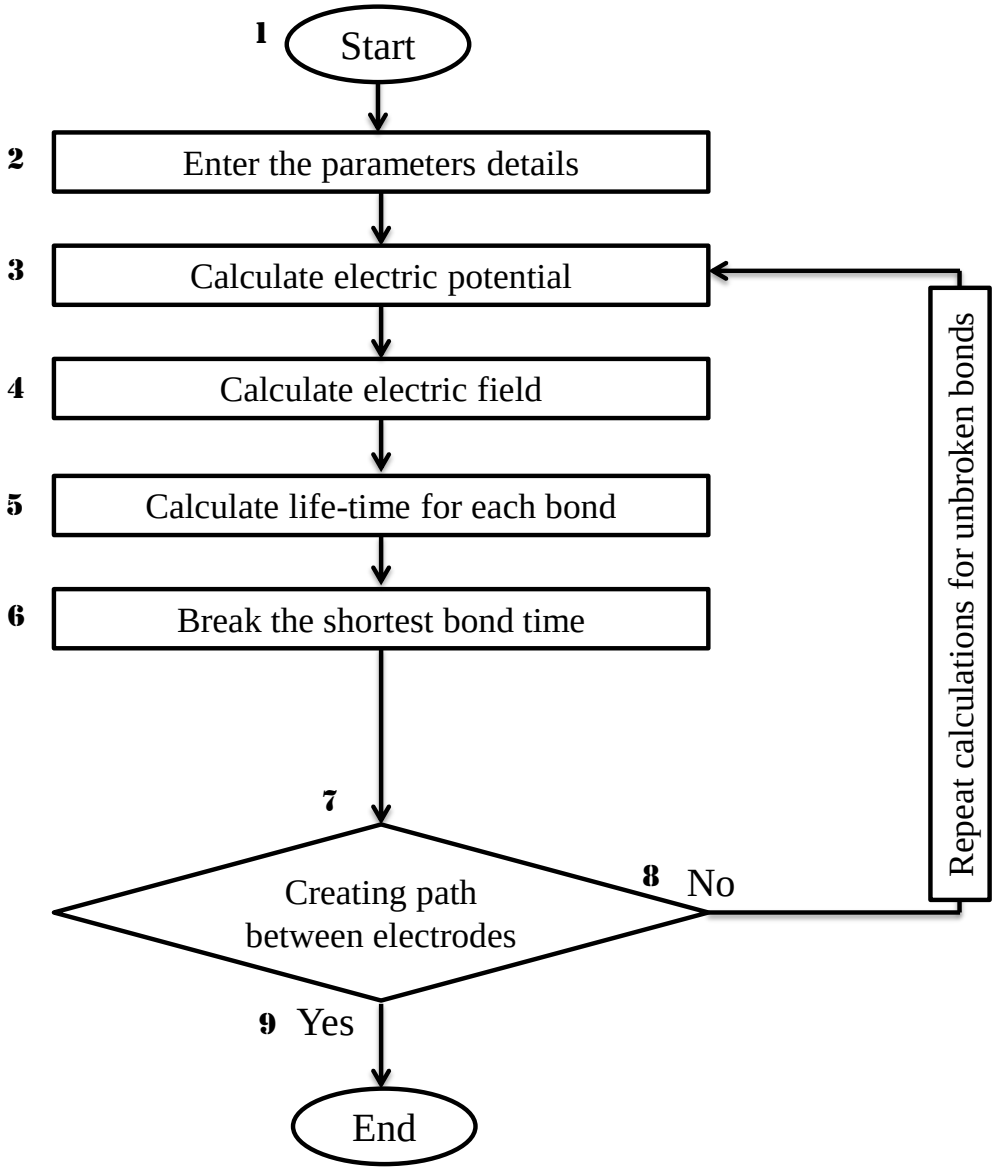

FIGURE 7.2: Flowchart diagram represents the simulation code working during ageing process under application of electric field.

To accomplish this simulation, a suitable method needs to be applied to distribute electric potential on the grid. Electric potential, V, at each point in the grid can play an important role in obtaining any information that relates to the electrostatic field. So, the easiest and convenient method is Finite Difference Method which is based on Laplace equation. To derive Laplace equation, it is necessary to obtain the relation between electric field intensity,E, and electric potential which is given by applying the gradient operation as:

$$E = -\nabla V \tag{7.1}$$

As the electric flux density $D = \varepsilon E$, then its divergence is differentiation in volume charge density ρ_v as:

$$\nabla \cdot D = \rho_v \tag{7.2}$$

Therefore, our objective should be to evaluate electric potential which of course can be found in terms of charge configuration. By substituting electric flux density and electric field into Equation 7.2, we can reach Poisson‘s equation as:

$$\nabla^2 V = -\frac{\rho_v}{\varepsilon} \tag{7.3}$$

Laplace‘s equation can be written from Equation 7.3when $\rho_v = 0$ as:

$$\nabla^2 V = 0 \tag{7.4}$$

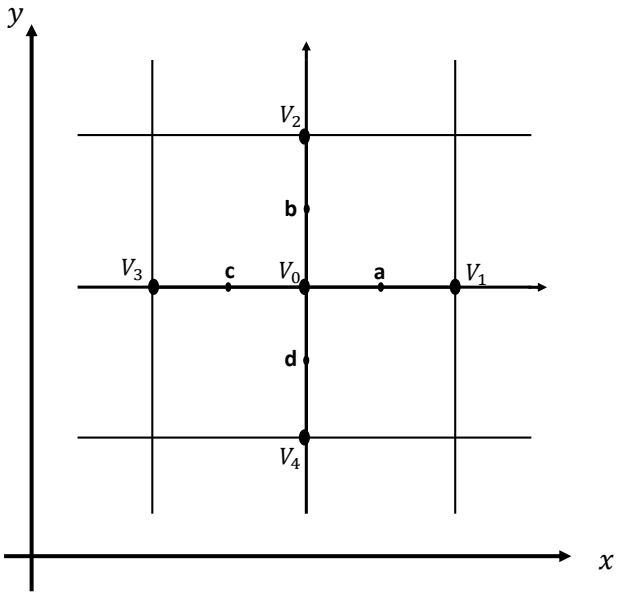

FIGURE 7.3: Figure of finite difference method in two dimensional potential field with similar distance between points [163].

According to Laplace equation, electric potential of V_o as shown in Figure 7.3 in the x-direction

$$\nabla^2 V_0 = \frac{\partial^2 V_0}{\partial x^2}\Big|_0 = \frac{\frac{\partial V_0}{\partial x}\Big|_a - \frac{\partial V_0}{\partial x}\Big|_c}{h} = \frac{V_1 - V_0 - V_0 + V_3}{h^2} \tag{7.5}$$

similarly for y-direction

$$\frac{\partial^2 V_0}{\partial y^2}\Big|_0 = \frac{\frac{\partial V_0}{\partial y}\Big|_b - \frac{\partial V_0}{\partial y}\Big|_d}{h} = \frac{V_2 - V_0 - V_0 + V_4}{h^2} \tag{7.6}$$

where h is the length of the bond in the grid. To calculate the potential at point V_0 by using Laplace equation

$$\frac{\partial^2 V_0}{\partial x^2}\Big|_0 + \frac{\partial^2 V_0}{\partial y^2}\Big|_0 = 0 \tag{7.7}$$

In another form

$$V_0 = \frac{1}{4}(V_1 + V_2 + V_3 + V_4) \tag{7.8}$$

This will be repeated several iterations until the error becomes less than the chosen tolerance. The error in this method is defined as the difference of the absolute value between the last approximated value for each single point in the grid, $V_{0_2}(i,j)$, with its previous value, $V_{0_1}(i,j)$, as:

$$Error(i,J) = \mid V_{0_2}(i,j) - V_{0_1}(i,j) \mid \tag{7.9}$$

$$Tolerance(i,j) > Error(i,J) \tag{7.10}$$

Then, the electric field between two electric potential points can be calculated by dividing the bond length h as:

$$E_0 = \frac{V_0}{h} \tag{7.11}$$

The simulation process has been performed through a series of steps based on Figure 7.2. Initially, the program requests the user to enter the main parameters of analysis. They are the electric potential at the upper electrode-insulation interface, the columns and rows number of the insulating grid, the bond length and the tolerance that is used for numerical method. Among these parameters, the electric potential at each point in the grid in the insulation can be calculated using Finite Difference Method FDM. Once the electric potential and the bond length are known, the electric field between two points either in the x or y direction is easily determined by using Equation 7.11. Each bond in the mesh represents a capacitor. This capacitor becomes a conductor when it broken

during the ageing process. Both terminals of the broken bond will take the same electric potential and, therefore, the electric field is zero.

The polymer chosen for this simulation is low-density polyethylene (LDPE), and the mean values of the model parameters for this material are shown in Table 7.1. These parameters have been used to describe properly the characteristic life of LDPE samples under the effect of DC electric field at temperature 80 ^oC. To simulate the LDPE sample on 2D square grid, it has been assumed that there are no metallic protrusions, inclusions or voids in the sample. On the grid mesh, the DC electric potential is sandwiched with the sample via an electrode at the top and the bottom. The simulation sample has a 40 $\times$ 40 mesh, and therefore each bond in the mesh has a length of 3.75 μm. As the edges may cause some effects to the bulk, we have attempted to reduce the edge effects by remaining the field uniform and excluding from consideration any simulation that ends upon the edge.

At the beginning, the state of each bond is assumed to be unfailed, which can be represented as a non-conducting capacitor. A set of the model parameter values is assigned for each bond. In these simulations, the activation energy barrier height, Φ, and the trap depth energy, E_T, have been kept at their characteristic value as the derivations of the life distribution based on material inhomogeneity and extreme value statistics show that there is very little spatial variation in their value [164]. With regards to the critical fraction of detrapped electrons, C^*, it has been chosen randomly from 0.48 to 0.2 which is an allowed range based on the characteristic value 0.34 as an average value. This range is reasonable regarding the characteristic value and considering to avoid affecting the simulation results.

The initial value of C_0 at all of the grid bonds is zero. Once the electric field is applied, all of the bonds are treated as accumulating elemental changes. This is expressed as a fraction of their local insulation life. The bond that has the shortest time to failure is identified by using the ageing model, and converted to a conductor. There is no restriction to the number of bonds that need to be reached to end the sample life. The amount of life lost in all other bonds during the simulation is converted to an equivalent bond-dependent value of C_0 relate to that time. At every time of breaking bond, the electric field distribution and C_0 in the simulation grid is recalculated. The remaining bonds with the shortest time after the updated field are identified and repeating the procedure. Eventually, a conducting path through the simulation sample is established across the failed bonds, and thereafter the simulation ends.

In regards to Equation 3.9, the assumption of C_0, which is the initial value, was chosen to be zero. It is only assumed to be zero only at detecting of the first bond. However, the Equation 3.19 in this case is written as:

$$t(E,T) = (K_T + K_D)^{-1} \ln \left[\frac{C(E) - C_0}{C(E) - C^*} \right] \tag{7.12}$$

The sequence of updating the value of C_0 of each grid bond can be described as:

1. Scan the whole grid to find the bond with the smallest lifetime T_1. Change the state of this bond to be a conductor and set the total lifetime T to be equal to T_1 (i.e. $T = T_1$).

2. Update C_0 for the second iteration C_{01} in all other bonds using:

$$\begin{aligned} C_{01}(j,i) = C_q(j,i) \times \{1 - \exp\left[-\left(K_T(j,i) + K_D(j,i)\right) T_1\right]\} \\ + C_0(j,i) \times \exp\left[-\left(K_T(j,i) + K_D(j,i)\right) T_1\right] \end{aligned} \tag{7.13}$$

   This gives the new value for C_0 in all of the grid bonds. Note: $(C_q = C(E))$.

3. Recalculate the local fields assuming that the failed bond is a conductor. This will give a new value of $C_q = C_{q_1}$.

4. Find the bond with the shortest time in the second iteration before it fails (i.e. T_2). This bond now becomes conducting, and the total lifetime becomes as $T = T_1 + T_2$.

5. Find the new value C_02 for all the grid bonds at the new time $T = T_1 + T_2$. This is given as:

$$\begin{aligned} C_{02}(j,i) = C_{q_1}(j,i) \times \{1 - \exp\left[-\left(K_T(j,i) + K_D(j,i)\right) T_2\right]\} \\ + C_01(j,i) \times \exp\left[-\left(K_T(j,i) + K_D(j,i)\right) T_2\right] \end{aligned} \tag{7.14}$$

6. Recalculate the fields and new value of $C_q = C_{q_2}$.

7. Repeat the previous steps until failure structure grows across the grid.

Parameter	**Unit**	**Value**
σ_T	m^2	6.55×10^{-16}
N_c	m^{-3}	$3.21 \times 10^{+25}$
v_{th}	ms^{-1}	$1.27 \times 10^{+5}$
E_T	J	3.94×10^{-19}
Φ	J	2.70×10^{-19}
T	K	353
C^*	-	0.34

TABLE 7.1: Values of the developed ageing model's parameters which are extracted and calculated in this thesis.

7.3 Results and Discussion

The reported results from simulations are performed on the applied fields range from 60 MV/m to 140 MV/m at temperature of 80 ^oC. An investigation on the spatial variation in C^* was carried out which gives each bond different value. A number of realizations have been considered for this variation range, and Figure 7.4 shows the failed structure when C^* is spatially distributed. The evolution time that corresponds to broken bonds is plotted in Figure 7.5.

During the ageing process, an inspection of the damage produced on the sample shows that only isolated bonds are damaged. The unconnected bonds to the breakdown path can be obviously seen in Figure 7.4. Even the value of C^* for these bonds are small, which are most susceptible to damage, their capability for extension were limited. A sample failure was initiated by the irreversible damage to a bond where its local electric field is increased, and therefore increasing in the mechanical energy that is produced in a trap. This mechanical energy is able to cause damage to the bond after being released due to detraping an electron. The initiation of breaking bonds takes a considerable time, and an acceleration of extending the damage occurs rapidly once one bond causes affect to fail neighbours and connect the two electrodes via the conducting path which causes a sample failure. Isolated damaged bonds lying next to or on the failure path are absorbed into the path. Some of these failed bonds causes minor deviation from a straight line. This pattern of behaviour is shown in all of the repeated simulations.

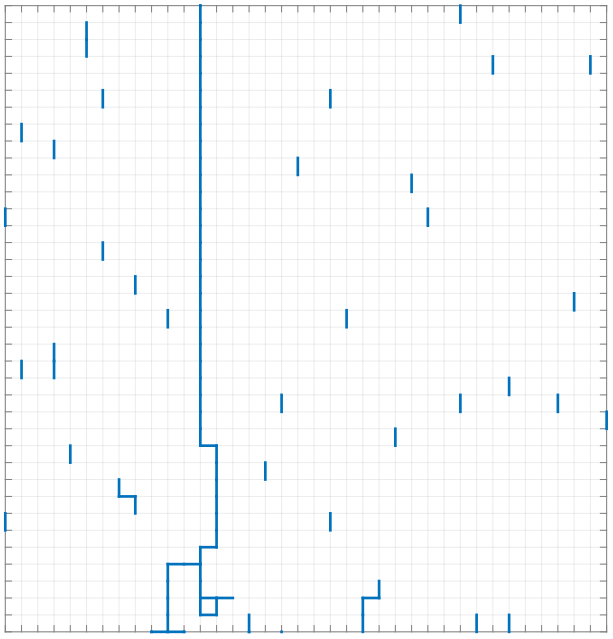

FIGURE 7.4: Damage produced by failure corresponding to the damage evolution in Figure 7.5.

Through the simulation results, the structure of isolated failures is similar to the expected form of a deterministic runaway process, where a filamentary conducting path is produced from a local reinforcement of damage generation [9], which is similar to the evolution of the isolated failures in this simulation as shown in Figure 7.5. The difference in the simulation is that the beginning of runaway is considerably delayed rather than being initiated at the most susceptible site. The key factor in determining the insulation life is not the susceptibility of individual local sites whereas the susceptibility of cluster sites together. This conclusion is illustrated by the results from simulations when C^* is given a spatial variation. A study of stochastic extension of the percolation model for breakdown represented similar results [165].

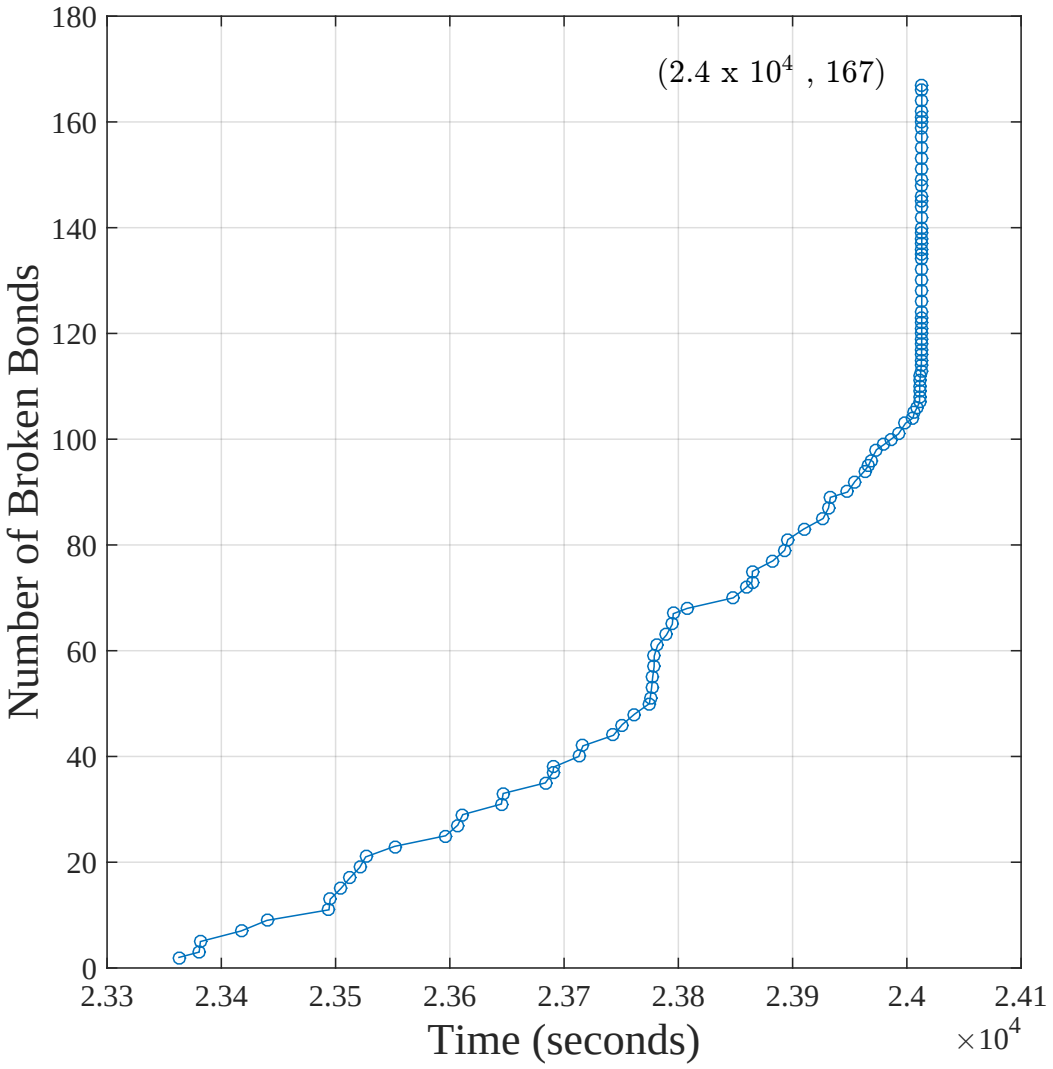

FIGURE 7.5: The damage evolution during the ageing process when electric field is 140 MV/m, temperature is 80 C^o, and spatial variation of C^* from 0.44 to 0.23.

The simulation results of the presented work show that a reasonable number of isolated failed regions occurs during the ageing period as can be seen in Figure 7.5. However, this conclusion is on the contrary to the study in [166] which states a few of bonds were failed during main part of the ageing period that would be detectable as nano voids, cracks or local conducting regions[167]. The rest of regions have not reached the critical situation for irreversibility as they assumed that detecting the changes during the main part of ageing period would be difficult.

The chosen lifetime at a specific field from repeated simulation results was by using the Weibull failure probability (P_F), which is given as: [168]:

$$P_F = 1 - \exp\left[-\left(\frac{t}{\alpha}\right)^{\beta}\right] \tag{7.15}$$

where α is the characteristic life, and β is the shape parameter of the distribution. Due to the limited number of sample tested for long ageing, the experimental evaluation of the parameters α and β still cannot be made precisely in the experiment.

According to the results of lifetime from repeating simulations for specific field, the variations among these results seems to be very small. This may be related to the fixed characteristic value of the model parameters which are not influenced during the simulation period such as variation of trap depth. Therefore, it has been assumed that five samples is sufficient to characterise the simulation lifetime for a chosen field since the aim is to investigate the effect of C^* variation on the ageing model. Moreover, the shape parameter of the distributed results, β, has a large value as they are close to each other. This result, however, would be expected to be in contrast with what can be seen from the empirical breakdown results. Figures 7.6 - 7.10 illustrate the Weibull distribution of several applied field with variation of C^*, and the characteristic lifetime of individual condition is provided in Tables 7.2-7.6.

A suitable modification on the value of the fraction C^* has been made to study its effect to the ageing of polymer. As an example, the characteristic lifetime of LDPE sample that stressed under 140 MV/m at a fixed value of C^* is around 11 hour, while it is at the same conditions with a range of C^* from 0.44 to 0.23 reduces to 7 hour, similarly the time at 60 MV/m is around 300 hours for the experimental work, and 200 hours with the range of C^*. The reason may be due to the most susceptible sites to ageing that have the smallest values of C^* and can fail earlier than the expected time. Figure 7.11 shows the simulation result of LDPE samples at fix and variant of C^*.

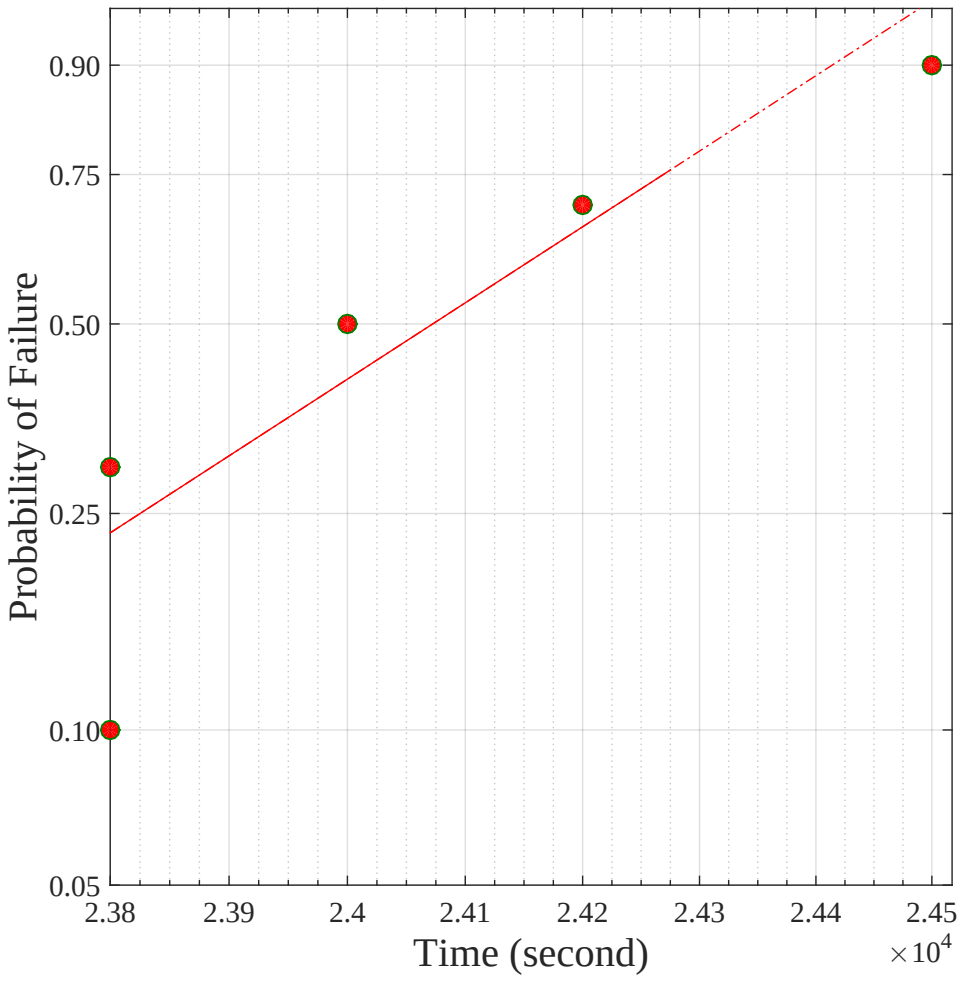

FIGURE 7.6: Plot of the simulation results by using Weibull distribution function with variation of C^* under 140 MV/m electric field and 80 ^oC temperature.

Sample Number	**Lifetime** (second)	**Characteristic Lifetime** (second)
1	2.38×10^4	2.42×10^4
2	2.42×10^4	
3	2.38×10^4	
4	2.45×10^4	
5	2.4×10^4	

TABLE 7.2: Time-to-failure for LDPE samples and the characteristic value by applying Weibull distribution function with variation of C^* under 140 MV/m electric field and 80 ^oC temperature.

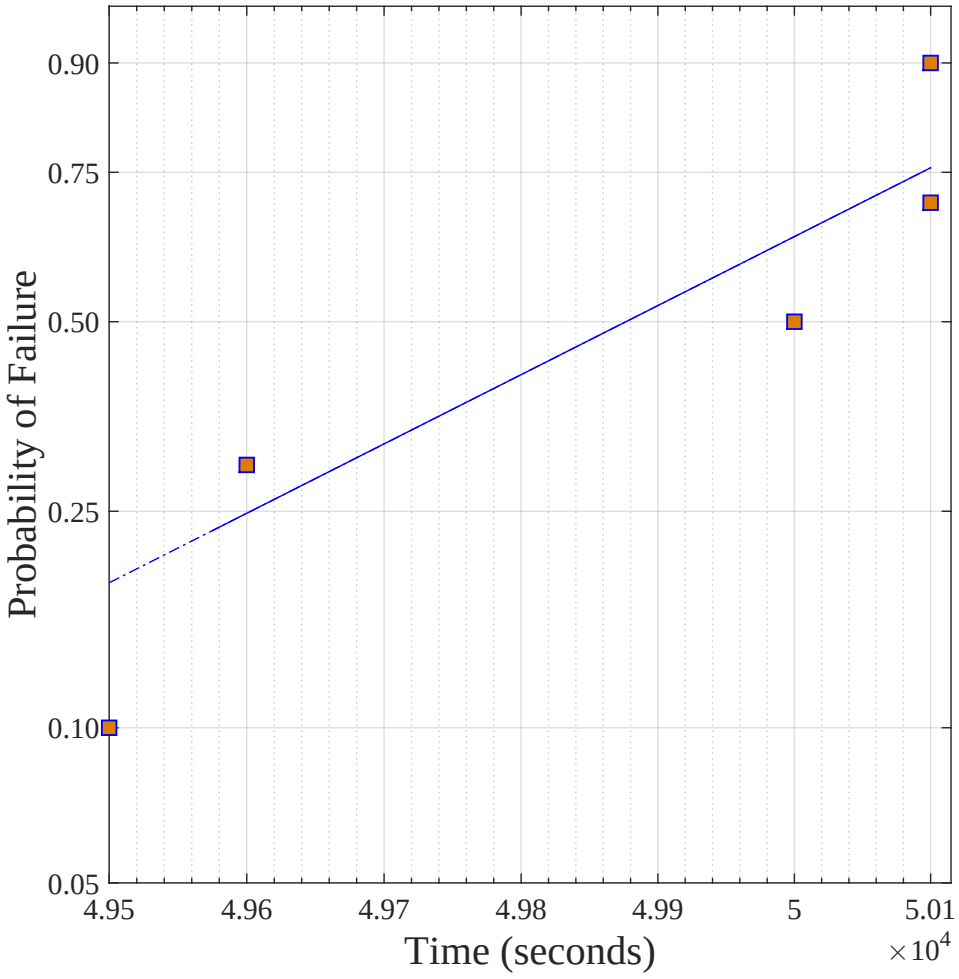

FIGURE 7.7: Plot of the simulation results by using Weibull distribution function with variation of C^* under 120 MV/m electric field and 80 ^oC temperature.

Sample Number	**Lifetime** (second)	**Characteristic Lifetime** (second)
1	5.01×10^4	5×10^4
2	4.96×10^4	
3	5.00×10^4	
4	5.01×10^4	
5	4.95×10^4	

TABLE 7.3: Time-to-failure for LDPE samples and the characteristic value by applying Weibull distribution function with variation of C^* under 120 MV/m electric field and 80 ^oC temperature.

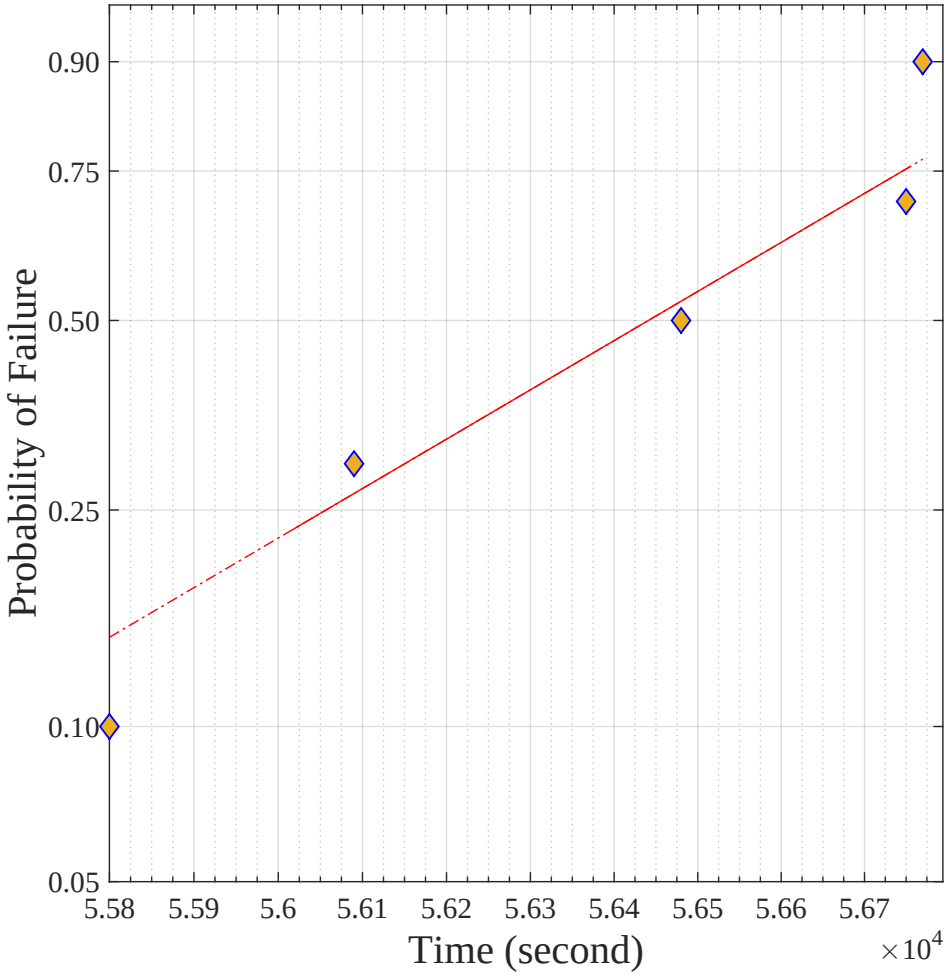

FIGURE 7.8: Plot of the simulation results by using Weibull distribution function with variation of C^* under 116 MV/m electric field and 80 ^oC temperature.

Sample Number	**Lifetime** (second)	**Characteristic Lifetime** (second)
1	5.65×10^4	5.66×10^4
2	5.67×10^4	
3	5.68×10^4	
4	5.61×10^4	
5	5.58×10^4	

TABLE 7.4: Time-to-failure for LDPE samples and the characteristic value by applying Weibull distribution function with variation of C^* under 116 MV/m electric field and 80 ^oC temperature.

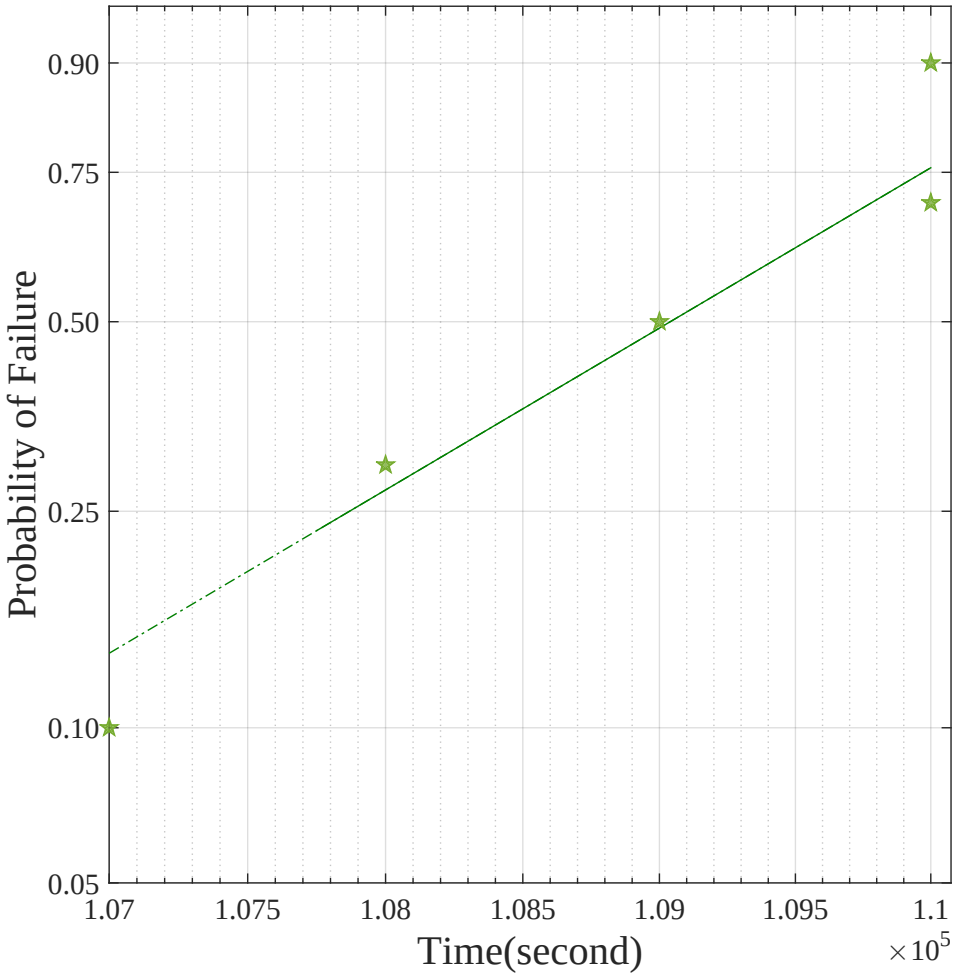

FIGURE 7.9: Plot of the simulation results by using Weibull distribution function with variation of C^* under 100 MV/m electric field and 80 ^oC temperature.

Sample Number	**Lifetime** (second)	**Characteristic Lifetime** (second)
1	1.08×10^5	1.1×10^5
2	1.10×10^5	
3	1.09×10^5	
4	1.1×10^5	
5	1.07×10^5	

TABLE 7.5: Time-to-failure for LDPE samples and the characteristic value by applying Weibull distribution function with variation of C^* under 100MV/m electric field and 80 ^oC temperature.

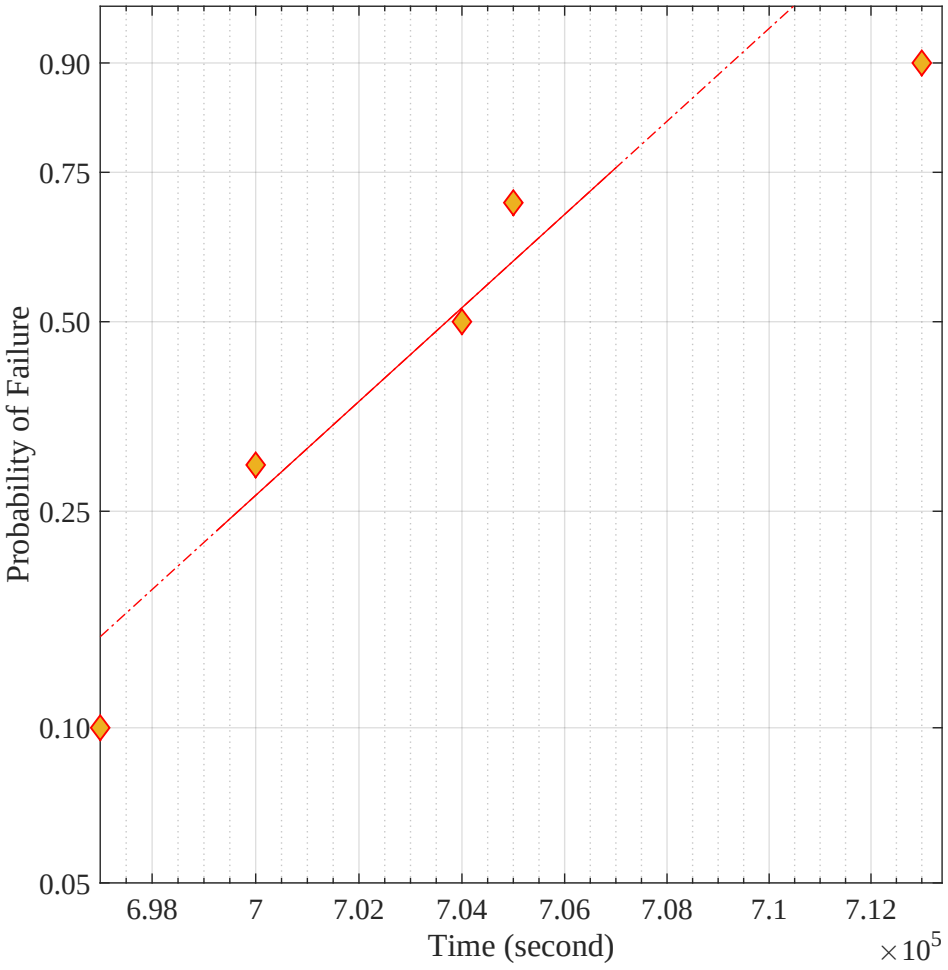

FIGURE 7.10: Plot of the simulation results by using Weibull distribution function with variation of C^* under 60 MV/m electric field and 80 ^oC temperature.

Sample Number	**Lifetime** (second)	**Characteristic Lifetime** (second)
1	7.05×10^5	7.07×10^5
2	7.00×10^5	
3	7.13×10^5	
4	6.97×10^5	
5	7.04×10^5	

TABLE 7.6: Time-to-failure for LDPE samples and the characteristic value by applying Weibull distribution function with variation of C^* under 60MV/m electric field and 80 ^oC temperature.

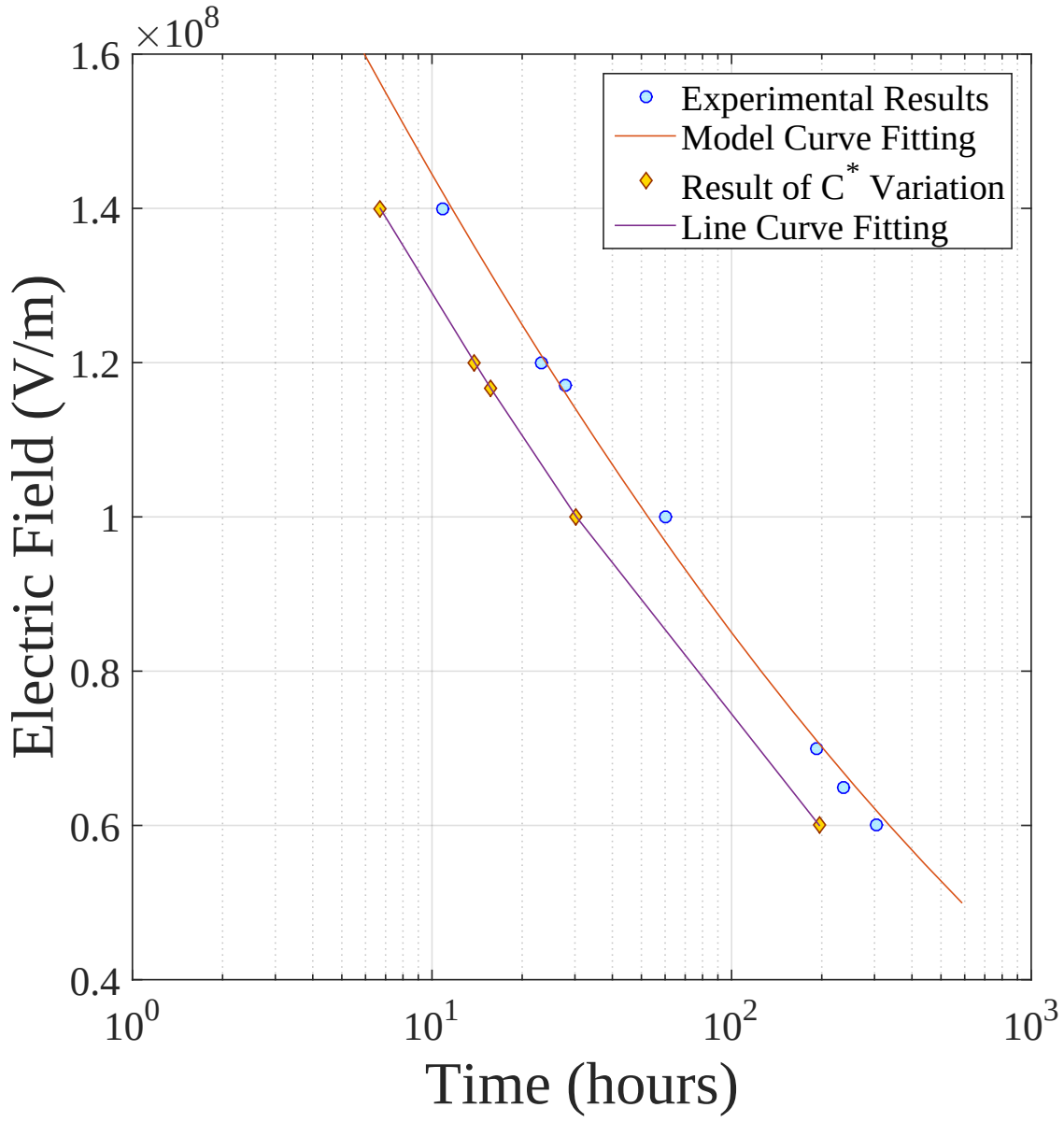

FIGURE 7.11: Comparison between the experimental and the simulation results of LDPE samples at different applied field and fixed temperature of 80 ^oC.

7.4 Summary

Simulations performed using the developed lifetime model with the spatial variation in the fraction of trapped charges C^* yield a form of a single filamentary path as a failure structure, with branching on a size scale that is not greater than 3.75 μm. A similar structure to a deterministic runaway process has been found for the time evolution of the damage during ageing process but the initiation of failing bonds is much delayed. Damage occurs when sufficient morphological changes exist in a region that is able to continually increase the local energy concentration and therefore increasing in the released energy from detrapping process. Simulations are performed at different applied field without distinguished number in the isolated failures.

The lifetime distribution that results from the simulations can be fitted to the Weibull distribution. The shape parameter reflects the variation between the simulation results at the same field. It has been found as a large value which means repeated simulation results are close together.

Chapter 8

Conclusion and Future work

8.1 Conclusion

An ageing model is developed based on the trapping and detrapping rate theories, and correlates well with the electro-thermal ageing of LDPE samples. The model has an interesting feature that its parameters have physical meaning.

In the case of trapping process, the dominant mechanism for electron injection is Schottky mechanism which was approved by characteristic of the current density versus the electric field. On the other hand, the accumulated charges in a trap produce a mechanical stress that is induced from the electrostatic field which reduces the trap depth in the thermal detrapping rate.

Apart from C^*, the model parameters could be determined by other kinds of investigation, rather than experimental life tests. Due to the resulting mechanical energy around a trapped charge, a local damage (ageing) or a catastrophic event (electrical breakdown, fracture, etc.) can occur from the released energy after detrapping the electrons. The proposed interpretation of ageing process strongly limits the lifetime of insulating materials which this work has shown and provided a good fit with experimental data.

The simulation part is the appropriate method that can assist to investigate the effect of each individual parameter with regards to the ageing process and the growth of breakdown path. This investigation can be performed on a mesh grid by selecting a narrow range for the investigated parameter that the allowed range is based on the characteristic value of the parameter as an average value. Simulations made using the developed ageing model with the varying spatially in the fraction C^* yield a failure structure with the form of a single filamentary path. The growth of the damage during the ageing process is similar to a deterministic runaway process, whereas a delay in the onset of which bond is damaged.

8.2 Future work

From the above results, some work can be proposed for further improvement of the developed ageing model. These improvements can be classified into two parts: experimental investigation and simulation analysis.

The parameters in the model do not relate directly to the type of the electric field (either AC or DC). However, when the model is extended to cover an AC field, the extracted parameters that are based on space charge profile will be influenced. The space charge profile in an AC field may be small or even insignificant, so the question that should be asked is how these parameters can be extracted in order to keep the model applicable to the AC field. In other words, the model parameters could be determined by using other kinds of experiments. Further research is required to extend the applicability of the model to both electric fields.

Although the experiments to verify the model were performed in the presence of an electric field, the space charge measurements were detected at the decay state after the removal of the electric field. This is due to the complication of extracting the ageing model parameters when the measurements were performed at the presence of electric field (volts ON). Consequently, the decay was used as an alternative and simple method to obtain the model parameters. However, it is significant to find a convenient method for extracting the model parameters in the presence of an electric field. In order to reach this direction, an assumption should be made between the trapping and detrapping rate constants with the electric field. Once these two constants are known, the rest of the parameters can be obtained.

The simulation can use the model to simulate the evolution of damage structures during the electro-thermal ageing of insulating polymers. Within this thesis, the simulation indirectly covered the effect of space charge by considering the modifications to the electric field during the ageing process. The effect of space charge would be understood better if the simulation is developed to find an explicit relationship between space charge and the ageing process. Further work on this particular point is recommended in order to realize this effect.

It is much worth for the developed model to be represented in three-dimension instead of two-dimension in this thesis as it becomes much explicit. In order to work for irregular three dimensional electric field by using the finite difference method, two obstacles may exist during ageing process and require further works to be developed. The first issue is related to the very large number of the electric potential values V(x, y, z) which require very large computer memory. The second is about the computation time for detecting each broken bond during ageing process. Hence, this suggestion of three-dimensional representation may help to explain the effect of space charge on the ageing of polymeric materials.

In addition, the simulation can also be used to investigate the effect of each single parameter of the model to the ageing process. Here, the critical fraction of the trapped electrons C^* that can cause sufficient released energy to break or weaken the bond is investigated by varying its value on a certain range. Moreover, other attempts to investigate other parameters, such as the trap-cross section and trap density, are suggested by using the developed ageing model in this thesis.

Appendix A

Space Charge Measurment at Volts ON

The preferable method for determining the injected space charge is when the voltage supply is switched on. Here, a new methodology has been performed to precise the quantity of charges at a specific time. Actually, this method is based on the chosen reference reading (for example $2kV$) that was detected for calibration. The second step is to multiply the reference by a ratio of at a certain voltage on which the measurement will be taken (for example $7kV$) to the reference voltage (i.e. $7kV/2kV$). At this stage, space charge is detected as normal by turning the voltage supply on and taking the reading at several different times. In order to know the exact amount of the injected charges is to subtract the multiplied reference reading from the space charge measurement at a specific time. This method is clearly detailed in Figure A.1.

It is more convenient for ageing study to carry-out space charge measurements when the power supply is active in order to simulate the normal situation of the cable. As several studies recognized that the space charge builds-up in the insulations with time, Figure A.2 shows the increase of injected charges with time.

The volt-on measurements, however, is too difficult to be applied for the developed model. The unknown parameters in Equation 5.7 are three, and this may make the solution more complicated. Furthermore, the exponential term in the model equation has a negative sign, which is opposite of the increase exponential term. Therefore, the appropriate way is to use the decay measurements as stated previously which make these parameters extracted and solved based on the space charge profiles.

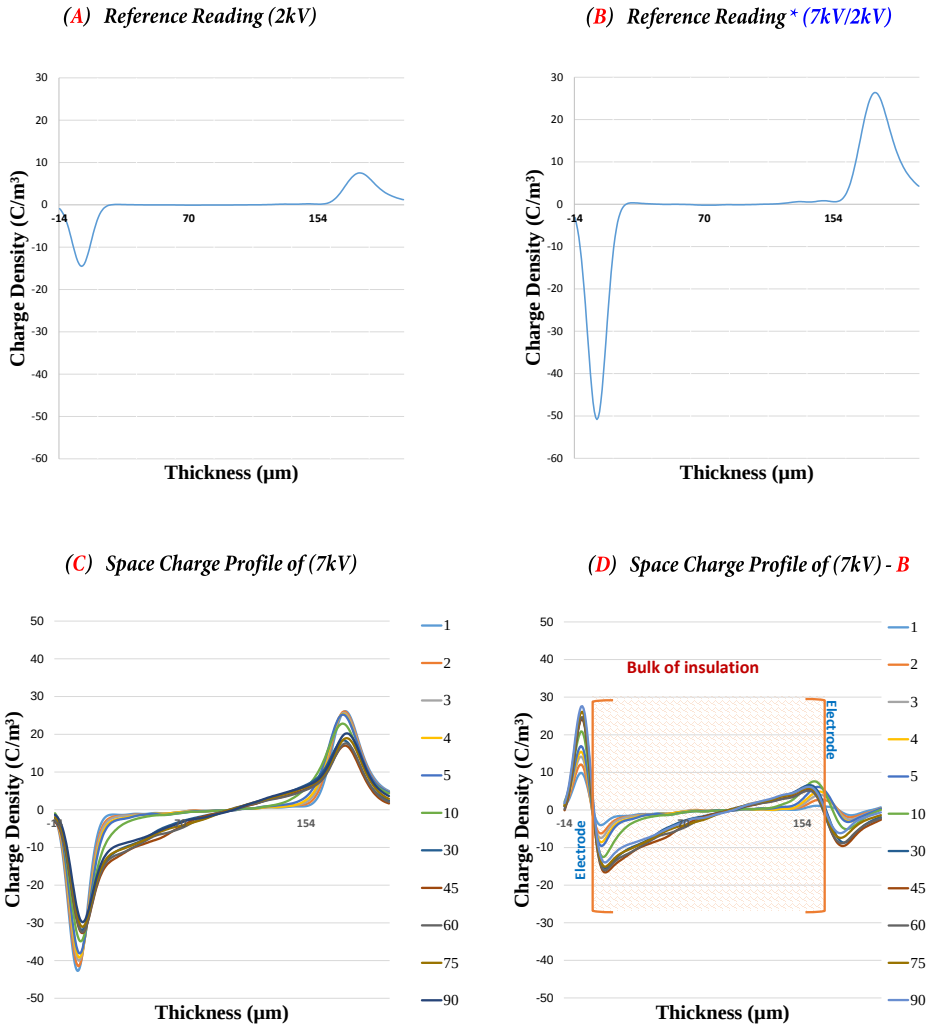

FIGURE A.1: Steps of measuring the total trapped charge while the voltage is switched on. (A) Represents the reference reading for the space charge profile. (B) The resulting reference signal after the maximisation. (C) Space charge profile at a chosen field. (D) Subtraction of maximised reference signal from the chosen applied voltage.

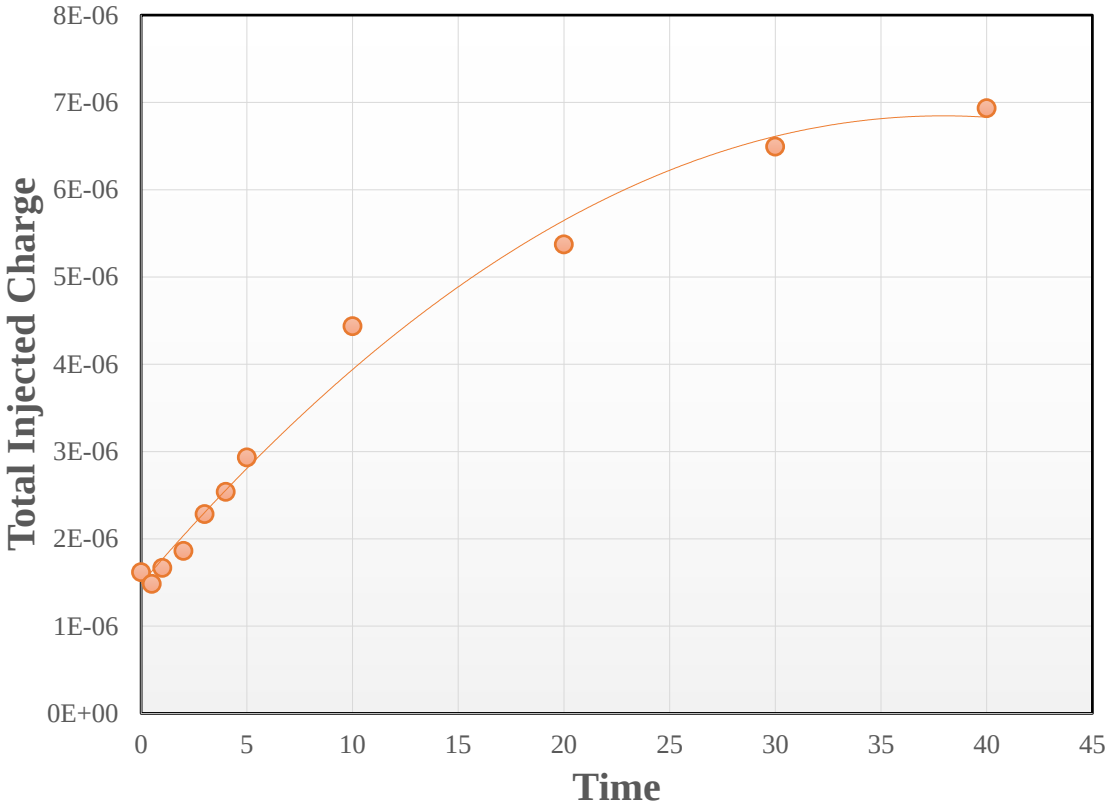

FIGURE A.2: Results of space charge amount at different selected times when the voltage source is switched on at 7KV for 40 mins..

Appendix B

Simulation Matlab Code

The matlab code is described individually step by step regarding to the flowchart in Figure 7.2. The first step started by asking the user to enter the input parameter values as shown in the code.

```
% entered values
Hboun= input('The high boundary value  = ');
a= input('The max value of X-axis (Columns) = ');
b= input('The max value of Y-axis (Rows) = ');
bond_size= input('The bond size = ');
tole= input('The tolerance value = ');
```

The next step is to create a random value of C^* for every single bond. As the simulation is performed in two-dimension, both bonds either in rows and columns are considered.

```
%to creat C* (for rows)
for i=1:a
for j=1:bb
Csr(j,i)= 0.23  + (0.44 -0.23 ).*rand(1,1);
end
end
%to creat C* (for columns)
for i=1:aa
for j=1:b
Csc(j,i)= 0.23  + (0.44-0.23 ).*rand(1,1);
end
end
```

As mentioned earlier in Chapter 7, the chosen method for distributing the electric potential is the finite difference method. This step is to show how to do the distribution among the cross points in the grid.

```
% Electric potential
for j = 1:a        % Columns
for i = 2:b-1      % Rows
if (j==1)
U2(i,j)=( U1(i,j+1)+ U1(i-1,j)+ U1(i,j+1)+ U1(i+1,j))/4;
elseif (j==a)
U2(i,j)=( U1(i-1,j)+ U1(i,j-1)+ U1(i,j-1)+ U1(i+1,j))/4;
elseif ((j≥2)&&(j≤(a-1)))
U2(i,j)=( U1(i+1,j)+ U1(i,j-1)+ U1(i,j+1)+ U1(i-1,j))/4;
end
end
%  check the tolerance
for j=1:a
for i=2:b-1
if abs(U1(i,j)-U2(i,j))>diff
diff= abs(U1(i,j)-U2(i,j));
end
U1(i,j)=U2(i,j);
end
end
```

Once the electric potential is calculated for every single cross-point, the electric field can be calculated using Equation 7.11.

```
%electric field for rows
for j=1:b-1
EFRR(j,:)= abs(U1(j,:)-U1(j+1,:))/bond_size;
end
%electric field for columns
for j=1:a-1
EFCC(:,j)= abs(U1(:,j)-U1(:,j+1))/bond_size;
end
```

Here is the fixed parameters during the ageing process. These parameters are either is taken from the literature or from other experimental work in the thesis.

```
%  The fixed parameters
q       =   1.6e-19;        %electron charge
T       =   273+80;         %Temperature
Cross   =   6.5462e-16;     %Trap cross-section
A       =   1.5564e+06;     %Richardson constant
Et      =   3.9422e-19;     %Trap depth
k       =   1.38e-23;       %Boltzmann constant
h       =   6.62606957e-34; %Planck constant
Nc      =   2*(2*pi*(9.10938291e-31)*k*T/(h^2))^(3/2);  %Effective ...
    state in the conduction band
Vth     =   (3*k*T/(9.10938291e-31))^0.5;  %Thermal velocity
```

```
Qw       =   2.7000e-19;   %Barrier heigh
Bs_row   = (((q^3)/(4*pi*2.3*8.854e-12))^0.5);
Bs_col   = (((q^3)/(4*pi*2.3*8.854e-12))^0.5);
```

When the above part is completed, the next part is to calculate the lifetime for every single bond in the mesh. For rows:

```
for j=1:aa  % Coulmns
for i=1:b   % Rows
W_row(j,i)  = (2e-55).*EFRR(j,i).^4;  %Mechanical energy
%-------------------
%  Check how to calculate the C0, at the first cycle is equal to 0
%-------------------
if (First_cycle==1)
Cr0_new(j,i)=Cr0(j,i);
elseif ((First_cycle ~= 1) & (Lr(j,i)~=36*10^(16)))
Cr0_new(j,i)= Cqr(j,i)*(1 - exp(- (Kf_r(j,i) + Kb_r(j,i)) * LLL ) ) ...
+ Cr0(j,i) * exp (- (Kf_r(j,i) + Kb_r(j,i)) *  LLL );
end
%-------------------
%  Update C0 for rows
%-------------------
Cr0(j,i)=Cr0_new(j,i);

%-------------------
%Trapping and Detrapping reaction rates - only rows
%-------------------
Kf_r(j,i) = (( A * T^2 * Cross)/(q)) * exp(-(Qw - Bs_row * ...
    (EFRR(j,i))^(0.5) )/(k * T));
Kb_r(j,i) = (Nc * Vth * Cross) * exp(-( Et - W_row(j,i) )/(k * T));

%-------------------
%  Calculate the equlibrium value
%-------------------
Cqr(j,i)=((1+ ((q * Nc * Vth)/(A * T^2))* exp(-((Et - W_row(j,i))-(Qw ...
    - Bs_row * (EFRR(j,i))^(0.5) ))/(k * T))   ).^-1);

%-------------------
% Check some conditions on the model
%-------------------
if ((Cqr(j,i) <= Csr(j,i)) & (Lr(j,i)~=36*10^(16)))
Lr(j,i)=36*10^(16);

%-------------------
% calculate if Cq > C*, and a bond has not been broken
%-------------------
elseif((Cqr(j,i) > Csr(j,i)) & (Lr(j,i)~=36*10^(16)))
Lr(j,i) = (Kf_r(j,i) + Kb_r(j,i))^(-1) * log((Cqr(j,i) - ...
    Cr0(j,i))/(Cqr(j,i) - Csr(j,i)));
```

```
end
end
end
```

Bellow is the calculation of the lifetime for columns.

```
for j=1:a     % Coulmns
for i=1:bb    % Rows
W_col(j,i)  = (2e-55).*EFCC(j,i).^4;   %Mechanical energy
%-----------------
%  Check how to calculate the C0, at the first cycle is equal to 0
%-----------------
if (First_cycle==1)
Cc0_new(j,i)=Cc0(j,i);
elseif ((First_cycle ~= 1) & (Lc(j,i)~=36*10^(16)))
Cc0_new(j,i)= Cqc(j,i)*(1 - exp(- (Kf_c(j,i) + Kb_c(j,i)) * LLL ) ) ...
+ Cc0(j,i) * exp (- (Kf_c(j,i) + Kb_c(j,i)) *  LLL );
end
%-----------------
%  Update C0 for columns
%-----------------
Cc0(j,i)=Cc0_new(j,i);
%-----------------
%Trapping and Detrapping reaction rates - only columns
%-----------------
Kf_c(j,i) = (( A * T^2 * Cross)/(q)) * exp(-(Qw - Bs_col * ...
    (EFCC(j,i))^(0.5) )/(k * T));
Kb_c(j,i) = (Nc * Vth * Cross) * exp(-( Et - W_col(j,i) )/(k * T));
%-----------------
%  Calculate the equlibrium value
%-----------------
Cqc(j,i)=((1+ ((q * Nc * Vth)/(A * T^2))* exp(-((Et - W_col(j,i))-(Qw ...
    - Bs_col * (EFCC(j,i))^(0.5) ))/(k * T))   ).^-1);
%-----------------
% Check some conditions on the model
%-----------------
if ((Cqc(j,i) <= Csc(j,i)) & (Lc(j,i)~=36*10^(16)))
Lc(j,i)=36*10^(16);
%-----------------
% calculate if Cq > C*, and a bond has not been broken
%-----------------
elseif((Cqc(j,i) > Csc(j,i)) & (Lc(j,i)~=36*10^(16)))
Lc(j,i) = (Kf_c(j,i) + Kb_c(j,i))^(-1) * log((Cqc(j,i) - ...
    Cc0(j,i))/(Cqc(j,i) - Csc(j,i)));
end
end
end
```

At this stage, it is possible to detect the minimum lifetime in the mesh for both directions; rows and columns.

```
Lowest_row=min(Lr(:))
Lowest_column=min(Lc(:))
%------------------
%Determine the x and y position for the lowest values of row and column
[Minval, Minidx] = min(Lr(:));
[minRow, minCol] = ind2sub(size(Lr),Minidx)
[MinvalC, MinidxC] = min(Lc(:));
[minRowC, minColC] = ind2sub(size(Lc),MinidxC)
```

Now, breaking the lowest time of either row or column.

```
%compartion between row and column and select the lowest value
if (Lowest_row< Lowest_column)
U3(minRow,minCol)=1;        %To creat the breakdown sign in the matrix
U3(minRow+1,minCol)=1;      %To creat the breakdown sign in the matrix
LLL=Lowest_row
time_total=time_total+LLL
Lr(minRow,minCol)=36*10^(16);

elseif (Lowest_column< Lowest_row)
U3(minRowC,minColC)=1;      %To creat the breakdown sign in the matrix
U3(minRowC,minColC+1)=1;    %To creat the breakdown sign in the matrix
LLL=Lowest_column
time_total=time_total+LLL
Lc(minRowC,minColC)=36*10^(16);

elseif (Lowest_column == Lowest_row)
U3(minRow,minCol)=1;        %To creat the breakdown sign in the matrix
U3(minRow+1,minCol)=1;      %To creat the breakdown sign in the matrix
LLL=Lowest_row
time_total=time_total+LLL
Lr(minRow,minCol)=36*10^(16);

elseif ((Lowest_column == 36*10^(16)) &  (Lowest_row == 36*10^(16)))
('Please stop here')
pause

end
```

Finally creating the path between the two electrodes (Top and Bottom), and stop simulation once completed.

```
[ch,bx] = islands(U3);bx(bx(:,end) ≠ 1,:) = ...
    [];ch(¬ismember(ch,bx(:,1))) = 0;
if (any(ismember(nonzeros(ch(1,:)),nonzeros(ch(end,:)))))
Check=0;
End_time=clock;
end
```

Bibliography

[1] D. Fabiani, G. Montanari, C. Laurent, G. Teyssedre, P. Morshuis, R. Bodega, L. Dissado, A. Campus, and U. Nilsson, "Polymeric hvdc cable design and space charge accumulation. part 1: insulation/semicon interface," *Electrical Insulation Magazine, IEEE*, vol. 23, no. 6, pp. 11–19, 2007.

[2] K. Bambery, R. Fleming, and J. Holbøll, "Space charge profiles in low density polyethylene samples containing a permittivity/conductivity gradient," *Journal of Physics D: Applied Physics*, vol. 34, no. 20, p. 3071, 2001.

[3] Y. Zhang, J. Lewiner, C. Alquie, and N. Hampton, "Evidence of strong correlation between space-charge buildup and breakdown in cable insulation," *Dielectrics and Electrical Insulation, IEEE Transactions on*, vol. 3, no. 6, pp. 778–783, 1996.

[4] M. Berthelot, "Action of heat on some hydrogenocarbon compounds," *CR Acad. Sci*, vol. 62, p. 905, 1866.

[5] H. Staudinger, "Über polymerisation," *Berichte der deutschen chemischen Gesellschaft (A and B Series)*, vol. 53, no. 6, pp. 1073–1085, 1920.

[6] R. J. Young and P. A. Lovell, *Introduction to polymers*, vol. 2. Chapman & Hall London, 1991.

[7] C. W. Hume, "Synthetic fiber," Sept. 20 1938. US Patent 2,130,948.

[8] J. C. Anderson, K. D. Leaver, R. D. Rawlings, and P. S. Leevers, *Materials science for engineers*. CRC Press, 2003.

[9] L. A. Dissado and J. C. Fothergill, "Electrical degradation and breakdown in polymers," vol. 9, 1992.

[10] G. Odian, *Principles of polymerization*. John Wiley & Sons, 2004.

[11] J.-P. Crine, J.-L. Parpal, and G. Lessard, "A model of aging of dielectric extruded cables," in *Conduction and Breakdown in Solid Dielectrics, 1989., Proceedings of the 3rd International Conference on*, pp. 347–351, IEEE, 1989.

[12] "Publication 505, guide for evaluation and identification of insulation systems of electrical equipment," Tech. Rep. 1975.

[13] C. Dang, J.-L. Parpal, and J.-P. Crine, "Electrical aging of extruded dielectric cables: review of existing theories and data," *Dielectrics and Electrical Insulation, IEEE Transactions on*, vol. 3, no. 2, pp. 237–247, 1996.

[14] L. Dissado, G. Mazzanti, and G. Montanari, "The role of trapped space charges in the electrical aging of insulating materials," *Dielectrics and Electrical Insulation, IEEE Transactions on*, vol. 4, no. 5, pp. 496–506, 1997.

[15] G. Blaise and W. Sarjeant, "Space charge in dielectrics. energy storage and transfer dynamics from atomistic to macroscopic scale," *Dielectrics and Electrical Insulation, IEEE Transactions on*, vol. 5, no. 5, pp. 779–808, 1998.

[16] T. W. Dakin, "Electrical insulation deterioration treated as a chemical rate phenomenon," *American Institute of Electrical Engineers, Transactions of the*, vol. 67, no. 1, pp. 113–122, 1948.

[17] L. Simoni, *Fundamentals of endurance of electrical insulating materials.* CLUEB, 1983.

[18] S. Zhurkov, "Kinetic concept of the strength of solids," *International Journal of Fracture*, vol. 26, no. 4, pp. 295–307, 1984.

[19] V. Montsinger, "Loading transformers by temperature," *American Institute of Electrical Engineers, Transactions of the*, vol. 49, no. 2, pp. 776–790, 1930.

[20] S. Glasstone, H. Eyring, and K. J. Laidler, *The theory of rate processes.* McGraw-Hill, 1941.

[21] T. Hibma and H. Zeller, "Space charges and dielectric ageing," in *Conference Record of the 1985 International Conference on Properties and Applications of Dielectric Materials*, pp. 230–233, 1985.

[22] J. Oudin, Y. Rerolle, and H. Thevenon, "Theorie statistique du claquage electrique," *Rev. Gen. Elec*, vol. 77, pp. 430–436, 1968.

[23] E. Occhini, "A statistical approach to the discussion of the dielectric strength in electric cables," *Power Apparatus and Systems, IEEE Transactions on*, no. 6, pp. 2671–2682, 1971.

[24] A. Gjerde, "Multifactor ageing models-origin and similarities," *Electrical Insulation Magazine, IEEE*, vol. 13, no. 1, pp. 6–13, 1997.

[25] H. Endicott, B. Hatch, and R. Sohmer, "Application of the eyring model to capacitor aging data," *Component Parts, IEEE Transactions on*, vol. 12, no. 1, pp. 34–41, 1965.

[26] B. Hemalatha and T. Ramu, "Insulation degradation under multifactor stress," in *Fifth International Symposium on High Voltage Engineering, Braunschweig, West Germany*, 1987.

[27] B. Fallou, C. Burguiere, and J. Morel, "First approach on multiple stress accelerated life testing of electrical insulation," *CEIDP Annual Report*, pp. 621–8, 1979.

[28] J.-P. Crine and A. Vijh, "A molecular approach to the physicochemical factors in the electric breakdown of polymers," *Applied physics communications*, vol. 5, no. 3, pp. 139–163, 1985.

[29] T. Lewis, "Ageing-a perspective," *Electrical Insulation Magazine, IEEE*, vol. 17, no. 4, pp. 6–16, 2001.

[30] L. Dissado, G. Mazzanti, and G. Montanari, "The incorporation of space charge degradation in the life model for electrical insulating materials," *Dielectrics and Electrical Insulation, IEEE Transactions on*, vol. 2, no. 6, pp. 1147–1158, 1995.

[31] L. Dissado, G. Mazzanti, and G. Montanari, "Discussion of space-charge life model features in dc and ac electrical aging of polymeric materials," in *Electrical Insulation and Dielectric Phenomena, 1997. IEEE 1997 Annual Report., Conference on*, vol. 1, pp. 36–40, IEEE, 1997.

[32] N. G. McCrum, B. E. Read, and G. Williams, "Anelastic and dielectric effects in polymeric solids," 1967.

[33] T. Lewis, J. Llewellyn, M. Van der Sluijs, J. Freestone, and R. Hampton, "A new model for electrical ageing and breakdown in dielectrics," in *Dielectric Materials, Measurements and Applications, Seventh International Conference on (Conf. Publ. No. 430)*, pp. 220–224, IET, 1996.

[34] J.-L. Parpal, J.-P. Crine, and C. Dang, "Electrical aging of extruded dielectric cables. a physical model," *Dielectrics and Electrical Insulation, IEEE Transactions on*, vol. 4, no. 2, pp. 197–209, 1997.

[35] J. Matthews, H. Peiser, and R. Richards, "The x-ray measurement of the amorphous content of polythene samples," *Acta Crystallographica*, vol. 2, no. 2, pp. 85–90, 1949.

[36] G. Challa, *Polymer chemistry: an introduction*. Prentice Hall, 1993.

[37] T. Lewis, "The micro-physics of charge in solid dielectrics," *Space charge in solid dielectrics*, pp. 1–17, 1998.

[38] G. Teyssedre and C. Laurent, "Charge transport modeling in insulating polymers: from molecular to macroscopic scale," *Dielectrics and Electrical Insulation, IEEE Transactions on*, vol. 12, no. 5, pp. 857–875, 2005.

[39] T. Lewis, J. Llewellyn, and M. Van der Sluijs, "Electrokinetic properties of metal-dielectric interfaces," *IEE Proceedings A (Science, Measurement and Technology)*, vol. 140, no. 5, pp. 385–392, 1993.

[40] T. Lewis, J. Llewellyn, and M. Van der Sluijs, "Electrically induced mechanical strain in insulating dielectrics," in *Electrical Insulation and Dielectric Phenomena, 1994., IEEE 1994 Annual Report., Conference on*, pp. 328–333, IEEE, 1994.

[41] J.-P. Crine, "A molecular approach to the electrical aging of xlpe cables," Jicable.

[42] J.-P. Crine, "Comparison between lewis and crine models for the electrical aging of dielectric polymers," in *Electrical Insulation and Dielectric Phenomena, 1999 Annual Report Conference on*, vol. 2, pp. 508–511, IEEE, 1999.

[43] P. Sayers, T. Lewis, J. Llewellyn, and C. Griffiths, "Investigation of the structural changes in ldpe and xlpe induced by high electrical stress," 2000.

[44] A. Griffith, "The phenomenon of rupture and now in solids," *Phil. Trans. R. Soc. A221*, vol. 163, 1920.

[45] J.-P. Crine, "A molecular model to evaluate the impact of aging on space charges in polymer dielectrics," *Dielectrics and Electrical Insulation, IEEE Transactions on*, vol. 4, no. 5, pp. 487–495, 1997.

[46] J.-P. Crine, "Aging and polarization phenomena in pe under high electric fields," *Dielectrics and Electrical Insulation, IEEE Transactions on*, vol. 9, no. 5, pp. 697–703, 2002.

[47] L. C. E. Struik, *Physical aging in amorphous polymers and other materials*. PhD thesis, TU Delft, Delft University of Technology, 1977.

[48] L. Reich and S. Stivala, "Elements of polymer degradation," 1971.

[49] K. Nakayama, "Triboemission of charged particles from various solids under boundary lubrication conditions," *Wear*, vol. 178, no. 1, pp. 61–67, 1994.

[50] B. Vallayer, G. Blaise, and D. Treheux, "Space charge measurement in a dielectric material after irradiation with a 30 kv electron beam: Application to single-crystals oxide trapping properties," *Review of scientific instruments*, vol. 70, no. 7, pp. 3102–3112, 1999.

[51] P. M. H. Janah and B. Aladenize, "Quality of hv cables insulators evaluated for their ability to trap and relax charges," *Suppl. Le Vide: Science, Technique et Applications*, vol. 275, pp. 454 –457, 1995.

[52] J. Nelson, "Breakdown strength of solids," *Engineering Dielectrics, Vol. IIA, ASTM Stol, Bartnikas/Eichhorn, Editors*, pp. 445–520, 1983.

[53] I. Chalmers and C. Wang, "Dielectric surface charge phenomena in simulated space conditions," in *Charging and Tracking of Insulators in Gaseous and Vacuum Environments, IEE Colloquium on*, pp. 511–515, IET, 1990.

[54] D. Wolters and J. Van der Schoot, "Dielectric breakdown in mos devices, part i: Defect-related and intrinsic breakdown," *Philips J. Res*, vol. 40, no. 3, pp. 115–136, 1985.

[55] H. C. Miller, "High voltage performance characteristics of solid insulators in vacuum," *High Voltage Vacuum Insulation, RV Latham, ed., Academic Press, London*, 1995.

[56] T. Mizutan, "Space charge measurement techniques and space charge in polyethylene," *Dielectrics and Electrical Insulation, IEEE Transactions on*, vol. 1, no. 5, pp. 923–933, 1994.

[57] H. Zeller, T. Baumann, and F. Stucki, "Microscopic models for ageing in solid dielectrics," in *Properties and Applications of Dielectric Materials, 1988. Proceedings., Second International Conference on Properties and Applications of*, pp. 13–15, IEEE, 1988.

[58] G. Blaise, "New approach to flashover in dielectrics based on a polarization energy relaxation mechanism," *Electrical Insulation, IEEE Transactions on*, vol. 28, no. 4, pp. 437–443, 1993.

[59] H. Eyring, J. Walter, and G. Kimball, *Quantum chemistry*. John Wiley & Sons Inc, 1944.

[60] G. Damamme, C. Le Gressus, and A. De Reggi, "Space charge characterization for the 21th century," *Dielectrics and Electrical Insulation, IEEE Transactions on*, vol. 4, no. 5, pp. 558–584, 1997.

[61] G. Damamme and C. Le Gressus, "Simulation of the triple junction effects in vacuum devices," in *Electrical Insulation and Dielectric Phenomena, 1996., IEEE 1996 Annual Report of the Conference on*, vol. 2, pp. 562–566, IEEE, 1996.

[62] D. Wolters and J. van der Schoot, "Breakdown by charge injection," *Insulating Films On Semiconductors*, 1985.

[63] D. Wolters and J. Van Der Schoot, "Kinetics of charge trapping in dielectrics," *Journal of applied physics*, vol. 58, no. 2, pp. 831–837, 1985.

[64] C. Williams, "Kinetics of trapping, detrapping, and trap generation," *Journal of electronic materials*, vol. 21, no. 7, pp. 711–720, 1992.

[65] J. Simmons, "Conduction in thin dielectric films," *Journal of Physics D: Applied Physics*, vol. 4, no. 5, p. 613, 1971.

[66] C. Sah, "Models and experiments on degradation of oxidized silicon," *Solid-state electronics*, vol. 33, no. 2, pp. 147–167, 1990.

[67] J. Albohn, W. Füssel, N. Sinh, K. Kliefoth, and W. Fuhs, "Capture cross sections of defect states at the si/sio2 interface," *Journal of Applied Physics*, vol. 88, no. 2, pp. 842–849, 2000.

[68] Y. Wang and K. Cheung, "Carrier capture at the sio 2–si interface: A physical model," *Applied Physics Letters*, vol. 91, no. 11, pp. 113509–113509, 2007.

[69] D. Goguenheim, D. Vuillaume, G. Vincent, and N. M. Johnson, "Accurate measurements of capture cross sections of semiconductor insulator interface states by a trap-filling experiment: The charge-potential feedback effect," *Journal of Applied Physics*, vol. 68, no. 3, pp. 1104–1113, 1990.

[70] T.-C. Zhou, G. Chen, R.-j. Liao, and Z. Xu, "Charge trapping and detrapping in polymeric materials: Trapping parameters," *Journal of Applied Physics*, vol. 110, no. 4, p. 043724, 2011.

[71] J. McPherson, J. Kim, A. Shanware, H. Mogul, and J. Rodriguez, "Proposed universal relationship between dielectric breakdown and dielectric constant," in *Electron Devices Meeting, 2002. IEDM'02. International*, pp. 633–636, IEEE, 2002.

[72] T. Burkes and W. Sarjeant, "Electromechanical shock in pulse power components," tech. rep., Los Alamos Scientific Lab., NM (USA), 1980.

[73] G. Blaise, "Charge detrapping induced dielectric relaxation. application to breakdown in insulating films," *Microelectronic Engineering*, vol. 28, no. 1, pp. 55–62, 1995.

[74] Y. Namiki, H. Shimanuki, F. Aida, and M. Morita, "A study on microvoids and their filling i crosslinked polyethylene insulated cables," *Electrical Insulation, IEEE Transactions on*, no. 6, pp. 473–480, 1980.

[75] J. G. Simmons, "Transition from electrode-limited to bulk-limited conduction processes in metal-insulator-metal systems," *Physical Review*, vol. 166, no. 3, p. 912, 1968.

[76] J. G. Simmons, "Poole-frenkel effect and schottky effect in metal-insulator-metal systems," *Physical Review*, vol. 155, no. 3, p. 657, 1967.

[77] J. Van der Waals and J. Platteeuw, "Clathrate solutions," *Advances in Chemical Physics, Volume 2*, pp. 1–57, 2007.

[78] A. Blythe, "Electrical properties of polymers. cambridge solid state science," 1979.

[79] D. A. Seanor, *Electrical properties of polymers*. Elsevier, 2013.

[80] N. F. Mott and E. A. Davis, *Electronic processes in non-crystalline materials.* Oxford University Press, 2012.

[81] D. Seanor, "Electronic and ionic conductivity in nylon 66," *Journal of Polymer Science Part A-2: Polymer Physics*, vol. 6, no. 3, pp. 463–477, 1968.

[82] D. Davies and D. Seanor, "Electrical properties of polymers," 1982.

[83] S. Saito, H. Sasabe, T. Nakajima, and K. Yada, "Dielectric relaxation and electrical conduction of polymers as a function of pressure and temperature," *Journal of Polymer Science Part A-2: Polymer Physics*, vol. 6, no. 7, pp. 1297–1315, 1968.

[84] T. Miyamoto and K. Shibayama, "Free-volume model for ionic conductivity in polymers," *Journal of applied physics*, vol. 44, no. 12, pp. 5372–5376, 1973.

[85] M. Kosaki, K. Sugiyama, and M. Ieda, "Ionic jump distance and glass transition of polyvinyl chloride," *Journal of Applied Physics*, vol. 42, no. 9, pp. 3388–3392, 1971.

[86] M. Mochizuki, M. Sawa, and K. Masuda, "Topical indomethacin in intracapsular extraction of senile cataract," *Japanese Journal of Ophthalmology*, vol. 21, no. 2, pp. p215–226, 1977.

[87] W. R. Moore, *An introduction to polymer chemistry.* Aldine Pub. Co., 1963.

[88] N. F. Mott and R. W. Gurney, "Electronic processes in ionic crystals," 1948.

[89] K. C. Kao, *Dielectric phenomena in solids.* Academic press, 2004.

[90] O. Yi, F. Xu, X. Xie, and D. Zhu, "Hopping current and charge storage in polymer electret," in *Electrets, 1996.(ISE 9), 9th International Symposium on*, pp. 54–59, IEEE, 1996.

[91] R. Bartnikas and R. Eichhorn, "Electrical properties of solid insulating materials," American Society for Testing and Materials, 1983.

[92] S. Le Roy, P. Segur, G. Teyssedre, and C. Laurent, "Description of bipolar charge transport in polyethylene using a fluid model with a constant mobility: model prediction," *Journal of physics D: Applied physics*, vol. 37, no. 2, p. 298, 2004.

[93] D. Emin, "On the existence of free and self-trapped carriers in insulators: an abrupt temperature-dependent conductivity transition," *Advances in Physics*, vol. 22, no. 1, pp. 57–116, 1973.

[94] S. Summerfield and P. Butcher, "Universal behaviour of ac hopping conductivity in disordered systems," *Journal of Non-Crystalline Solids*, vol. 77, pp. 135–138, 1985.

[95] J. Frenkel, "On pre-breakdown phenomena in insulators and electronic semiconductors," *Physical Review*, vol. 54, no. 8, p. 647, 1938.

[96] R. Ongaro and A. Pillonnet, "Poole-frenkel (pf) effect high field saturation," *Revue de Physique Appliquée*, vol. 24, no. 12, pp. 1085–1095, 1989.

[97] F.-C. Chiu, "A review on conduction mechanisms in dielectric films," *Advances in Materials Science and Engineering*, vol. 2014, 2014.

[98] R. M. Hill, "Poole-frenkel conduction in amorphous solids," *Philosophical magazine*, vol. 23, no. 181, pp. 59–86, 1971.

[99] J. Yeargan and H. Taylor, "The poole-frenkel effect with compensation present," *Journal of Applied Physics*, vol. 39, no. 12, pp. 5600–5604, 1968.

[100] S. Sze, "Physics of semiconducting devices," *End of Bibliographic Section*, 1981.

[101] S. Sze, "Current transport and maximum dielectric strength of silicon nitride films," *Journal of Applied Physics*, vol. 38, no. 7, pp. 2951–2956, 1967.

[102] C. Mead, "Electron transport mechanisms in thin insulating films," *Physical Review*, vol. 128, no. 5, p. 2088, 1962.

[103] A. G. Milnes, "Deep impurities in semiconductors," 1973.

[104] J. J. O'Dwyer, *The theory of electrical conduction and breakdown in solid dielectrics*. Clarendon Press, 1973.

[105] G. Khan and C. Hogarth, "Electrical conduction through mim structures of evaporated v2o5 and v2o5/b2o3 amorphous thin films," *Journal of materials science*, vol. 25, no. 12, pp. 5014–5018, 1990.

[106] S. O. Kasap, *Principles of electronic materials and devices*, vol. 81. McGraw-Hill New York, NY, 2006.

[107] A. Sommerfield, "Partial differential equations in physics new york," 1949.

[108] R. H. Fowler and L. Nordheim, "Electron emission in intense electric fields," in *Proceedings of the Royal Society of London A: Mathematical, Physical and Engineering Sciences*, vol. 119, pp. 173–181, The Royal Society, 1928.

[109] G. Wentzel, "Eine verallgemeinerung der quantenbedingungen für die zwecke der wellenmechanik," *Zeitschrift für Physik*, vol. 38, no. 6-7, pp. 518–529, 1926.

[110] H. Kramers, "Some remarks on the theory of absorption and refraction of x-rays," *Nature*, vol. 117, no. 2952, pp. 774–775, 1926.

[111] L. Brillouin, "La mécanique ondulatoire de schrödinger; une méthode générale de résolution par approximations successives," *CR Acad. Sci*, vol. 183, no. 11, pp. 24–26, 1926.

[112] T. Lewis, "Some factors influencing field emission and the fowler-nordheim law," *Proceedings of the Physical Society. Section B*, vol. 68, no. 11, p. 938, 1955.

[113] A. International, *Standard Test Methods for DC Resistance Or Conductance of Insulating Materials*. ASTM International, 2007.

[114] J. F. Fowler and F. Farmer, "Effect of temperature on the conductivity induced in insulators by x-rays," 1953.

[115] R. Neagu, J. Marat-Mendes, and E. Neagu, "Electrical conduction of ldpe at moderate fields," in *Electrets, 2002. ISE 11. Proceedings. 11th International Symposium on*, pp. 118–121, IEEE, 2002.

[116] M. Ieda, "Carroer injection, space charge and electrical breakdown in insulating polymers," *Electrical Insulation, IEEE Transactions on*, no. 3, pp. 261–267, 1987.

[117] J. Lewiner, "Evolution of experimental techniques for the study of the electrical properties of insulating materials," *Electrical Insulation, IEEE Transactions on*, no. 3, pp. 351–360, 1986.

[118] S. B. Lang and D. Das-Gupta, "A technique for determining the polarization distribution in thin polymer electrets using periodic heating," *Ferroelectrics*, vol. 39, no. 1, pp. 1249–1252, 1981.

[119] T. Maeno, H. Kushibe, T. Takada, and C. Cooke, "Pulsed electroacoustic method for the measurement of volume charges in e-beam irradiated pmma," *CEIDP Annual Report*, pp. 389–393, 1985.

[120] A. Migliori and T. Hofler, "Use of laser-generated acoustic pulses to measure the electric field inside a solid dielectric," *Review of Scientific Instruments*, vol. 53, no. 5, pp. 662–666, 1982.

[121] G. Sessler, J. West, and R. Gerhard, "Measurement of charge distribution in polymer electrets by a new pressure-pulse method," *Polymer Bulletin*, vol. 6, no. 1-2, pp. 109–111, 1981.

[122] N. Ando and F. Numajiri, "Experimental investigation of space charge in xlpe cable using dust figure," *Electrical Insulation, IEEE Transactions on*, no. 1, pp. 36–42, 1979.

[123] M. S. Khalil and B. S. Hansen, "Investigation of space charge in low-density polyethylene using a field probe technique," *Electrical Insulation, IEEE Transactions on*, vol. 23, no. 3, pp. 441–445, 1988.

[124] M. Ieda, T. Mizutani, Y. Suzuoki, and Y. Yokota, "Study of space charge effects in polyethylene by thermal-pulse current techniques," *Electrical Insulation, IEEE Transactions on*, vol. 25, no. 3, pp. 509–514, 1990.

[125] Y. Tanaka, H. Kitajima, M. Kodaka, and T. Takada, "Analysis and discussion on conduction current based on simultaneous measurement of tsc and space charge distribution," *Dielectrics and Electrical Insulation, IEEE Transactions on*, vol. 5, no. 6, pp. 952–956, 1998.

[126] R. Ono, M. Nakazawa, and T. Oda, "Charge storage in corona-charged polypropylene films analyzed by lipp and tsc methods," *Industry Applications, IEEE Transactions on*, vol. 40, no. 6, pp. 1482–1488, 2004.

[127] S. Bamji and A. Bulinski, "Luminescence in polymeric insulation and its implication on insulation aging," in *Electrical Insulating Materials, 2001.(ISEIM 2001). Proceedings of 2001 International Symposium on*, pp. 453–458, IEEE, 2001.

[128] M. Ieda, "Dielectric breakdown process of polymers," *Electrical Insulation, IEEE Transactions on*, no. 3, pp. 206–224, 1980.

[129] R. Collins, "Distribution of charge in electrets," *Applied Physics Letters*, vol. 26, no. 12, pp. 675–677, 1975.

[130] J. Giacometti, G. Minami, A. De Reggi, B. Dickens, and D. Chinaglia, "Thermal pulse measurements on electron-beam irradiated fluoroethylene-propylene copolymer," in *Electrets, 1994.(ISE 8), 8th International Symposium on*, pp. 212–217, IEEE, 1994.

[131] A. Mellinger, R. Singh, and R. Gerhard-Multhaupt, "Fast thermal-pulse measurements of space-charge distributions in electret polymers," *Review of scientific instruments*, vol. 76, no. 1, p. 013903, 2005.

[132] G. M. Sessler, J. E. West, R. Gerhard-Multhaupt, and H. von Seggern, "Nondestructive laser method for measuring charge profiles in irradiated polymer films," *Nuclear Science, IEEE Transactions on*, vol. 29, no. 6, pp. 1644–1649, 1982.

[133] D. Malec, "Technical problems encountered with the laser induced pressure pulse method in studies of high voltage cable insulators," *Measurement Science and Technology*, vol. 11, no. 5, p. N76, 2000.

[134] G. Chen, T. Tay, A. Davies, Y. Tanaka, and T. Takada, "Electrodes and charge injection in low-density polyethylene using the pulsed electroacoustic technique," *Dielectrics and Electrical Insulation, IEEE Transactions on*, vol. 8, no. 6, pp. 867–873, 2001.

[135] Y. Li, J. Kawai, Y. Ebinuma, Y. Fujiwara, Y. Ohki, Y. Tanaka, and T. Takada, "Space charge behavior under ac voltage in water-treed pe observed by the pea method," *Dielectrics and Electrical Insulation, IEEE Transactions on*, vol. 4, no. 1, pp. 52–57, 1997.

[136] T. Takada and T. Sakai, "Measurement of electric fields at a dielectric/electrode interface using an acoustic transducer technique," *Electrical Insulation, IEEE Transactions on*, no. 6, pp. 619–628, 1983.

[137] Z. Xu, *Space charge measurement and analysis in low density polyethylene films.* PhD thesis, University of Southampton, 2009.

[138] N. L. Dao, *Impulse ageing of polymeric materials.* PhD thesis, University of Southampton, 2011.

[139] T. Takada, T. Maeno, and H. Kushibe, "An electric stress-pulse technique for the measurement of charges in a plastic plate irradiated by an electron beam," *Electrical Insulation, IEEE Transactions on*, no. 4, pp. 497–501, 1987.

[140] D. D. Gupta and M. Barbarez, "On electronic conduction in polyethylene films," *Journal of Physics D: Applied Physics*, vol. 6, no. 7, p. 867, 1973.

[141] J. Hageman, G. de Wijs, R. de Groot, and R. J. Meier, "Bond scission in a perfect polyethylene chain and the consequences for the ultimate strength," *Macromolecules*, vol. 33, no. 24, pp. 9098–9108, 2000.

[142] L. Dissado, G. Mazzanti, and G. Montanari, "Elemental strain and trapped space charge in thermoelectrical aging of insulating materials. part 1: elemental strain under thermo-electrical-mechanical stress," *Dielectrics and Electrical Insulation, IEEE Transactions on*, vol. 8, no. 6, pp. 959–965, 2001.

[143] J. Kuffel, E. Kuffel, and W. S. Zaengl, *High voltage engineering fundamentals.* Newnes, 2000.

[144] B. S. Bernstein and J. W. Tarpey, "Electrical insulation materials," *Electrical Power Cable Engineering: Second: Edition*, p. 58, 2003.

[145] L. Dissado, J. Fothergill, S. Wolfe, and R. Hill, "Weibull statistics in dielectric breakdown; theoretical basis, applications and implications," *Electrical Insulation, IEEE Transactions on*, no. 3, pp. 227–233, 1984.

[146] G. Stone and J. Lawless, "The application of weibull statistics to insulation aging tests," *Electrical Insulation, IEEE Transactions on*, no. 5, pp. 233–239, 1979.

[147] H. C. Miller, "Flashover of insulators in vacuum: review of the phenomena and techniques to improved holdoff voltage," *Electrical Insulation, IEEE Transactions on*, vol. 28, no. 4, pp. 512–527, 1993.

[148] N. Klein, "Electrical breakdown in solids," *Advances in electronics and electron physics*, vol. 26, pp. 309–424, 1969.

[149] S. Whitehead, *Dielectric breakdown of solids*, vol. 8. Clarendon Press, 1953.

[150] K. Stark and C. Garton, "Electric strength of irradiated polythene," 1955.

[151] M. Nagao, T. Amura, Y. Mizuno, M. Kosaki, and M. Ieda, "Localized heat generation before dielectric breakdown of polyethylene films," in *Conduction and Breakdown in Solid Dielectrics, 1989., Proceedings of the 3rd International Conference on*, pp. 77–81, IEEE, 1989.

[152] N. Zebouchi and D. Malec, "Combination of thermal and electromechanical breakdown mechanisms to analyze the dielectric breakdown in polyethylene terephthalate," *Journal of applied physics*, vol. 83, no. 11, pp. 6190–6192, 1998.

[153] W. Weibull, "Wide applicability," *Journal of applied mechanics*, vol. 103, 1951.

[154] G. Sncdccor and W. Cochran, "Statistical methods, 6th cdn," 1976.

[155] R. Ross, "Graphical methods for plotting and evaluating weibull distributed data," in *Properties and Applications of Dielectric Materials, 1994., Proceedings of the 4th International Conference on*, vol. 1, pp. 250–253, IEEE, 1994.

[156] J. Fothergill, "Estimating the cumulative probability of failure data points to be plotted on weibull and other probability paper," *Electrical Insulation, IEEE Transactions on*, vol. 25, no. 3, pp. 489–492, 1990.

[157] M. Fukuma, K. Fukunaga, and T. Maeno, "Space charge dynamics in ldpe films immediately before breakdown," *Dielectrics and Electrical Insulation, IEEE Transactions on*, vol. 8, no. 2, pp. 304–306, 2001.

[158] T. Tanaka and A. Greenwood, "Effects of charge injection and extraction on tree initiation in polyethylene," *Power Apparatus and Systems, IEEE Transactions on*, no. 5, pp. 1749–1759, 1978.

[159] B. Halperin, S. Feng, and P. Sen, "Differences between lattice and continuum percolation transport exponents," *Physical review letters*, vol. 54, no. 22, p. 2391, 1985.

[160] W. Curtin and H. Scher, "Time-dependent damage evolution and failure in materials. mi. mtheory," *Physical Review B*, vol. 55, no. 18, p. 12038, 1997.

[161] M. I. Zeifman and D. Ingman, "A percolation model for lifetime variability in polymeric materials under creep conditions," *Journal of Applied Physics*, vol. 88, no. 1, pp. 76–87, 2000.

[162] J. D. French and S. M. Wiederhorn, "Tensile specimens from ceramic components," *Journal of the American Ceramic Society*, vol. 79, no. 2, pp. 550–552, 1996.

[163] C. Wadhwa, *High voltage engineering*. New Age International, 2007.

[164] L. A. Dissado, "Predicting electrical breakdown in polymeric insulators. from deterministic mechanisms to failure statistics," *Dielectrics and Electrical Insulation, IEEE Transactions on*, vol. 9, no. 5, pp. 860–875, 2002.

[165] K. Wu and Y. Cheng, "Simulation on the time dependence of breakdown strength in insulating polymers," *Journal of applied physics*, vol. 101, no. 6, p. 064113, 2007.

[166] L. A. Dissado and A. Thabet, "Simulation of electrical ageing in insulating polymers using a quantitative physical model," *Journal of Physics D: Applied Physics*, vol. 41, no. 8, p. 085412, 2008.

[167] L. Dissado, A. Thabet, and S. Dodd, "Simulation of dc electrical ageing in insulating polymer films," *Dielectrics and Electrical Insulation, IEEE Transactions on*, vol. 17, no. 3, pp. 890–897, 2010.

[168] "Ieee guide for the statistical analysis of electrical insulation breakdown data," *IEEE Std 930-2004 (Revision of IEEE Std 930-1987)*, pp. 1–41, 2005.

List of Publications

Journals

1. Hisham Alghamdi, George Chen and Alun Vaughan. "The Electro-Mechanical Effect from Charge Dynamics on Polymeric Insulation Lifetime ." AIP Advances 5, no. 12 (2015).

2. Liu, Ning, Miao He, Hisham Alghamdi, George Chen, Mingli Fu, Ruihai Li, and Shuai Hou. "An improved model to estimate trapping parameters in polymeric materials and its application on normal and aged low-density polyethylenes ." Journal of Applied Physics 118, no. 6(2015).

Conferences

1. Hisham Alghamdi, George Chen and Alun Vaughan. "Simulation of electro-thermal aging based on the generic life-expression ."International Conference on Condition Monitoring and Diagnosis (CMD), 2012 , pp. 421-424, IEEE.

2. Hisham Alghamdi, George Chen and Alun Vaughan. "Comparison of two schools of polymeric ageing models: Causes and effects of space charge ."Annual Report Conference on Electrical Insulation and Dielectric Phenomena (CEIDP), 2012, pp. 827-830, IEEE.

3. Hisham Alghamdi and George Chen. "Relation between trapping parameters and ageing based on a new electro-thermo kinetic equation ."IEEE Conference on Electrical Insulation and Dielectric Phenomena (CEIDP), 2014, pp. 421-424, IEEE.

4. Hisham Alghamdi, George Chen and Alun Vaughan. "Simulation of the developed electro-thermal aging model based on trapping and detrapping process ."Annual Report Conference on Electrical Insulation and Dielectric Phenomena (CEIDP), 2015, IEEE.